The Dissertation Committee for Ping Xia
certifies that this is the approved version of the following dissertation:

Interference Management in Heterogeneous Cellular Networks

Committee:

Jeffrey G. Andrews, Supervisor

Gustavo de Veciana

Robert W. Heath

Sundeep Rangan

Sriram Vishwanath

Interference Management in Heterogeneous Cellular Networks

by

Ping Xia, B.E.; M.S.E.

DISSERTATION

Presented to the Faculty of the Graduate School of

The University of Texas at Austin

in Partial Fulfillment

of the Requirements

for the Degree of

DOCTOR OF PHILOSOPHY

THE UNIVERSITY OF TEXAS AT AUSTIN

December 2012

Dedicated to my family.

Acknowledgments

First of all, special thanks and appreciation are for my supervisor Professor Jeff Andrews, for his continual inspiration and guidance during my time at UT. I am indebted to him for helping me find the right problem to focus and teaching me to skillfully motivate my research to the readers/audience. Professionally, I owe most of my improvements to his insightful feedbacks and great writing and presentation skills. In addition to my advisor, I would like to thank my committee members Professor Gustavo de Veciana, Professor Robert Heath, Professor Sundeep Rangan and Professor Sriram Vishwanath for their constructive research advice on my dissertation. I gratefully acknowledge Motorola Solutions (now Nokia Siemens) for supporting my research, and Dr. Amitava Ghosh and Dr. Bishwarup Mondal for their valuable technical inputs.

I would like to express my thanks to my colleagues in Wireless Networking and Communications Group (WNCG), especially Chun-Hung Liu, Han-Shin Jo, Vikram Chandrasekhar, Jun Zhang, Yudong Chen and Beiyu Rong for their helpful discussions at so many times. I also thank Melanie Gulick of ECE graduate office and Janet Preuss, Jennifer Graham and Karen Little of WNCG office for providing comfortable research environment and taking care my tuition bills, course registrations and many other paperworks.

Most importantly, I would like to thank my parents, Zhengrong Xia and Youmei Chen, for their unconditional love and care throughout my life. I also would like to thank my girlfriend Wen Zhu for her long-standing support, patience and encouragement during the past years. It is a great sacrifice of them to support me pursuing graduate school thousands of miles away. I could not have accomplished it without them.

Interference Management in Heterogeneous Cellular Networks

Publication No. _____

Ping Xia, Ph.D.
The University of Texas at Austin, 2012

Supervisor: Jeffrey G. Andrews

Heterogeneous cellular networks (HCNs) – comprising traditional macro base stations (BSs) and heterogeneous infrastructure such as microcells, picocells, femtocells and distributed antennas – are fast becoming a cost-effective and essential way of handling explosive wireless data traffic demands. Up until now, little basic research has been done on the fundamentals of managing so much infrastructure – much of it unplanned – together with the carefully planned macro-cellular network. This dissertation addresses the key technical challenges of inter-cell interference management in this new network paradigm.

This dissertation first studies uplink femtocell access control in *uncoordinated* two-tier networks, i.e. where the femtocells cannot coordinate with macrocells. Closed access allows registered home users to monopolize their own femtocell and its backhaul connection, but also results in severe interference between femtocells and nearby unregistered macro users. Open access reduces

such interference by handing over such users, at the expense of femtocell resource sharing. In the first analytical work on this topic, we studied the best femtocell access technique from the perspectives of both network operators and femtocell owners, and show that it is strongly contingent on parameters such as multiple access schemes (i.e. orthogonal vs. non-orthogonal) and cellular user density (in TDMA/OFDMA).

To study *coordinated* algorithms whose success depends heavily on the rate and delay (vs. user mobility) of inter-cell overhead sharing, this dissertation develops various models of overhead signaling in general HCNs and derives the *overhead quality contour* – the achievable set of overhead packet rate and delay – under general assumptions on overhead arrivals and different overhead signaling methods (backhaul and/or wireless). The *overhead quality contour* is further simplified for two widely used models of overhead arrivals: *Poisson* and *deterministic*.

Based on the *overhead quality contour* that is applicable to generic coordinated techniques, this dissertation develops a novel analytical framework to evaluate downlink coordinated multi-point (CoMP) schemes in HCNs. Combined with the signal-to-interference-plus-noise-ratio (SINR) characterization, this framework can be used for a class of CoMP schemes without user data sharing. As an example, we apply it to downlink CoMP inter-cell interference cancellation (ICIC), after deriving SINR results for it using the spatial Poisson Point Process (PPP) to capture the uncertainty in base station locations.

Table of Contents

List of Tables

List of Figures

Chapter 1

Introduction

One remarkable trend in recent years is the proliferation and relentless penetration of new generation mobile devices such as smartphones and tablets. Their annual shipments have already overtaken those of personal computers in 2011 [128] and will be more than the global population in next year [116]. The prevalence of powerful devices combined with plentiful online content has opens up new dimensions of mobile usage: cloud computing, video/music streaming, social networking, gaming and news [128]. Not surprisingly, it has raised customers' expectation of ubiquitous data service and leaded to a stunning increase in mobile data traffic in recent years. According to forecasts from Ericsson, Qualcomm, Cisco and 3GPP [20, 57, 116, 117, 128], such a trend is going to accelerate, rather than slow down, in the next 5 – 10 years. If history is any indication, the actual growth in data demands is likely to be even stronger than these seemingly aggressive forecasts [56, 115]. Therefore, improving cellular network capacity cost-effectively is a particularly serious and urgent concern of network operators. To meet this challenge, the possible approaches are few, and can be summarized below [7, 16, 20, 100].

Use More Cellular Spectrum. This approach is technically simple

but effective, as Shannon capacity scales linearly with the signal bandwidth. However, available spectrum is scarce, expensive and usually fragmented. Proposals of utilizing the ultra-wide bands beyond 60 GHz are not feasible any time soon, as it takes time for hardware to mature and system design to adjust. For example, traditional silicon analog circuits, amplifiers and even transceiver architecture are not suitable for 60 GHz communications and completely redesigns are usually required [29, 45, 49, 64, 107]. From system level, new PHY and/or MAC protocols are needed because of the change in signal propagation characteristics (e.g. channel attenuation, multipath and time variation) and that the system is turning from bandwidth limited to power limited [45, 136].

Improve Radio Link Performance. The goal of this approach is to improve spectral efficiency (bps/Hz) by using advanced PHY and MAC techniques such as multiple-input-multiple-output (MIMO) and efficient user scheduling. These techniques are the main focus of previous academic research and industrial implementations, from perspectives such as information-theoretic limits, communication theory and signal processing algorithms [148]. By now, they are widely adopted as essential components in existing and upcoming cellular standards. However, as the point-to-point link performance is already approaching its theoretic limit, their gains are expected to be small in 4G and beyond [50, 100]. One of few exceptions may be massive MIMO, where BSs with very large number of antennas serve many users simultaneously [102]. In theory, it can translate into huge spatial multiplexing gains and is now under active research [31, 68].

Deploy More Cells. Since not much gain can be expected from a single point-to-point link, network operators can instead increase the cell density to create as many links as possible in a given area. In this way, the spectrum is reused and the area spectral efficiency (bps/Hz/km^2) is improved. Another benefit of this approach, although diminishing as cell density increases, is the better signal-to-noise-ratio (SNR) because of reduced transmit distance. Shown from the history of cellular networks, this approach has brought most of the capacity gains, significantly more than other factors combined [36]. Because cells can be deployed indefinitely (if their footprints shrink appropriately), there is no hard limit on the capacity gains in the future [12]. Seemingly, this approach is a scalable way for network operators to keep pace with the explosive data demands.

One way of increasing cell density is to deploy more macrocells. Macrocells are primarily used in the past for seamless coverage in cellular networks, but are expensive for network operators in terms of both capital expense (CAPEX) and operational expense (OPEX). Because of the size, backhaul and power consumption of macrocells, their deployment is slow and faces site limitations, especially in dense urban environments where most data demand is generated. For these reasons, deploying more macrocells is not a desirable choice for network operators.

Another way of deploying more infrastructure is to overlay low-power low-cost small cells (e.g. microcells, picocells, femtocells and distributed antennas) on top of existing macrocells, and therefore transform the conventional

macrocell networks into heterogeneous cellular networks (HCNs). An example of HCN is shown in Fig. 1.1. Different from traditional macrocells, small cells allow much faster deployment in a variety of environments (e.g. on top of traffic lights and even in end-users' houses) and are orders of magnitude cheaper in terms of backhaul cost, power consumption, site rent price and installation labour fee. In short, with the help of such overlaid infrastructure, the network operator is able to extend high quality coverage and create high-capacity hotspots wherever the demand occurs, without the need of additional expensive cellular towers. Not surprisingly, there has been enthusiastic interest in industry towards making HCNs a reality. Academic research however, has been slower to embrace this new paradigm.

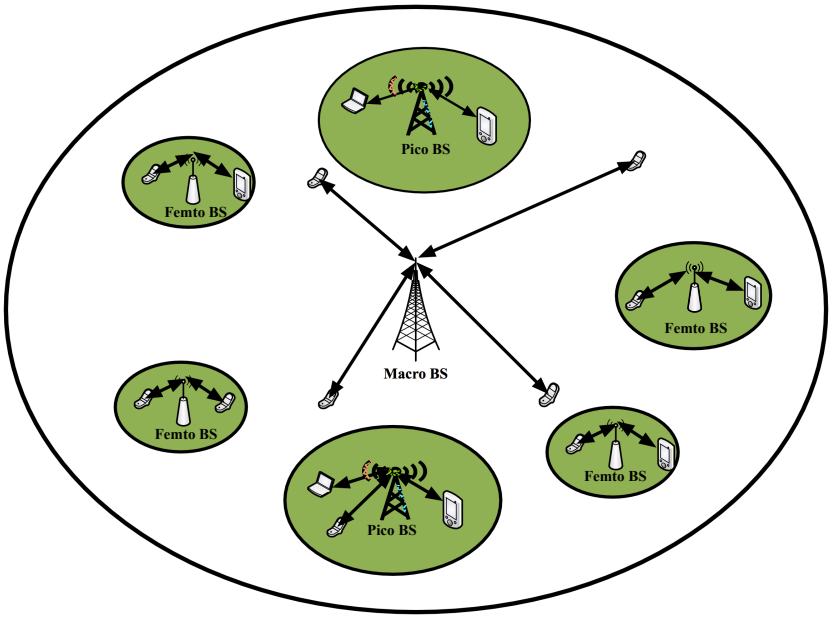

Figure 1.1: A heterogeneous cellular network consisting of macrocells, picocells and femtocells.

1.1 Interference Management Issues in HCNs

The market for small base stations (BSs) is in an early phase but projected to reach a significant level in the near future [15,36,85]. Tens of millions of arbitrarily-located devices that interfere with the carefully planned and deployed macrocell network is a source of serious concern for network operators. How can the potentially large benefits of HCN deployments be balanced with their potentially deleterious effect on the existing cellular network? A key technical challenge is interference management in HCNs, to make sure different infrastructure components behave in a way that increases, rather than decreases, the key quality of service (QoS) metrics.

Several particular aspects of small cells make the interference management in HCNs more challenging than traditional macrocell-only case. First, unlike Wi-Fi access points, small cells serve users in licensed spectrum, to guarantee Quality-of-Service (QoS) and because the devices they communicate with are developed for these frequencies. Compared to allocating separate channels inside the licensed spectrum exclusively to small cells, sharing spectrum would be preferred from an operator perspective. Secondly, the overlaid small cells will often be added over time in unpredictable locations: they can be deployed anywhere inside the macrocell area with no prior warning [36, 85, 118, 164]. Therefore, significant interference is not restrict at the edges of macrocells any more. Instead, it is now ubiquitous in the network, even in the interior of macrocells. Further, to balance the user load in the network and fully utilize the spectrum resource at small cells, range extension is proven to be essential

for HCN capacity improvement [44, 85, 89, 160]. Otherwise, not much capacity gain can be expected from deploying small cells, because they essentially serve very few mobile users and the macrocell is still overloaded. However, an inevitable side-effect of range extension is the deteriorated interference: mobile users in the extended areas (see Fig. 1.2 for an example) suffer stronger interference than their signals. For these reasons, interference in HCNs is quite different from in conventional cellular networks, and potentially endangers their successful co-existence [35, 91].

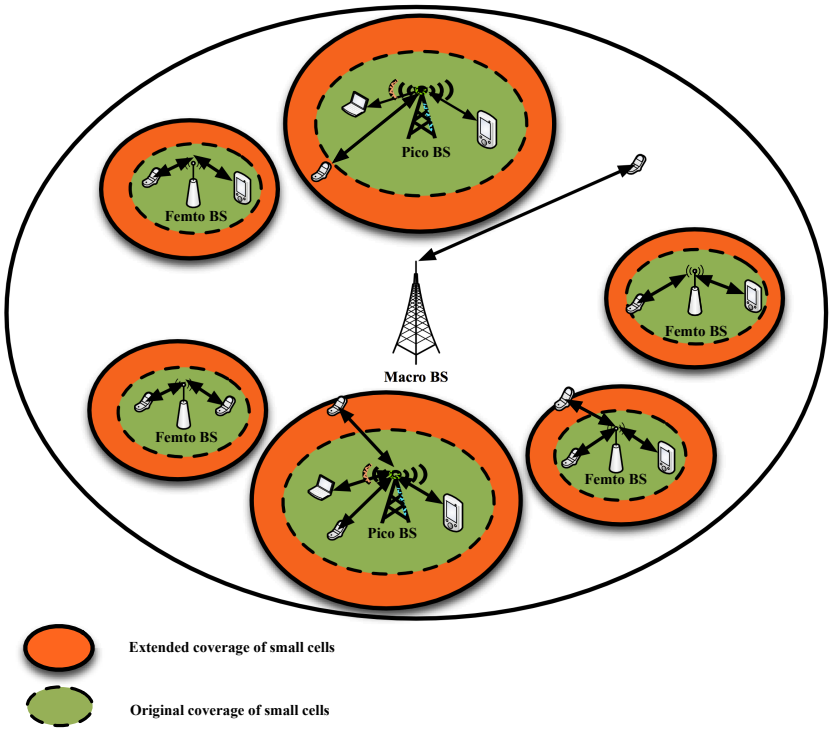

Figure 1.2: Range extension in heterogeneous cellular networks, which offloads more mobile users to small cells, by either increasing their pilot powers or adding an artificial biasing factor in favour of them during cell association.

Therefore, interference management techniques are of critical importance in HCNs. They can be divided into the following categories, based on whether inter-cell overhead signaling is required among different cells.

Decentralized Interference Management. Techniques in this category do not require any cooperation among cells, as each cell observes and acts on its own. Common examples are fractional frequency reuse, advanced receivers, distributed power control and static resource partition [34, 37, 44, 85, 111]. One obvious advantage of these techniques is that they do not bring additional inter-cell overhead into the system, which can otherwise be capacity consuming in dense networks like HCNs. They also relieve the requirements on base station backhaul – a significant cost for network operators considering the overwhelming number of small cells. On the other hand, an unavoidable shortcoming of decentralized algorithms is sub-optimal performance in general, because cooperative gains among cells can be potentially large, if various practical challenges are robustly addressed.

Coordinated Interference Management. As the name implies, techniques in this category allow inter-cell overhead messaging among neighboring cells to cooperatively manage interference in the network, with examples being enhanced inter-cell interference coordination (eICIC), joint power control and coordinated multipoint (CoMP) communications [20, 44, 59]. Intuitively, with relaxed constraint on inter-cell information sharing, these techniques are expected to bring larger performance gains than decentralized algorithms. However in reality, their success depends heavily on how the overhead

is shared, and the rate and delay (vs. mobility) of the overhead sharing. For example, without particular optimizations on inter-cell overhead channel, coordinated multi-cell beamforming/scheduling is even worse than distributed resource partition in HCNs [20]. Therefore, practical issues on inter-cell overhead sharing must be considered in the study of coordinated interference management techniques.

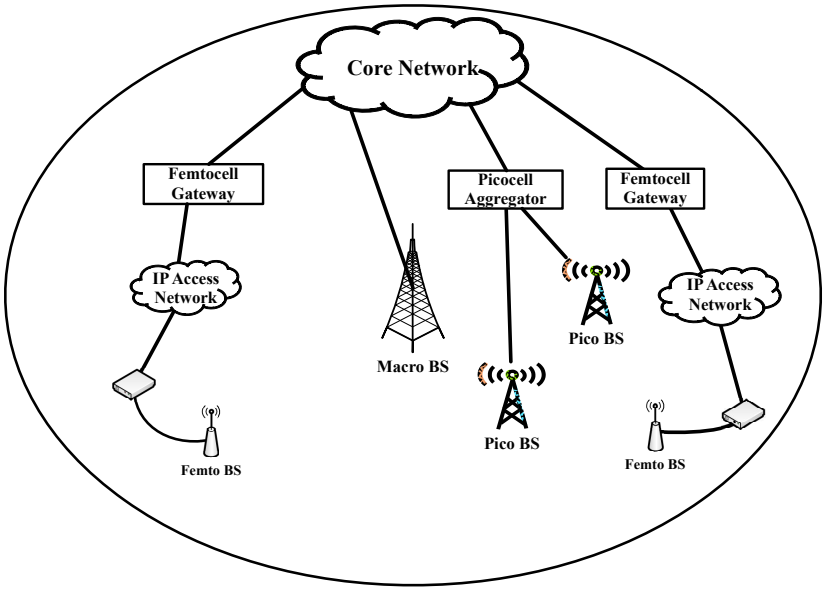

Figure 1.3: An example of the backhaul deployment of a heterogeneous cellular network.

Both decentralized and coordinated interference managements assume great importance in HCNs, because different types of base stations have vastly different backhaul capabilities and protocols (see Fig. 1.3). For example, femtocells often use third-party IP based backhaul (e.g. DSL and cable modem) that is aggregated by a gateway and so has much lower capacity and much

longer delay. Therefore, the only option for femtocell interference management is to develop algorithms with very low inter-cell overhead [15, 34, 36, 37]. On the other extreme, picocells in the same cluster are connected using high-speed backhaul (e.g. fiber optics) with few intermediate gateways [119]. Algorithms with intense inter-cell overhead are thus preferred to them for higher performance gains. Therefore, this dissertation studies interference management techniques from both categories.

1.2 Overview of Contributions

This dissertation focuses on the inter-cell interference management in the new paradigm of heterogeneous cellular networks. Because different types of BSs have distinct backhaul and processing capabilities, we study both decentralized and coordinated interference management techniques, with the main contributions summarized in the following.

Uplink Access Control in Uncoordinated Femtocell Networks. Cross-tier interference in femtocell networks is contingent on the femtocell access decision – that is, which users in the network should be allowed to use it. *Closed access* restricts the use of the femtocell to users explicitly approved by the owner, whereas *open access* allows an arbitrary nearby cellular user to use the femtocell. Seemingly, the network operator would prefer an open access deployment for traffic offloading and interference mitigation, while the femtocell owner would prefer closed access, in order to keep the femtocell's capacity and backhaul to himself. We show mathematically and through simulations that

the reality is more complicated for both parties, and that the best approach is very different between orthogonal (TDMA or OFDMA, per subband) and non-orthogonal (CDMA) multiple accesses. In a TDMA/OFDMA network, closed access is typically preferable at high user densities, whereas in CDMA, open access can provide gains of more than 300% for the *home user* by reducing the near-far problem experienced by the femtocell. The results of this paper suggest that the interests of the femtocell owner and the network operator are more compatible than typically believed, and that CDMA femtocells should be configured for open access whereas OFDMA or TDMA femtocells should adapt to the cellular user density.

Overhead Signaling characterization in Inter-cell Coordination. The success of inter-cell coordination (e.g. CoMP communications) depends heavily on how the overhead is shared, and the rate and delay (vs. mobility) of the overhead sharing. We develop various models of overhead signaling for generic inter-cell coordination schemes, which are usually ignored in traditional 1-tier networks, and assumes even more importance in multi-tier HCNs. We then derive the overhead delay distributions for general K-tier HCNs in closed-form expressions or computable integrals under general assumptions on overhead arrivals and different overhead signaling methods (*backhaul* and/or *wireless*). The delay distributions are further simplified for two widely used models of overhead arrivals: *Poisson* and *deterministic* arrival process. Note that these models and results are general and independent on the spatial distributions of BS locations. they can be used in the design and

evaluation of any inter-cell coordination scheme. For example, they are used in Chapter 4 for downlink CoMP schemes. They also provide design insights on backhaul and wireless overhead channels to handle specific overhead signaling requirements.

Downlink Coordinated Multi-Point. We present the evaluation of CoMP techniques in HCNs by using novel models of inter-cell overhead messaging and BS locations. Previous approaches to CoMP ignore the inter-cell overhead delay, which results in an irreducible performance bound in theory and significant performance degradations in practice. Besides, they consider the grid or Wyner model for base station locations, which is not appropriate for HCN BS locations which are numerous and haphazard. Even for conventional macrocell networks without overlaid small cells, SINR results are not tractable in the grid model nor accurate in the Wyner model. In contrast, we develop a novel analytical framework to quantify the impact of overhead delay and inaccuracy for CoMP evaluation in HCNs. This framework can be used for a class of CoMP schemes without user data sharing. As an example, we apply it to downlink CoMP inter-cell interference cancellation (ICIC), after deriving clean-form SINR results for it by using the spatial Poisson Point Process (PPP) to capture the uncertainty in base station locations. Our results diverge significantly from previous works on downlink CoMP ICIC. For example, we show that CoMP ICIC does not bring any throughput gain when the overhead channel delay is larger than 60% of the channel coherence time. We also find that, in most cases, coordinating with only one other cells is nearly

optimum for downlink CoMP ICIC.

1.3 Organization

The remainder of this dissertation is organized as follows. Chapter 2 compares femtocell closed access with open access (a decentralized way of interference mitigation) from the perspective of network operators and femtocell owners. Chapter 3 presents various models on inter-cell overhead messaging in HCNs and quantifies the delay distributions. The results are applicable to generic inter-cell coordination schemes, and used in Chapter 4 for CoMP evaluation. Chapter 4 studies downlink CoMP techniques by developing a novel framework to quantify the impact of overhead messaging and using the Poisson Point Process to model BS randomness in SINR characterization. Conclusion and Future work are summarized in Chapter 5.

Chapter 2

Uplink Access Control in Uncoordinated Two-tier Femtocell Networks

In two-tier femtocell networks, cross-tier interference depends heavily on the femtocell access decision – that is, which users in the network should be allowed to use it. A typical scenario is called the "Dead Zone" or "Loud Neighbor" problem, where mobile users are very near to a femtocell but unable to use it. These users have to connect to the regular macrocell BSs that may be far away. They cause significant macro-to-femto interference in the uplink, and likewise suffer from low signal-to-interference-ratios (SIRs) in the downlink because of the strong interference from the femtocells. These affects are akin to the well known near-far problem, but exacerbated by the de-centralization and lack of coordinated power control inherent in a two-tier network.

Because of the presently non-existent coordination between femtocells and macrocell BSs, centralized cooperation to mitigate cross-tier interference is infeasible in the near future, and thus a two-tier network needs to adopt decentralized strategies for interference management [34, 37] such as femtocell access control [15, 36, 41, 46, 61, 84, 90, 135, 141]. Femtocells can be configured to be either *closed access* or *open access*. Femtocells only provide service to

specified subscribers in closed access, to ensure they can monopolize their own femtocell and its backhaul with privacy and security. However this potentially leads to severe cross-tier interference as described above. On the contrary, open access allows arbitrary nearby cellular users to use the femtocell and thus reduces the strong cross-tier interference from and to them. Seemingly, open access is beneficial to network operators, by providing an inexpensive way to expand their network capacities by leveraging third-party backhaul for free. However, the femtocell owners will lose the monopoly on their femtocell resources when enjoying a lower macro-to-femto interference in open access. Crucial unanswered questions remain in femtocell access control, such as:

1. Which mode meets the interests of femtocell owners? Which mode is preferable to the network operator? Are these two choices the same or different?

2. How does the answer depend on factors such as multiple access protocol (e.g. OFDMA, CDMA), user densities, user scheduling, and femtocell backhaul constraints?

2.1 Related Work

The uplink interference in two-tier femtocell networks was evaluated in [35], showing that tier-based open access can reduce the interference and offer an improvement in the network-wide area spectral efficiency – the feasible number of femtocells and macrocell users per cell-site. Similar conclusions were presented in many simulation-centric studies accomplished by the 3GPP RAN

4 group [1,106,108]. Downlink network capacities under open and closed access were explored in [108]; Feasible combinations of femtocells and macrocells under the constraint of network interference were examined in [106]; Various scenarios were presented in [1] to compare femtocell open and closed access. All these simulations show that with adaptive open access, the interference in two-tier networks is mitigated and the deployment of co-channel femtocells becomes feasible. However, since femtocells are installed and paid for by their owners, it is necessary to evaluate their loss of femtocell resources in open access. It is important that the benefits of mitigated interference are not undermined by the loss of femtocell resources, such as over-the-air (OTA) and backhaul capacity.

The issues of femtocell backhaul sharing in open access were examined in [41], which simulated open and closed access in HSDPA, with the thesis that completely open access is problematic because of sharing limited femtocell backhaul among a potentially large number of mobile users. Based on simulations incorporating femtocell backhaul issues and cross-tier interference, this work concludes that open access with a restriction on the number of supported users at the femtocell is the preferred approach. Based on both analytical and simulation results, this chapter shows that such a conclusion strongly depends on whether the multiple access scheme is orthogonal (TDMA or OFDMA) or non-orthogonal (CDMA).

The increased handover frequency and hence overhead signaling in open access is a possible challenge to its implementation. A technique combining

intracell handovers with power control was proposed in [91], and a *hybrid access* model – open access with a cap on the amount of resources allocated to the cellular users – was simulated in [46]. Both of these approaches substantially reduce the number of handovers in open access while mitigating the cross-tier interference. In this chapter, the hybrid access model is simply called open access, since in the system model open access is assumed to have an upper limit of K users, where K could become arbitrarily large to conform to fully open access.

2.2 Contributions

This chapter evaluates the performance of femtocell open and closed access in the uplink, from the viewpoints of both the femtocell owner (owner's achieved rate) and the network operator (cellular users' sum throughput).

First, the cumulative distribution function (CDF) for uplink cross-tier interference is derived in orthogonal multiple access schemes (TDMA or OFDMA). The capacity tradeoffs for both the femtocell owner and cellular users are then presented. In TDMA or OFDMA, the preferences of the femtocell owner and the network operator are highly dependent on cellular user density: Their choices are incompatible/ open access/ closed access in low/ medium/ high cellular user density respectively. Thus, for 4G networks (LTE & WiMAX) that use OFDMA, the femtocell access control should likely be adaptive to the cellular user density.

Second, by deriving lower bounds on the performance of open access,

this chapter shows that in non-orthogonal multiple access (i.e. CDMA) open access is a strictly better choice for the home user. In typical propagation scenarios, it provides more than a factor of 3 rate gain to the femtocell owner by lowering interference. From the viewpoint of the network operator, open access is also preferred. In the less important regime of low cellular user density, open access achieves almost the same performance as closed access, while in the important regime of high cellular user density, it improves performance significantly. The results suggest that femtocell open access is the preferred approach for CDMA femtocells (i.e. 3G), from the viewpoints of both femtocell owners and network operators.

2.3 System Model

In the interior area of a macrocell of radius R, the macrocell BS is located at the center, with a single femtocell at a distance D away from it. Suppose there are N cellular users, denoted as $U_1, U_2, \ldots, U_N$, roaming inside the macrocell. Their positions are i.i.d. random variables, uniformly distributed in the macrocell area. The femtocell owner, or alternatively the home user, is denoted as U_0. Since the home user is transmitting and receiving inside the small area of a house, we could assume it is located at a *deterministic* position, with a distance of d from the femtocell. As the subscriber, the home user would always talk to the femtocell. On the other hand, cellular users can be served by the macrocell BS, or the femtocell if it employs open access. Femtocell-to-femtocell interference has been neglected for reasons of

analytical tractability. However, because uplink femtocell transmissions typically originate and terminate indoors and are of low power, their contribution to the overall interference is expected to be negligible compared to the more numerous and high power outdoor (macro-cellular) users.

2.3.1 Channel Model and Interference

We consider path loss attenuation effects only and ignore short-term fading in our channel model. This assumption is reasonable because fading does not have a large effect in a wideband system with sufficient diversity, e.g. RAKE receiver (CDMA), or multi-antenna diversity or distributed subcarrier allocation (OFDMA). The path-loss exponent of outdoor (indoor) transmission is denoted by α (β). In particular, the channel model is given by

$$H(|x|) = \begin{cases} |x|^{-\alpha} & \text{outdoor \& cross-wall transmission} \\ |x|^{-\beta} & \text{indoor transmisstion} \end{cases} \tag{2.1}$$

Here, $|x|$ is the distance from the transmitter to the respective base station. Setting $\alpha > \beta$ incorporates wall penetration loss in our channel model.

Assumption 1. *We assume that there is no coordination between the femtocell and the macrocell BS, nor between different femtocells, in terms of power control or resource scheduling.*

In the uplink, denote P_c and P_f as the received power at the macrocell BS and the femtocell respectively. Through uplink power control, a macrocell user U_j causes interference of $P_c h_j / g_j$ to the femtocell, where h_j (g_j) is its

channel to the femtocell (the macrocell BS). Conversely, a femtocell user U_i causes interference of $P_f g_i/h_i$ to the macrocell BS.

Definition 1. *For $U_j \in \{U_0, U_1, \ldots, U_N\}$, its* interference factor *I_j is defined as h_j/g_j. $\{I_1, I_2, \ldots, I_N\}$ are i.i.d. random variables, and we define their ordered statistics as*

$$I_{(1)} = \min(I_1, \ldots, I_N), \quad I_{(N)} = \max(I_1, I_2, \ldots, I_N)$$

and for $1 < k < N$,

$$I_{(k)} = \min(\{I_1, \ldots, I_N\} \backslash \{I_{(1)}, \ldots, I_{(k-1)}\})$$

Correspondingly cellular users are reordered as $\{U_{(1)}, U_{(2)}, \ldots, U_{(N)}\}$.

Assumption 2. *We assume $I_0 \geq I_{(N)}$ holds, because the home user is closer to the femtocell, and the indoor channel has a smaller path loss exponent.*

Lemma 2.3.1. *The cumulative distribution function for the interference factor of each cellular user is*

$$F_I(i) = \begin{cases} (r/R)^2 & 0 \leq i < (\frac{R}{R+D})^\alpha \\ L(i) & (\frac{R}{R+D})^\alpha \leq i < 1 \\ \frac{\pi - \varphi + 0.5\sin(2\varphi)}{\pi} & i = 1 \\ 1 - L(i) & 1 < i \leq (\frac{R}{R-D})^\alpha \\ 1 - (r/R)^2 & (\frac{R}{R-D})^\alpha < i \end{cases} \tag{2.2}$$

where r, L(i), φ are given by:

$$r = \frac{i^{1/\alpha} D}{|1 - i^{2/\alpha}|}, \quad \varphi = \arccos\left(\frac{D}{2R}\right),$$

$$L(i) = \frac{\pi(R^2 + r^2) - (\pi - \theta + 0.5\sin 2\theta)r^2 - (\pi - \phi + 0.5\sin 2\phi)R^2}{\pi R^2},$$

where $x_c = \frac{D i^{2/\alpha}}{|1 - i^{2/\alpha}|}$, $\theta = \arccos\left(\frac{r^2 + x_c^2 - R^2}{2 r x_c}\right)$ and $\phi = \arccos\left(\frac{x_c^2 + R^2 - r^2}{2 x_c R}\right)$.

Proof. See Appendix 2.8.1 □

In non-orthogonal multiple access (CDMA), the interference is additive. For a set of k *interference factors* $\{I_{n_1}, I_{n_2}, \ldots, I_{n_k}\}$, denote function $G_I(k, \cdot)$ as the CDF of $\sum_{j=n_1}^{n_k} I_j$, which is given by

$$G_I(k, i) = \mathbb{P}(\sum_{j=n_1}^{n_k} I_j \leq i).$$

$G_I(k, \cdot)$ is the same for whatever k *interference factors*, since the *interference factors* are i.i.d..

Lemma 2.3.2. *An upper bound on the CDF function $G_I(k, \cdot)$ is given by*

$$G_I(k, i) \leq G_I^{ub}(k, i) = (F_I(i))^k \triangleq F_I^k(i) \tag{2.3}$$

Proof. Without loss of generality, we assume I_{n_1} is the maximum *interference factor* of $\{I_{n_1}, \ldots, I_{n_k}\}$. Therefore $\mathbb{P}(I_{n_1} \leq i) = F_I^k(i)$, which provides an upper bound on $G_I(k, \cdot)$.

$$G_I(k, i) = \mathbb{P}\left(\sum_{j=n_1}^{n_k} I_j \leq i\right) = 1 - \mathbb{P}\left(\sum_{j=n_1}^{n_k} I_j > i\right) \leq 1 - \mathbb{P}\left(I_{n_1} > i\right) = F_I^k(i) \tag{2.4}$$

□

To summarize, in this subsection we derived the CDF $F_I(\cdot)$ for each *interference factor* and an upper bound on the CDF $G_I(\cdot, \cdot)$ for the sum of these *interference factors*. These two CDFs will be will be used to calculate outage probability for orthogonal and non-orthogonal multiple access respectively.

2.3.2 Hand over Metric and Procedure

When the femtocell deploys open access control, it can choose to serve cellular users based on certain metrics. A typical metric is that it provides service to cellular users if both of the following two conditions hold: 1) these cellular users cause outage to the home user, and 2) the femtocell has available resources. Such a metric allows cellular users to share the femtocell resources when they can potentially boost the capacity of femtocell owners by reducing co-channel interference. Suppose the maximum number of additional cellular users that the femtocell can serve is K.

Assumption 3. *When cellular users cause outage to the home user, the femtocell picks the most noisy interferer from the macrocell to serve. This hand over procedure continues as long as the home user still experiences outage and the number of handed over cellular users does not exceed K.*

Based on this assumption, when the femtocell provides service to L cellular users, these users must be the strongest interferers $U_{(N)}, \ldots U_{(N-L+1)}$, which reduce the macro-to-femto interference to the largest extent possible. When served by the femtocell, these cellular users cause interference $P_f/I_{(N)}, \ldots$, $P_f/I_{(N-L+1)}$ to the macrocell respectively, which are also the smallest possible. Therefore, the proposed procedure is preferable for the two parties, since it maximally reduces the interference they experience after the handover.

2.3.3 Resource Allocation and Ergodic Rate

From Assumption 1, we consider distributed resource allocation in two-tier femtocell networks.

Backhaul Allocation. The macrocell BS usually has a large backhaul capacity. So when a cellular user is served by the macrocell BS, its rate will not be constrained by the backhaul. However, the femtocell backhaul capacity, denoted as $\mathcal{C}_b$, is typically modest and often shared, common examples being DSL and cable modem. Thus it is necessary to incorporate the femtocell's backhaul allocation into the analysis. As the femtocell serves additional L $(0 \leq L \leq K)$ cellular users, the home user is allocated with a portion λ_L of this backhaul capacity, while each of the L cellular users is assigned a portion μ_L of the femtocell backhaul capacity. In both closed and open access, when the femtocell does not serve any cellular users, there is no backhaul issue, i.e. $\lambda_0 = 1$ and $\mu_0 = 0$.

Assumption 4. *For* $\{\lambda_0, \lambda_1, \ldots, \lambda_K\}$ *defined above, the following inequality holds:*

$$\lambda_0 \geq \lambda_1 \geq \ldots \geq \lambda_K \tag{2.5}$$

Because as users are added, the fraction of resources allocated to the home user should not increase.

Time Allocation (in TDMA/OFDMA per subband). In the macrocell network, since all the users have the same rate requirement and

they are i.i.d. located inside the macrocell, the time resources will be fairly allocated among them. Therefore, when the macrocell BS is serving M cellular users, each user enjoys an average time fraction[1] of $1/M$. In the femtocell network, when the femtocell serves additional L cellular users, the time fraction allocated to the home user and each of the L cellular users should be λ_L and μ_L respectively, according to the allocation in backhaul capacity.

Assumption 5. *Each macrocell user has a target rate* $\mathcal{C}$*, while each femtocell user has a rate requirement of* $\min\{\mathcal{C}, \lambda\mathcal{C}_b\}$*, where* $\lambda\mathcal{C}_b$ *is its allocated backhaul capacity.*

Assumption 6. *According to its rate requirement, each user has a SINR target. The user achieves its required rate when the received SINR (we assume additive white Gaussian noise with variance of* σ^2*) at or above its SINR target. Otherwise it is in outage and the rate is zero.*

Definition 2. *The event* $A_L(L \in \{0, 1, 2, \ldots, K\})$ *is defined as the femtocell provides service to* L *additional cellular users. In event* A_L*, denote the SINR targets of the home user, handed over* L *cellular users and the remaining* $N-L$ *cellular users as* $\Gamma_{f,L}$*,* $\Gamma_{h,L}$ *and* $\Gamma_{c,L}$ *respectively. Their success probabilities are denoted as* $p_{f,L}$*,* $p_{h,L}$ *and* $p_{c,L}$ *accordingly.*

Definition 3. *A user's* ergodic rate *is its rate requirement multiplied by its success probability.*

[1]Although in practice the time slot assigned to a mobile user can only be a group of discrete values, the average time fraction of the mobile user can be any value between 0 and 1. The same argument is applicable to the value of λ_L and μ_L.

We evaluate open vs. closed access from the viewpoints of the femtocell owner – the home user's *ergodic rate* $\mathcal{C}_0$, and the network operator – cellular users' *sum throughput* $\mathcal{C}_{sum}$, which is defined as the sum of all cellular users' *ergodic rates*. Although we use the hybrid model in [46] as a more general form of open access, the overhead signaling from handovers still would affect the rates of mobile and femtocell users. However, since it is difficult to quantify precisely, often involves separate overhead channels, and the exact implementation varies significantly from protocol to protocol, we do not include the impact of handover signalling in the analysis.

2.4 Capacity Contours in Orthogonal Multiple Access Schemes

In LTE and WiMAX, which both use a similar form of OFDMA, the end-user is assigned a portion of the spectrum for a (sub)frame, which is identical to being allocated the entire spectrum for certain time slots (i.e. TDMA) from an analysis perspective. Besides, each subband in OFDMA is orthogonal and allocated in a TDMA fashion along the time axis. Therefore in this section, we analyze a TDMA scenario, which can also be viewed as OFDMA on a per subband basis. We first consider the scenario when the femtocell can serve K cellular users. We then focus on the important special case of $K = 1$.

In an arbitrary time slot, suppose users U_i and U_j are active at the femtocell and the macrocell respectively, causing interference of P_f/I_j and

$P_c I_j$ at macro and femto BSs accordingly.

Theorem 2.4.1. *In TDMA or OFDMA, the home user's ergodic rate and the cellular users' sum throughput in femtocell closed access are given by*

$$\mathcal{C}_0 = \min(\mathcal{C}, \lambda_0 \mathcal{C}_b) F_I \left(\frac{P_f}{P_c \Gamma_{f,0}} - \frac{\sigma^2}{P_c} \right), \tag{2.6}$$

$$\mathcal{C}_{sum} = N \mathcal{C} \mathbb{P} \left(\frac{P_c}{P_f / I_0 + \sigma^2} \geq \Gamma_{c,0} \right) \tag{2.7}$$

Proof. Since at the macrocell BS, each cellular user causes interference to the home user during its time slot, namely $1/N$, the *ergodic rate* of the home user is

$$\begin{aligned} \mathcal{C}_0 &= \min(\mathcal{C}, \lambda_0 \mathcal{C}_b) \sum_{j=1}^{N} \frac{1}{N} \mathbb{P} \left(\frac{P_f}{P_c I_j + \sigma^2} \geq \Gamma_{f,0} \right) \\ &= \min(\mathcal{C}, \lambda_0 \mathcal{C}_b) F_I \left(\frac{P_f}{P_c \Gamma_{f,0}} - \frac{\sigma^2}{P_c} \right) \end{aligned} \tag{2.8}$$

On the other hand, each cellular user experiences an interference of P_f / I_0 from the home user. Their sum rate is

$$\mathcal{C}_{sum} = N \mathcal{C} p_c = N \mathcal{C} \mathbb{P} \left(\frac{P_c}{P_f / I_0 + \sigma^2} \geq \Gamma_{c,0} \right) \tag{2.9}$$

□

Remark 1. *In TDMA the macro-to-femto interference is time shared, so the home user's probability of success is averaged over time and consequently not scaled by N. Therefore, the home user's* ergodic rate *in closed access is independent of the number of cellular users. Things are different in CDMA, as shown in the next section.*

It is an important fact that the SINR target of cellular users in the macrocell (in both open and closed access) is an increasing function of their density. Intuitively, when the macrocell BS serves more mobile users, each of them has a smaller time fraction and must increase its SINR target to achieve a given rate requirement.

In closed access, since the received SINR of a cellular user in the macrocell is a constant value of $\frac{P_c}{P_f/I_0+\sigma^2}$, there is a cutoff user loading N_c^*, such that: 1) when $N \leq N_c^*$, each cellular user's SINR target constraint is satisfied and their *sum throughput* is the maximum possible, $\mathcal{C}_{sum} = N\mathcal{C}$; 2) when $N > N_c^*$, each cellular user's SINR target is infeasible and $\mathcal{C}_{sum} = 0$. The value of N_c^* is governed by the inequality $\frac{P_c}{P_f/I_0+\sigma^2} \geq \Gamma$ (SINR target), which for example in a Gaussian channel is $N_c^* = \lfloor \frac{1}{\mathcal{C}} \log_2(1 + \frac{P_c}{P_f/I_0+\sigma^2}) \rfloor$.

It is less clear if there is such a cutoff value N_o^* in open access, because the received SINR of each cellular user in the macrocell is not constant, due to the random interference from the cellular users supported at the femtocell. The simulation results show that such a cutoff value N_o^* occurs under practical network configurations, which is essentially due to two particular aspects of open access. First, the femtocell predictably allocates a large portion of OTA resources to the home user. Therefore the femto-to-macro interference is still a constant value for a large portion of time. Second, the cellular users served by the femtocell must be very close to the femtocell according to the handover criteria, which greatly reduces the randomness of their locations. As a result, their interference to the macrocell is also nearly deterministic. The numerical

relation between N_c^* and N_o^* is discussed later in Remark 3.

In femtocell open access, events $\{A_L, L = 0, 1, 2, \ldots, K\}$ can occur. From Assumption 3, femtocell will pick the strongest interferers sequentially, so

$$\mathbb{P}(A_L) = \begin{cases} \mathbb{P}(\bigcap_{j=0}^{L-1} B_j, \overline{B}_L) & L < K \\ \mathbb{P}(\bigcap_{j=0}^{K-1} B_j) & L = K \end{cases} \tag{2.10}$$

where for $0 \leq j \leq K$, event $B_j = \{\frac{P_f}{P_c I_{(N-j)} + \sigma^2} < \Gamma_{f,j}\}$ and its complementary event is denoted as $\overline{B}_j$.

Lemma 2.4.2. *In TDMA or OFDMA, the ergodic rate of the home user and sum throughput of the cellular users in open access are given by*

$$\mathcal{C}_0 = \sum_{L=0}^{K} \min(\mathcal{C}, \lambda_L \mathcal{C}_b) p_{f,L} \tag{2.11}$$

$$\mathcal{C}_{sum} = N\mathcal{C}p_{c,0} + \sum_{L=1}^{K} \{(N-L)\mathcal{C}p_{c,L} + L\min(\mathcal{C}, \mu_L \mathcal{C}_b) p_{h,L}\} \tag{2.12}$$

where $p_{f,L}$,$p_{h,L}$ and $p_{c,L}$ are success probabilities of the home user, the supported cellular users at the femtocell and the remaining cellular users at the macrocell

respectively, which are given by

$$p_{f,L} = \begin{cases} \mathbb{P}(A_L) & L < K \\ \frac{1}{N-K} \sum_{j=1}^{N-K} \mathbb{P}\left(\frac{P_f}{P_c I_{(j)} + \sigma^2} \geq \Gamma_{f,K}, A_K \right) & L = K \end{cases} \tag{2.13}$$

$$p_{h,L} = \frac{1}{N-L} \sum_{j=1}^{N-L} \mathbb{P}\left(\frac{P_f}{P_c I_{(j)} + \sigma^2} \geq \Gamma_{h,L}, A_L \right) \tag{2.14}$$

$$\begin{aligned} p_{c,L} =& \lambda_L \mathbb{P}\left(\frac{P_c}{P_f / I_0 + \sigma^2} \geq \Gamma_{c,L} \right) \mathbb{P}(A_L) \\ &+ \mu_L \sum_{j=N-L+1}^{N} \mathbb{P}\left(\frac{P_c}{P_f / I_{(j)} + \sigma^2} \geq \Gamma_{c,L}, A_L \right) \end{aligned} \tag{2.15}$$

Proof. Denote S_f as the event that the home user succeeds in its communication process. When $L < K$, we have

$$p_{f,L} = \mathbb{P}(S_f, A_L) = \mathbb{P}(S_f | A_L) \mathbb{P}(A_L) = \mathbb{P}(A_L) \tag{2.16}$$

When the femtocell serves only L ($L < K$) cellular users, it implies the home user experiences no outage at this point based on Assumption 3. Therefore $\mathbb{P}(S_f | A_L) = 1$ and the last equality holds. When $L = K$, the remaining $N - K$ cellular users in the macrocell, which correspond to $\{I_{(1)}, I_{(2)}, \ldots, I_{(N-K)}\}$, can possibly cause outage to the home user. Since they are fairly scheduled, they are equally likely interfering the home user with probability $\frac{1}{N-K}$. So in the event of A_K, the success probability of the home user is

$$p_{f,K} = \sum_{j=1}^{N-K} \frac{1}{N-K} \mathbb{P}\left(\frac{P_f}{P_c I_{(j)} + \sigma^2} \geq \Gamma_{f,K}, A_K \right) \tag{2.17}$$

Similar arguments hold for $p_{h,L}$ and $p_{c,L}$. □

In open access, due to the random macro-to-femto and femto-to-macro interference, the cellular users' *sum throughput* is strictly between 0 and $N\mathcal{C}$, which are two possible *sum throughput* in closed access. Therefore, the network operator's choice between open vs. closed access is fairly clear.

Remark 2. *According to the value of N_c^*, the network operator prefers closed access when $N \leq N_c^*$, while embracing open access when $N > N_c^*$.*

The reason why open access reduces the *sum throughput* when $N \leq N_c^*$ is explained as follows. The femto-to-macro interference is P_f/I_0 in closed access for all time slots, which in open access after handover will increase to (due to Assumption 2) $P_f/I_{(i)}$ in the time slot of $U_{(i)}$, the cellular user served by the femtocell. The increased femto-to-macro interference from the handed over cellular users indeed bottlenecks the performance of open access by reducing *sum throughput*.

Remark 3. *When the amount of cellular users in the macrocell is over N_c^*, the femto-to-macro interference in closed access causes their* sum throughput *to be zero, which should also be true in open access due to the increased femto-to-macro interference. Considering the at most K cellular users served by the femtocell, the cutoff value N_o^* should be given by $N_o^* \leq N_c^* + K$.*

In the following, we focus on a special case of $K = 1$. Such a case is important because femtocell owners can be reasonably expected as selfish users with their infrastructure.

Theorem 2.4.3. *In TDMA or OFDMA, when the femtocell is set to serve at most one cellular user, namely $K = 1$, the ergodic rate of home user and the sum throughput of cellular users in open access are given by*

$$\begin{aligned}\mathcal{C}_0 =& \min(\mathcal{C}, \lambda_0 \mathcal{C}_b) F_I^N(\frac{P_f}{P_c \Gamma_{f,0}} - \frac{\sigma^2}{P_c}) + \min(\mathcal{C}, \lambda_1 \mathcal{C}_b) p_{f,1} \qquad (2.18)\\ \mathcal{C}_{sum} =& N\mathcal{C}\mathbb{P}\left(\frac{P_c}{P_f/I_0 + \sigma^2} \geq \Gamma_{c,0}\right) F_I^N(\frac{P_f}{P_c \Gamma_{f,0}} - \frac{\sigma^2}{P_c})\\ &+ \mathcal{C}(N-1) p_{c,1} + \min(\mathcal{C}, \mu_1 \mathcal{C}_b) p_{h,1} \qquad (2.19)\end{aligned}$$

Where $p_{f,1}$, $p_{c,1}$ and $p_{h,1}$ are given by

$$\begin{aligned}p_{f,1} =& \frac{N}{N-1} F_I(\frac{P_f}{P_c \Gamma_{f,1}} - \frac{\sigma^2}{P_c}) \left(1 - F_I^{N-1}(\frac{P_f}{P_c \Gamma_{f,0}} - \frac{\sigma^2}{P_c})\right)\\ p_{c,1} =& \lambda_1 \mathbb{P}\left(\frac{P_c}{P_f/I_0 + \sigma^2} \geq \Gamma_{c,1}\right)\\ &+ \mu_1 \left[1 - \max\left(F_I^N(\frac{P_f}{P_c \Gamma_{f,0}} - \frac{\sigma^2}{P_c}), F_I^N(\frac{P_f \Gamma_{c,1}}{P_c - \Gamma_{c,1}\sigma^2})\right)\right]\\ p_{h,1} =& \frac{N}{N-1} F_I(\frac{P_f}{P_c \Gamma_{h,1}} - \frac{\sigma^2}{P_c}) \left(1 - F_I^{N-1}(\frac{P_f}{P_c \Gamma_{f,0}} - \frac{\sigma^2}{P_c})\right)\end{aligned}$$

Proof. See Appendix 2.8.2 □

Note that the SINR target of a femtocell user is a non-increasing function of its allocated time fraction. For example, in a Gaussian Channel, a femtocell user U_i has a SINR target $\Gamma = 2^{\min(\mathcal{C}, \lambda \mathcal{C}_b)/\lambda} - 1 = 2^{\min(\mathcal{C}/\lambda, \mathcal{C}_b)} - 1$ as λ is its time fraction. Thus, the observation below follows.

Remark 4. *From Theorem 2.4.3, it is seen that the* ergodic rate *of the home user in open access is an increasing function of λ_1: As stated above $\Gamma_{f,1}$ dose*

not increase when λ_1 *gets larger, then both* $F_I(\frac{P_f}{P_c\Gamma_{f,1}} - \frac{\sigma^2}{P_c})$ *and* $\min(\mathcal{C}, \lambda_1\mathcal{C}_b)$ *are non-decreasing functions w.r.t.* λ_1.

The remark above implies that with a large enough value of λ_1, the home user's *ergodic rate* can possibly be higher than that in closed access. However, the following corollary shows that such a rate gain in open access is not possible in the regime of very large cellular user density.

Corollary 2.4.4. *If the values of* λ_1 *is independent of* N*, then as the number of cellular user goes to arbitrarily large, that is* $N \to \infty$*, the ergodic rate of home user in TDMA becomes*

$$\mathcal{C}_0 = \begin{cases} \min(\mathcal{C}, \lambda_0\mathcal{C}_b)F_I(\frac{P_f}{P_c\Gamma_{f,0}} - \frac{\sigma^2}{P_c}) & \textit{Closed Access} \\ \min(\mathcal{C}, \lambda_1\mathcal{C}_b)F_I(\frac{P_f}{P_c\Gamma_{f,1}} - \frac{\sigma^2}{P_c}) & \textit{Open Access} \end{cases} \tag{2.20}$$

Remark 5. *Since* $\lambda_1 \leq \lambda_0 = 1$, $\Gamma_{f,1}$ *is greater than* $\Gamma_{f,0}$*. Therefore, as shown in Corollary 2.4.4, with infinitely large user density, open access is inferior to closed access in terms of home user's rate.*

Numerical Simulations show that open access provides a very marginal rate gain to the home user in high user density (e.g. on the order of hundred users per macrocell). This observation, along with Corollary 2.4.4, indicates that open access is not a suitable choice in densely populated scenarios. The reason is explained as follows. When the number of cellular users increases, the amount of time occupied by each interferer decreases. Thus, in high cellular user density, handing over a small group of interferers (Corollary 2.4.4 is derived in the case of $K = 1$, but the argument can be extended) lowers

the macro-to-femto interference merely for a small portion of time, i.e. very short time length originally occupied by them. The home user's signal quality is still inhibited by the residual interference from the remaining cellular users. Thus in high user density, the femtocell will be reluctant to admit the interferers even if they cause outage. Note that this conclusion is possibly contingent on the assumption of no coordination between femtocell and macrocell BS. Our conjecture is that open access with inter-BS coordination will be the appropriate solution in high user density.

2.5 Capacity Contours in Non-Orthogonal Multiple Access Scheme

3G CDMA networks have been launched worldwide in recent years and will be in wide service for at least a decade. This necessitates research and standardization for incorporating femtocells in CDMA cellular networks [73, 86, 87, 159]. Even if both TDMA and CDMA are part of the medium access (e.g. HSPA in 3GPP and EVDO in 3GPP2), we restrict our attention to the CDMA aspect here, and this analysis would thus be valid per time or frequency slot. We show that in CDMA the interests of the femtocell owner and the network operator are compatible: Open access is the appropriate approach for both two parties.

In CDMA, suppose L cellular users are served by the femtocell, and

the received SIRs at the two BSs are

$$\begin{cases} \frac{P_f}{LP_f+P_c\sum_{j=1}^{N-L} I_{(j)}+\sigma^2} & \text{SINR at the femtocell} \\ \frac{P_c}{P_f/I_0+\sum_{j=N-L+1}^{N} P_f/I_{(j)}+(N-L-1)P_c+\sigma^2} & \text{SINR at macro BS} \end{cases} \tag{2.21}$$

To be consistent with previous analysis in TDMA, we use the same notations of users' target SIRs, but note that their values change as the rate-SINR mapping function in CDMA is different due to spreading.

Theorem 2.5.1. *In CDMA, the ergodic rate of the home user and the sum throughput of cellular users in femtocell closed access are given by*

$$\mathcal{C}_0 = \min(\mathcal{C}, \lambda_0 \mathcal{C}_b) G_I(N, \frac{P_f}{P_c \Gamma_{f,0}} - \frac{\sigma^2}{P_c}) \tag{2.22}$$

$$\mathcal{C}_{sum} = N\mathcal{C}\mathbb{P}\left(\frac{P_c}{P_f/I_0 + (N-1)P_c + \sigma^2} \geq \Gamma_{c,0}\right) \tag{2.23}$$

Proof. In closed access, no cellular user is served by the femtocell, meaning that the value of L in equation (2.21) is zero. Thus, the success probabilities of the home user and the cellular users are given by

$$\begin{aligned} p_f &= \mathbb{P}\left(\sum_{j=1}^{N} I_j \leq \frac{P_f}{P_c\Gamma_{f,0}} - \frac{\sigma^2}{P_c}\right) = G_I\left(N, \frac{P_f}{P_c\Gamma_{f,0}} - \frac{\sigma^2}{P_c}\right) \\ p_c &= \mathbb{P}\left(\frac{P_c}{P_f/I_0 + (N-1)P_c + \sigma^2} \geq \Gamma_{c,0}\right) \end{aligned} \tag{2.24}$$

Then the results of $\mathcal{C}_0$ and $\mathcal{C}_{sum}$ follow. □

Similar to TDMA or OFDMA, there exist cutoff user loadings N_c^* and N_o^* for *sum throughput* in CDMA as well. For example, in a Gaussian channel, the value N_c^* is governed by

$$\frac{2^{\mathcal{C}} - 1}{G} = \frac{P_c}{P_f/I_0 + (N_c^* - 1)P_c + \sigma^2} \tag{2.25}$$

In femtocell open access, the mathematical expression of $\{A_L, L = 0, 1, 2, \ldots, K\}$ is given by

$$\mathbb{P}(A_L) = \begin{cases} \mathbb{P}(\bigcap_{j=0}^{L-1} B_j, \overline{B}_L) & L < K \\ \mathbb{P}(\bigcap_{j=0}^{K-1} B_j) & L = K \end{cases} \tag{2.26}$$

where for $0 \leq j \leq K$, event B_j is defined as

$$B_j = \left\{ \frac{P_f}{jP_f + P_c \sum_{m=1}^{N-j} I_{(m)} + \sigma^2} < \Gamma_{f,j} \right\} = \left\{ \sum_{m=1}^{N-j} I_{(m)} > \frac{P_f}{P_c \Gamma_{f,j}} - \frac{\sigma^2 + jP_f}{P_c} \right\} \tag{2.27}$$

and its complementary event is denoted as $\overline{B}_j$.

The general form of capacity contours in open access in CDMA are the same as those in Lemma 2.4.2, however in which the success probabilities are different.

Lemma 2.5.2. *In CDMA, the success probabilities of the home user, the supported cellular users at the femtocell and the remaining cellular users at the macrocell are given by*

$$p_{f,L} = \begin{cases} \mathbb{P}(A_L) & L < K \\ \mathbb{P}\left(\frac{P_f}{P_c \sum_{m=1}^{N-K} I_{(m)} + KP_f + \sigma^2} \geq \Gamma_{f,K}, A_K \right) & L = K \end{cases} \tag{2.28}$$

$$p_{h,L} = \mathbb{P}\left(\frac{P_f}{P_c \sum_{m=1}^{N-L} I_{(m)} + LP_f + \sigma^2} \geq \Gamma_{h,L}, A_L \right) \tag{2.29}$$

$$p_{c,L} = \mathbb{P}\left(\frac{P_c}{X_L + \sigma^2} \geq \Gamma_{c,L}, A_L \right) \tag{2.30}$$

where $X_L = (N - L - 1)P_c + P_f/I_0 + \sum_{m=N-L+1}^{N} P_f/I_{(m)}$.

Proof. The proof is very similar to Lemma 2.4.2, so is omitted. □

Based on Lemma 2.5.2, we derive two helpful lower bounds in the following theorems.

Theorem 2.5.3. *In CDMA, the home user's ergodic rate in open access is*

$$\mathcal{C}_0 = \min(\mathcal{C}, \lambda_0 \mathcal{C}_b) G_I(N, \frac{P_f}{P_c \Gamma_{f,0}} - \frac{\sigma^2}{P_c}) + \sum_{L=1}^{K} \min(\mathcal{C}, \lambda_L \mathcal{C}_b) p_{f,L} \tag{2.31}$$

a lower bound on $p_{f,L}$ is given by

$$p_{f,L} \geq \left[1 - L\binom{N}{L} B\left(F_I(x); N - L + 1, L\right)\right] G_I\left(N - L, y\right) \tag{2.32}$$

Where $x = \frac{P_f}{P_c \Gamma_{f,L-1}} - \frac{\sigma^2}{P_c}$, $y = \frac{P_f(1-\Gamma_{f,L}) - \sigma^2 \Gamma_{f,L}}{P_c \Gamma_{f,L}}$ and the function $B(s; a, b)$ is the incomplete beta function

$$B(s; a, b) = \int_0^s t^{a-1}(1-t)^{b-1} dt \tag{2.33}$$

Proof. See Appendix 2.8.3. □

Remark 6. *Theorem 2.5.3 shows that in CDMA, open access has strictly better performance than closed access in terms of the home user's rate, irrespective of the femtocell resource allocation after handover.*

In CDMA, interference is additive. So handing over a small group of strongest interferers always means a significant reduction in macro-to-femto interference and consequently an improvement in the home user's rate. On the contrary, interference is time shared in TDMA. Thus handing over a small group of interferers for just part of the time does not guarantee an appreciable reduction of cross-tier interference.

Theorem 2.5.4. *In CDMA, when the femtocell is set to serve one cellular user at most, namely $K = 1$, the sum throughput of cellular users in open access is given by*

$$\begin{aligned}\mathcal{C}_{sum} =&(N-1)\mathcal{C}p_{c,1} + \min(\mathcal{C}, \mu_1\mathcal{C}_b)p_{h,1} \\ &+ N\mathcal{C}\mathbb{P}(\frac{P_c}{P_f/I_0 + (N-1)P_c + \sigma^2} \geq \Gamma_{c,0})G_I\left(N, x\right) \end{aligned} \tag{2.34}$$

where lower bounds of $p_{h,1}$ and $p_{c,1}$ are given by

$$p_{h,1} \geq \left(1 - F_I^N(x)\right) G_I\left(N-1, y\right) \tag{2.35}$$

$$p_{c,1} \geq 1 - F_I^N\left(z - \frac{\sigma^2}{P_c}\right) \tag{2.36}$$

where x and y are given by

$$\begin{aligned} x &= \frac{P_f}{P_c\Gamma_{f,0}} - \frac{\sigma^2}{P_c} \\ y &= \frac{P_f(1-\Gamma_{h,1}) - \sigma^2\Gamma_{h,1}}{P_c\Gamma_{h,1}} \\ z &= \max\left(\frac{P_f\Gamma_{c,1}}{P_c - (N-2)P_c\Gamma_{c,1} - P_f\Gamma_{c,1}/I_0}, \frac{P_f}{P_c\Gamma_{f,0}}\right) \end{aligned}$$

Proof. we first deploy the same technique as in the proof of theorem 2.5.3 in deriving the lower bound of $p_{h,1}$. According to equation (2.29), we have

$$\begin{aligned} p_{h,1} &= \mathbb{P}\left(\sum_{m=1}^{N} I_m \geq x, \sum_{m=1}^{N-1} I_{(m)} \leq y\right) \\ &\geq \mathbb{P}\left(I_{(N)} > x\right) G_I\left(N-1, y\right) \\ &= \left(1 - F_I^N(x)\right) G_I\left(N-1, y\right) \end{aligned} \tag{2.37}$$

A similar proof applies to the lower bound of $p_{c,1}$ □

After the femtocell serves L cellular users, the femto-to-macro interference in CDMA is $(N-L)P_c + P_f/I_0 + \sum_{j=N-L+1}^{N} P_f/I_{(j)}$, smaller than $(N-1)P_c + P_f/I_0$ in closed access with high probability (according to Definition 1 of ordered *interference factors*). However, due to the resulting variance, the femto-to-macro interference in open access can exceed a certain threshold with a positive possibility, consequently causing outage to cellular users remaining in the macrocell. Open access thus causes a minor loss of *sum throughput* in CDMA, as shown in numerical simulations.

Remark 7. *In CDMA, open access is also the preferred choice for the network operator, since it is almost as good as (strictly better than) closed access in the regime of small (large) N.*

2.6 Numerical Results and Conclusion

Notations and system parameters are given in Table 2.1. Note that in our plots, the home user's *ergodic rate* and cellular users' *sum throughput* are normalized by $\mathcal{C}$.

2.6.1 TDMA or OFDMA Access

Cellular User Density. Fig. 2.1 and 2.2 depict the home user's *ergodic rate* and cellular users' *sum throughput* w.r.t. cellular user density. For the purpose of fair comparison, the values of μ_L and λ_L in these two plots are set as $\frac{1}{N}$ and $1-\frac{L}{N}$ respectively.In low user density ($N \leq N_c^* = 49$), open access provides an appreciable rate gain to the home user, however which also

Table 2.1: Notations and Parameters

Symbol	Description	Sim. Value
R	macrocell radius	300 meters
D	Distance between macro & femto BSs	150 meters
d	Distance between home user and femto BS	5 meters
α, β	Path loss exponents	$4, 2$
P_f/σ^2	Femtocell BS received SNR	20 dB
P_c/σ^2	Macrocell BS received SNR	20 dB
G	Spreading factor (for CDMA)	64
$\mathcal{C}$	User rate requirement	0.5 bps/Hz
$\mathcal{C}_b$	Femtocell backhaul capacity	2 bps/Hz
λ_L	The home user's portion of femtocell resources with L handed over cellular users	N/A
μ_L	Portion of femtocell resources allocated to each of the L handed over cellular users	$\frac{1-\lambda_L}{L}$
$\Gamma_{f,L}$	home user's SINR target in TDMA	$2^{\min(\frac{\mathcal{C}}{\lambda_L}, \mathcal{C}_b)} - 1$
	home user's SINR target in CDMA	$\frac{1}{G}(2^{\min(\mathcal{C}, \lambda_L \mathcal{C}_b)} - 1)$
$\Gamma_{h,L}$	SINR target of cellular user supported in the femtocell in TDMA	$2^{\min(\frac{\mathcal{C}}{\mu_L}, \mathcal{C}_b)} - 1$
	SINR target of cellular user supported in the femtocell in CDMA	$\frac{1}{G}(2^{\min(\mathcal{C}, \mu_L \mathcal{C}_b)} - 1)$
$\Gamma_{c,L}$	SINR target of cellular user remaining in the macrocell in TDMA	$2^{(N-L)\mathcal{C}} - 1$
	SINR target of cellular user remaining in the macrocell in CMDA	$\frac{1}{G}(2^{\mathcal{C}} - 1)$

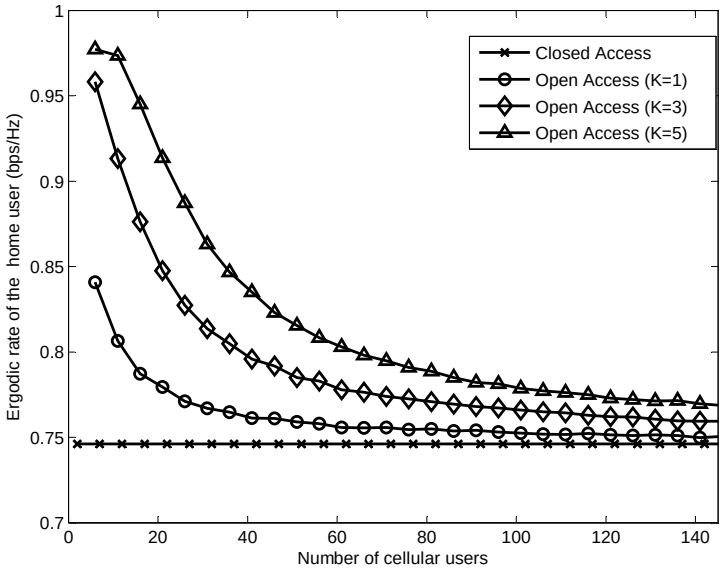

Figure 2.1: The home user's *ergodic rate* versus cellular user density in TDMA. We have $\lambda_L = 1 - \frac{L}{N}$ and $\mu_L = \frac{1}{N}$ for fair comparison, $0 \leq L \leq K$.

causes a noticeable decrease in cellular users' *sum throughput*. It is seen that the rate gain and loss are about the same in terms of percentage: For $K = 3$ case at $N = 20$, as an example, the rate gain of the home user is about 15%, and the rate loss of cellular users is almost 20%. Indeed, the choices of the two parties in low cellular user density are incompatible.

As predicted previously (below Remark 1), there is a cutoff user loading N_o^* in open access. Indeed, further simulations show as long as $\lambda \gtrsim 30\%$, N_o^* equals $N_c^* + K$. In other words, single open access femtocell expands the macrocell network capacity by K. Therefore when $N_c^* \leq N \leq N_o^*$, open access is appropriate for both parties, especially to the network operator by offloading traffic from overloaded macrocell.

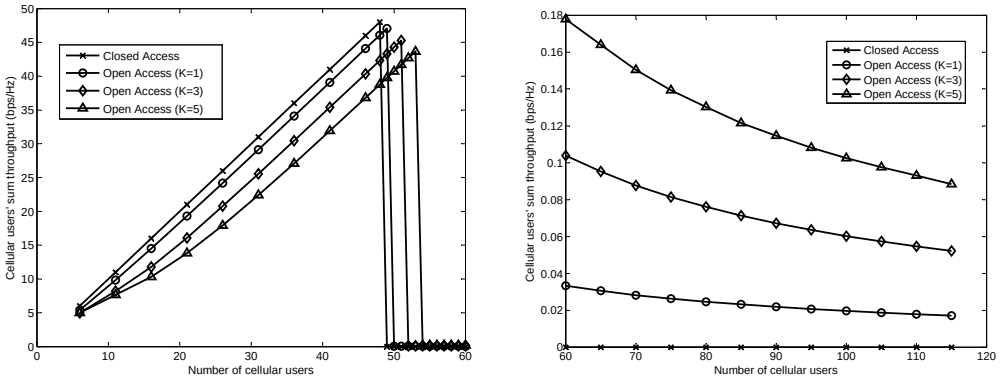

(a) Regime of low cellular user density (b) Regime of high cellular user density

Figure 2.2: Cellular users' sum throughput versus cellular user density in TDMA. We have $\lambda_L = 1 - \frac{L}{N}$ and $\mu_L = \frac{1}{N}$ for fair comparison, $0 \leq L \leq K$.

In high user density ($N \geq N_o^* = 55$), open access provides only a very small rate gain to the home user. Its rate gain to the cellular user is also marginal because the macro BS remains overloaded even after handover K users to the femtocell. Note that we assume that the overloaded macro BS does not "turn off" any cellular users even when the outage becomes high. Obviously admission control could be used to improve the sum rate, so this can be considered a worst case scenario for closed access since the sum throughput tends to zero. Even with this assumption favoring open access – which maintains a low but strictly positive sum throughput due to the handoffs – not much gain is observed for open access. If the overloaded macrocell BS randomly blocks users to avoid congestion, the curves in Fig. 2.2 would flatten beyond the cut-off, which implies lower sum throughput to the cellular users in open access. We summarize our observations in Table 2.2.

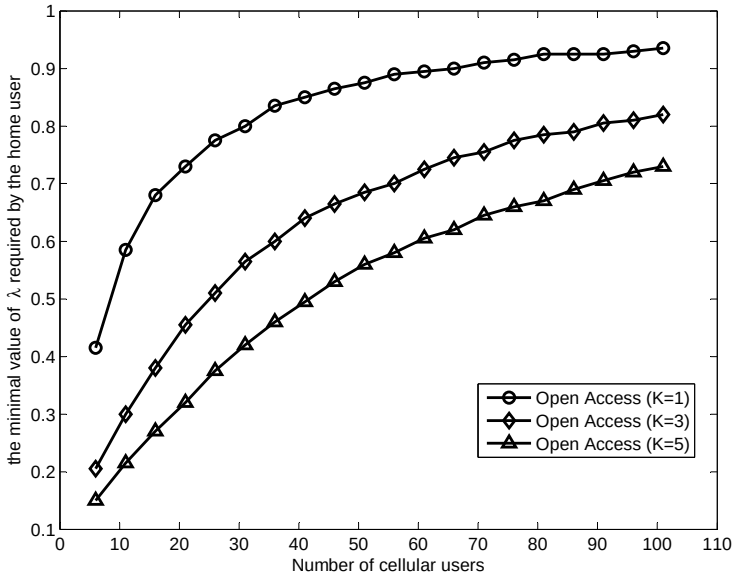

Figure 2.3: The value of λ^*, i.e. the minimal proportion of femtocell resources required by the home user in TDMA open access, versus cellular user density.

Femtocell Resource Allocation. In this subsection, we identify the appropriate fraction of femtocell resources allocated to the home user in open access. Note that in this subsection, λ_L is assumed to be the same for all L and we simply denote it as λ here. As stated in Remark 4, the home user's *ergodic rate* is an increasing function of λ. Therefore, to ensure the home user's *ergodic rate* is not reduced after the handover, the value of λ must be above some threshold λ^*. It is shown in Fig. 2.3 that λ^* is an increasing function of cellular user density N. In higher cellular user density N, the reduction of macro-to-femto interference is diminishing (as stated below Remark 5), the home user will require more time resources, and therefore larger value of λ^*, to lower its SINR target and consequently be more tolerant to the interference. Hence

the femtocell resource allocation in TDMA or OFDMA should be adaptive to cellular user density, which is potentially difficult due to no coordination between the femtocell and the macrocell BS. Otherwise, the performance of open access is very likely to degrade sharply, because the home user's *ergodic rate* is sensitive to the value of λ, as shown in Fig. 2.4.

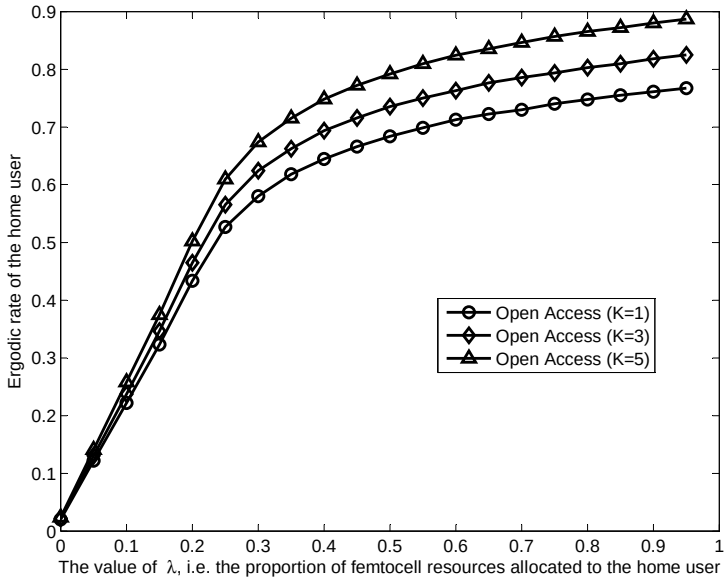

Figure 2.4: The home user's *ergodic rate* versus the portion of femtocell resources allocated to him in TDMA, i.e. the value of λ in open access. The cellular user density $N = 30$.

Summary for TDMA/OFDMA Access. In orthogonal multiple access, the choices of the two parties are highly dependent on the cellular user density, with both preferring open access in medium density, closed access in high density, and they are in disagreement at low density. Therefore, our results suggest that when deploying OFDMA, femtocell access control should

be adaptive based on the estimated cellular user density. Note that this conclusion is possibly contingent on our analysis assumptions, among which the following two may be the most critical: 1) the assumption of no inter-BS coordination both among and cross the two tiers. Possible coordination schemes include time/spectrum splitting between femtocells and macrocells [34]; 2) the assumption on handoff policy. More sophisticated handoff policy may further improve the performance of open access [38]. Investigations on the impact of these assumptions are important related topics for future research.

Table 2.2: Choices of Two Parties w.r.t. Cellular User Density

	TDMA or OFDMA		CDMA	
Cellular Use density	Femtocell Owner	Network Operator	Femtocell Owner	Network Operator
Low ($N < N_c^*$)	Open Access	Closed Access	Open Access	Indifferent
Medium ($N_c^* \leq N \leq N_o^*$)	Open Access	Open Access	Open Access	Open Access
High ($N > N_o^*$)	Closed Access	Indifferent	Open Access	Indifferent
Choices	Highly Dependent on Cellular User Density		Open Access	

2.6.2 CDMA Access

Cellular User Density. Fig. 2.5 and 2.6 present the home user's *ergodic rate* and cellular users' *sum throughput* in CDMA. To be consistent with TDMA/OFDMA case, the values of μ_L and λ_L in these two plots are also set as $\frac{1}{N}$ and $1 - \frac{L}{N}$ respectively. Theorem 2.5.3 states that the home

user will always experience a rate gain in open access in CDMA, which is over 300% (5 dB) for a vast range of cellular user density, as shown in Fig. 2.5. In the regime of small N ($N \leq N_c^* = 155$), open access in CDMA only leads to a negligible loss of cellular users' *sum throughput*, as shown in Fig. 2.6. Open access in CDMA will strictly improve cellular users' *sum throughput* when $N \geq N_c^* = 155$, for the same reason in TDMA or OFDMA. Therefore, in CDMA open access is an appropriate approach for both parties in the whole range of cellular user density.

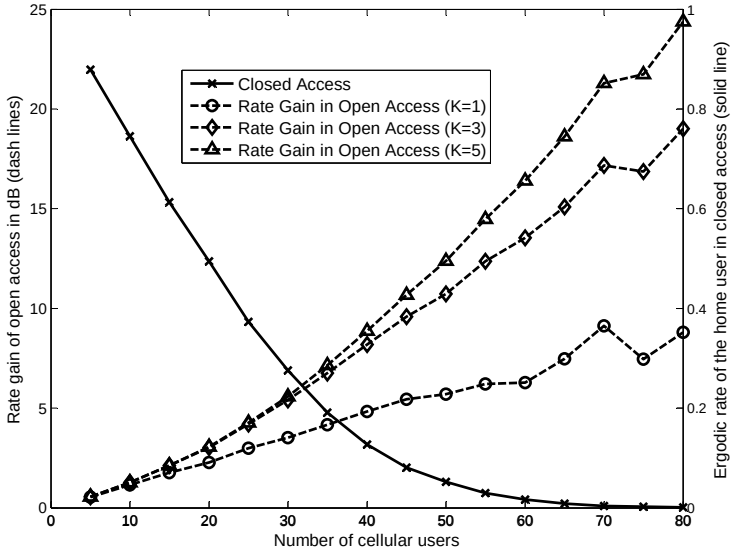

Figure 2.5: The home user's rate gains in dB (dash lines) in CDMA open access compared with closed access (solid line). For the purpose of comparison with TDMA/OFDMA case, we have $\lambda_L = 1 - \frac{L}{N}$ and $\mu_L = \frac{1}{N}$, $0 \leq L \leq K$.

Femtocell Resource Allocation. As stated in Theorem 2.5.3 and Remark 6, open access improves the home user's rate, no matter how the femtocell backhaul is shared among users and what the cellular user density

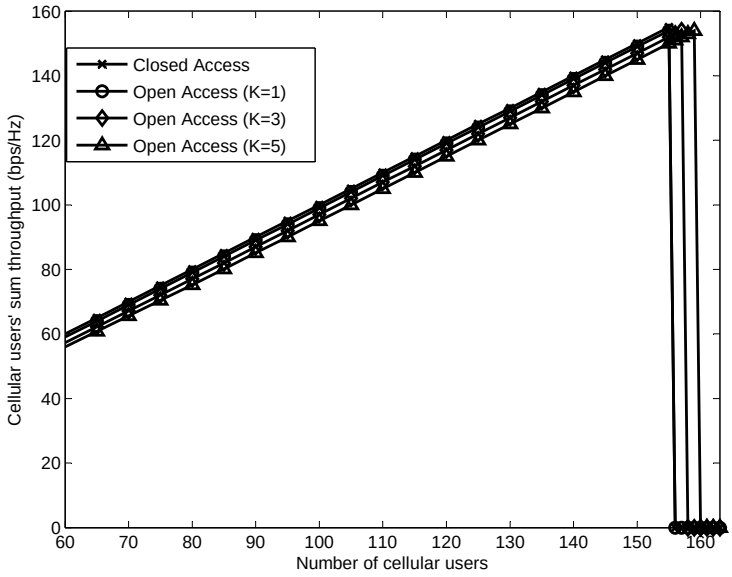

Figure 2.6: Cellular users' sum throughput versus cellular user density in TDMA. For the purpose of comparison with TDMA/OFDMA case, we have $\lambda_L = 1 - \frac{L}{N}$ and $\mu_L = \frac{1}{N}$, $0 \leq L \leq K$.

is. Indeed, when $\lambda \mathcal{C}_b \geq \mathcal{C}$, the home user's rate is not affected by the femtocell resource allocation. This observation provides insight into the optimal value of K, which is the maximum number of additional cellular users the femtocell can support. Compared with smaller values of K, the choice of $K = \max\{K : \lambda_K \geq \frac{\mathcal{C}}{\mathcal{C}_b}\}$ is preferred by the home user, which can significantly reduce the interference while still not affecting its available resources. In short, the optimal value of K should be not less than $\max\{K : \lambda_K \geq \frac{\mathcal{C}}{\mathcal{C}_b}\}$.

Summary for CDMA Access. Open access in CDMA benefits both parties in almost the whole range of cellular user density. Moreover, these appreciable benefits do not require the femtocell to deploy adaptive resource

allocation. Therefore, open access is conclusively preferred in 3G CDMA networks.

2.6.3 Discussion on Shadowing

We investigate the impact of large-scale random channel effects in this subsection by incorporating lognormal shadowing with standard deviation $\sigma_s = 10$ dB in the channel model. Simulation results show that shadowing affects the performance of open and closed access as one would expect, but it does not change the main conclusions about the optimal access policy. Consider the home user's *ergodic rate* in TDMA for instance. By comparing Fig. 2.1 (path loss only) and Fig. 2.7 (path loss and shadowing), it is seen that shadowing lowers the rates by approximately $5\% \sim 10\%$, but the main trends of the curves are preserved: open access in TDMA still has a diminishing rate gain for the home user as cellular user density becomes large. Therefore, in the presence of shadowing, open access in TDMA is preferred by the femtocell owner in low user density, the same conclusion as in the path loss only case. Further simulation results (not included due to space limitations) confirm that our main conclusions listed in Table 2.2 are unchanged in view of shadowing.

2.7 State-of-the-Art

After our work on this topic, femtocell access tradeoffs are further investigated in [19, 40, 51, 54, 82, 103, 104, 170] from different perspectives and under more sophisticated models. [51] compares open vs. closed access from

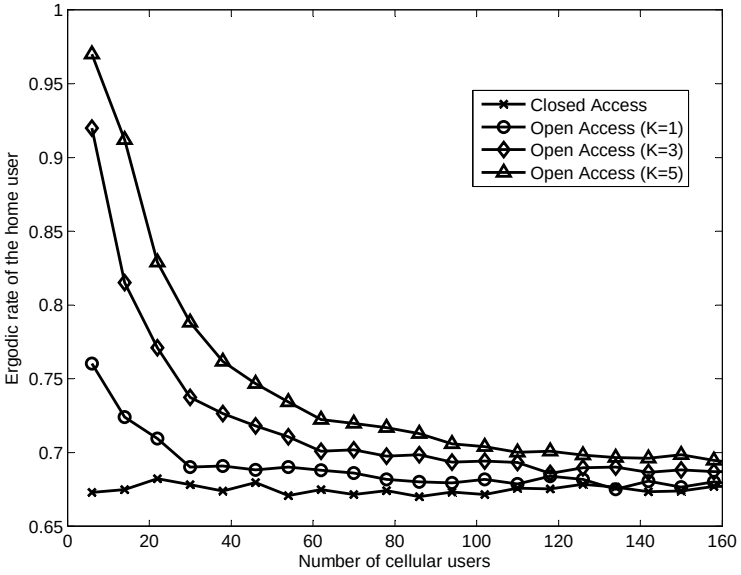

Figure 2.7: The home user's *ergodic rate* in TDMA by incorporating the shadowing effect into the channel model. We assume a lognormal shadowing with standard deviation $\sigma_s = 10$ dB. For the purpose of comparison with Fig. 2.1 (which includes path loss attenuation only), we have $\lambda_L = 1 - \frac{L}{N}$ and $\mu_L = \frac{1}{N}$, $0 \leq L \leq K$.

the perspective of diversity and multiplexing tradeoff. As the interfering mobile users are not always in the full buffer state, [19] uses Markov chains to model their transceiver activities and investigates the interference in femtocell open vs. closed access. Femtocell access control is also jointly considered with spectrum allocation for throughput optimization [40, 54]. Many other works focus on studying the best access approach in the downlink [82, 103, 104, 170]. They use the spatial Poisson Point Process to model the ad-hoc femtocell locations, and then quantify the SINRs of home users and macro users in open, close and hybrid femtocell accesses. They show that the interests of network

operators and femtocell owners are incompatible in the downlink: network operators prefer open access while femtocell owners perfer closed access. This is not surprising, because femtocell owners are not victims in the downlink (different from the uplink case) and thus do not have much incentive for open access. Optimizations on hybrid access to improve network capacity under femtocell QoS constraints are also considered in these works.

As open access does not gain much incentive from home users except in CDMA uplink, many works consider various incentive mechanisms for femtocell owners to enable open access [38, 65, 113, 157, 162]. Several works consider advanced user association policies to further improve the performance of open access [38, 39].

2.8 Appendix

2.8.1 Proof of Lemma 2.3.1

Denote (x, y) as the location of a cellular user. Thus the CDF of its *interference factor* I is

$$\begin{aligned} F_I(i) &= \mathbb{P}(I \leq i) \\ &= \mathbb{P}\left((1-i^{2/\alpha})x^2 + (1-i^{2/\alpha})y^2 + 2Di^{2/\alpha}x - D^2 i^{2/\alpha} \leq 0\right) \\ &= S/(\pi R^2). \end{aligned} \tag{2.38}$$

S is the area inside the macrocell, and governed by

$$(1-i^{2/\alpha})x^2 + (1-i^{2/\alpha})y^2 + 2Di^{2/\alpha}x - D^2 i^{2/\alpha} \leq 0$$

When $i \neq 1$, the above equation defines a circle area, with center of $x_c = \frac{Di^{2/\alpha}}{|1-i^{2/\alpha}|}$ and radius of $r = \frac{i^{1/\alpha}D}{|1-i^{2/\alpha}|}$. Moreover, when $i < 1$, S is the area inside the circle, while $i > 1$, S is the area outside the circle. Therefore, according to the range of i, $F_I(i)$ can be divide into 5 segments:

1. when $0 \leq i < (\frac{R}{R+D})^\alpha$ (note that *interference factor* is a non-negative r.v., we must have $i \geq 0$), the circle is contained in macrocell ($|x_c| + |r| \leq R$). Thus $S = \pi r^2$.

2. when $(\frac{R}{R+D})^\alpha \leq i < 1$, the circle intersects with macrocell ($|x_c| + |r| \geq R$). Using the method in [164], we get:

$$S = \pi(R^2 + r^2) - (\pi - \theta + 0.5 \sin 2\theta)\, r^2 - (\pi - \phi + 0.5 \sin 2\phi)R^2$$

   where $\theta = \arccos(\frac{r^2+x_c^2-R^2}{2rx_c})$ and $\phi = \arccos(\frac{x_c^2+R^2-r^2}{2x_cR})$.

3. when $i = 1$, the area of S is a half plane ($x \leq \frac{D}{2}$) intersected with the macrocell. Thus $S = (\pi - \varphi + 0.5 \sin 2\varphi)R^2$, where $\varphi = \arccos(\frac{D}{2R})$.

4. when $1 < i \leq (\frac{R}{R-D})^\alpha$, the circle intersects with macrocell ($|x_c| + |r| \geq R$). Note that now S is the area outside the circle. Therefore

$$S = \pi R^2 - \pi(R^2 + r^2) + (\pi - \theta + 0.5 \sin 2\theta)\, r^2 + (\pi - \phi + 0.5 \sin 2\phi)R^2$$

5. when $(\frac{R}{R-D})^\alpha < i$, the circle is contained in macrocell ($|x_c| + |r| \leq R$). Similarly, $S = \pi(R^2 - r^2)$.

2.8.2 Proof of Theorem 2.4.3

As $K = 1$, there are only two events A_0 and A_1, with probabilities of

$$\mathbb{P}(A_0) = F_I^N(\frac{P_f}{P_c\Gamma_{f,0}} - \frac{\sigma^2}{P_c})$$
$$\mathbb{P}(A_1) = 1 - F_I^N(\frac{P_f}{P_c\Gamma_{f,0}} - \frac{\sigma^2}{P_c})$$

The key in the proof is the calculation of $p_{f,1}$, $p_{h,1}$ and $p_{c,1}$. Applying (2.13), we have

$$p_{f,1} = \frac{\sum_{j=1}^{N-1} \mathbb{P}\left(I_{(j)} \leq \frac{P_f}{P_c\Gamma_{f,1}} - \frac{\sigma^2}{P_c}, I_{(N)} > \frac{P_f}{P_c\Gamma_{f,0}} - \frac{\sigma^2}{P_c}\right)}{N-1}$$

Denote $\mathbb{P}(I \leq \frac{P_f}{P_c\Gamma_{f,1}} - \frac{\sigma^2}{P_c})$ as p, and $\mathbb{P}(I \leq \frac{P_f}{P_c\Gamma_{f,0}} - \frac{\sigma^2}{P_c})$ as q, then we have

$$\begin{aligned}
&\sum_{j=1}^{N-1} \mathbb{P}(I_{(j)} \leq \frac{P_f}{P_c\Gamma_{f,1}} - \frac{\sigma^2}{P_c}, I_{(N)} > \frac{P_f}{P_c\Gamma_{f,0}} - \frac{\sigma^2}{P_c}) \\
=&\sum_{j=1}^{N-1}\sum_{k=j}^{N-1}\left\{\binom{N}{k}p^k(1-p)^{N-k} - \binom{N}{k}p^k(q-p)^{N-k}\right\} \\
=&Np(1-q^{N-1})
\end{aligned}$$

Substituting back for p and q, $p_{f,1}$ is given by

$$p_{f,1} = \frac{N}{N-1}F_I(\frac{P_f}{P_c\Gamma_{f,1}} - \frac{\sigma^2}{P_c})\left(1 - F_I^{N-1}(\frac{P_f}{P_c\Gamma_{f,0}} - \frac{\sigma^2}{P_c})\right) \tag{2.39}$$

The success probability $p_{h,1}$ of handover user $U_{(N)}$ follows by applying the same technique.

In the femtocell, the home user is allocated a time fraction of λ_1, and the handed over user $U_{(N)}$ is assigned a time fraction of μ_1. Therefore, the

success probability of a cellular user in the macrocell network is

$$\begin{aligned} p_{c,1} =& \lambda_1 \mathbb{P}\left(\frac{P_c}{P_f/I_0+\sigma^2} \geq \Gamma_{c,1}\right) \\ &+ \mu_1 \mathbb{P}\left(\frac{P_c}{P_f/I_{(N)}+\sigma^2} \geq \Gamma_{c,1}, \frac{P_f}{P_c I_{(N)}+\sigma^2} < \Gamma_{f,0}\right) \\ =& \lambda_1 \mathbb{P}\left(\frac{P_c}{P_f/I_0+\sigma^2} \geq \Gamma_{c,1}\right) \\ &+ \mu_1 \left[1 - \max\left(F_I^N(\frac{P_f}{P_c\Gamma_{f,0}} - \frac{\sigma^2}{P_c}), F_I^N(\frac{P_f\Gamma_{c,1}}{P_c - \Gamma_{c,1}\sigma^2})\right)\right] \end{aligned} \tag{2.40}$$

2.8.3 The Proof of Theorem 2.5.3

As $L = 0$, we have

$$p_{f,0} = \mathbb{P}\left(\frac{P_f}{P_c\sum_{m=1}^{N} I_{(m)}+\sigma^2} \geq \Gamma_{f,0}\right) = G_I\left(N, \frac{P_f}{P_c\Gamma_{f,0}} - \frac{\sigma^2}{P_c}\right) \tag{2.41}$$

For $1 \leq L \leq K$, it is easy to check that $p_{f,L}$ has the same form, which are lower bounded as below. The constants x and y are as defined in the statement of

Theorem 2.5.3.

$$
\begin{aligned}
p_{f,L} &= \mathbb{P}(\bigcap_{j=0}^{L-1} B_j, \overline{B}_L) \\
&\overset{(a)}{\geq} \mathbb{P}\left(\bigcap_{j=0}^{L-1}\left\{\sum_{m=1}^{N-j} I_{(m)} > \frac{P_f}{P_c\Gamma_{f,j}} - \frac{\sigma^2}{P_c}\right\}, \sum_{m=1}^{N-L} I_{(m)} \leq y\right) \\
&\overset{(b)}{\geq} \mathbb{P}\left(\sum_{m=1}^{N-L+1} I_{(m)} > x, \sum_{m=1}^{N-L} I_{(m)} \leq y\right) \\
&\geq \mathbb{P}\left(I_{(N-L+1)} > x, \sum_{m=1}^{N-L} I_{(m)} \leq y\right) \\
&\overset{(c)}{\geq} \mathbb{P}\left(I_{(N-L+1)} > x\right) G_I\left(N-L, y\right) \\
&= \left[1 - L\binom{N}{L} B\left(F_I(x); N-L+1, L\right)\right] G_I\left(N-L, y\right) \qquad (2.42)
\end{aligned}
$$

The inequality (a) comes from the lower bound on the probability of B_j (see equation (2.27)). It is important to note that in CDMA $\Gamma_{f,L}$ is a non-decreasing function of λ_L. In a Gaussian channel, for example, $\Gamma_{f,L} = \left(2^{\min(\mathcal{C},\lambda_L \mathcal{C}_{sum})} - 1\right)/G$. Since λ_L does not increase as L goes larger, $\Gamma_{f,L}$ is also a non-increasing function of L. Thus the inequality (a) holds. Instead of making $\sum_{m=1}^{N-L} I_{(m)}$ smaller than a certain constant, we randomly pick $N-L$ elements from the set of $\{I_{(1)}, I_{(2)}, \ldots, I_{(N)}\}$, which are also independent of $I_{(N-L+1)}$. Therefore inequality (b) holds.

Chapter 3

Fundamentals of Overhead Signaling in Inter-cell Coordination

Inter-cell coordination is in principle an effective way of managing HCNs for interference mitigation, end-user SINR enhancement and system efficiency improvement. Common examples include coordinated multipoint (CoMP) communications, cooperative scheduling and handoffs. Many coordination techniques are shown to have large cooperative gains in theory. However, the assessment of these gains usually ignores the inherent cost of overhead sharing: the overhead (e.g. CSI and user scheduling) is shared at limited rate with quantization error and delay [123, 124]. Practical concerns on overhead lead to non-trivial gaps between real and theoretical cooperative gains. An example is downlink joint processing COMP in the 1-tier case, which ideally introduces a multi-fold throughput improvement [59, 133, 138]. However, industrial simulations and field trials show that real throughput gain is disappointing – less than 20% – and the major limiting factor is sharing CSI and other overhead among cells [17, 75, 123, 124]. Mathematically, the achievable gain is a function of overhead parameters: 1) $\mathcal{T}$, the overhead packet interarrival time (the expected value of $\mathcal{T}$ is the inverse of the expected packet rate); 2) B, the overhead packet bit size; and 3) $\mathcal{D}$, the overhead delay. It is therefore

important to evaluate cooperative gains in terms of the achievable values of these overhead signaling parameters.

3.1 Previous Models for the Overhead Parameters

The model of limited overhead bit rate, which is the product of overhead packet rate $1/\mathbb{E}[\mathcal{T}]$ and packet size B, is previously considered for wireless overhead signaling [96]. It is not considered for backhaul signaling in the traditional 1-tier macrocell case (except that overhead includes user data [131,139]), assuming macro BSs are equipped with high capacity backhaul. However, it is not always the case for BSs in HCNs. In particular, femtocells often use third-party IP based backhaul (e.g. DSL and cable modem) that is aggregated by a gateway and so has much lower rate [3, 36].

Besides average rate, the natural dynamics in overhead interarrival time $\mathcal{T}$ are often ignored. In coordination techniques where inter-cell overhead is driven or influenced by unplanned incidents (e.g. during inter-cell handoffs overhead is generated when a user crosses cell boundaries), the interarrival time $\mathcal{T}$ varies over time. However, previous works simply assume $\mathcal{T}$ as a constant value (e.g. several symbol time [165]).

Perhaps the most important piece missing from previous works is an appropriate model on overhead delay $\mathcal{D}$ in general multi-tier HCNs. In 1-tier macrocell case, the backhaul interface between neighboring BSs is modeled as nearly delay-free [58, 59, 133, 138]. This assumption may hold if macrocells are directly interconnected by high speed Ethernet [75], but is far from reality in

most network configurations [123, 124, 154]. More than likely, it is not applicable to overlaid BSs with generally lower capacities and more complicated protocols [3, 36]. For wireless signaling (e.g. to-be-defined overhead channels in LTE-A), the overhead delay is also very different from the 1-tier case due to distinct statistics of spatial interference in HCNs [14, 48, 55]. With even moderate mobility, delay in side information results in an irreducible performance bound that cannot be overcome even with much higher rate and more frequent overhead messages [98].

In summary, the appropriate models on overhead parameters in multi-tier HCNs are currently missing but of critical importance for the design and evaluation of coordination techniques. It is thus desirable to develop a general framework to quantify the feasible set of overhead parameters $(\mathcal{T}, B, \mathcal{D})$ as a function of various HCNs setups, rather than heuristically for each possible network realization.

3.2 Contributions

We first develop general models for inter-cell overhead parameters in HCNs: 1) a Gamma distribution model on overhead interarrival time $\mathcal{T}$, which contains two important and opposite special cases: *deterministic* and *Poisson* overhead arrivals; 2) queuing models on backhaul servers (e.g. switches, routers and gateways) to characterize backhaul overhead delay $\mathcal{D}$; and 3) a stochastic geometry model on HCN spatial interference to characterize wireless overhead delay $\mathcal{D}$.

From such models, we propose a novel framework *overhead quality contour* to quantify feasible overhead parameters $(\mathcal{T}, B, \mathcal{D})$ as a function of overhead channel realizations and overhead arrivals. We derive its general expressions in computable integrals for backhaul and wireless overhead signaling, which are simplified to closed-form results in two widely assumed overhead arrivals: *deterministic* and *Poisson*. We show mathematically and through numerical simulations that previous models, compared with our framework, are over-optimistic about achievable overhead rate, delay and outage probability, which explains the non-trivial gaps between their predictions and the real cooperative gains.

The *overhead quality contour* can be used for the following general purposes.

The Evaluation and Optimization of HCN Coordination. The *overhead quality contour* can be directly used for the analysis of specific HCN coordination techniques by determining: 1) the feasibility of these techniques, i.e. if their overhead requirements (e.g. overhead outage below some threshold) lie in the *overhead quality contour*; 2) if feasible, their possible overhead signaling options, i.e. achievable set of $(\mathcal{T}, B, \mathcal{D})$ in different overhead signaling methods (backhaul and/or wireless). The gains of proposed coordination techniques can then be maximized by choosing the appropriate overhead signaling option. For example, the results in this chapter is used in CoMP study in Chapter 4.

The Design of HCN Overhead Channels. During the deployment

of HCNs, the proposed framework is also useful in providing design insights on overhead channel setups to facilitate inter-cell coordination. Based on the overhead quality contour, we derive tight lower bound on backhaul servers' rate as a function of overhead signaling requirements and backhaul connection scenarios (i.e. the number of backhaul servers). Similarly, we characterize the lower bound on wireless overhead channel bandwidth. The optimal setups to achieve these lower bounds are also identified.

3.3 System Model

We consider a downlink heterogeneous cellular network consisting of K different types of base stations (e.g. macrocells, microcells, picocells, femtocells and distributed antennas). We refer to a specific type of BSs as *a tier*, and thus call the network a K-tier HCN. In a K-tier HCN, a base station BS_0 intends to coordinate with its neighbouring base station BS_n, from whom its user receives the strongest long-term average power (which means strongest interference if not coordinated). Therefore, frequent overhead messaging is required between them, to exchange cooperation-dependent parameters such as user scheduling information and/or the scheduled user's CSI. The overhead messaging is either through backhaul (termed *backhaul signaling*) or wireless overhead channels (termed *wireless signaling*).

Assumption 7. *We do not consider retransmission schemes of overhead messages due to their time sensitivity. Thus one overhead message will be outdated once a new overhead message is generated.*

Denote B as the bit size of each overhead message. In the following, we describe the models on other overhead parameters: message interarrival time $\mathcal{T}$ and delay $\mathcal{D}$.

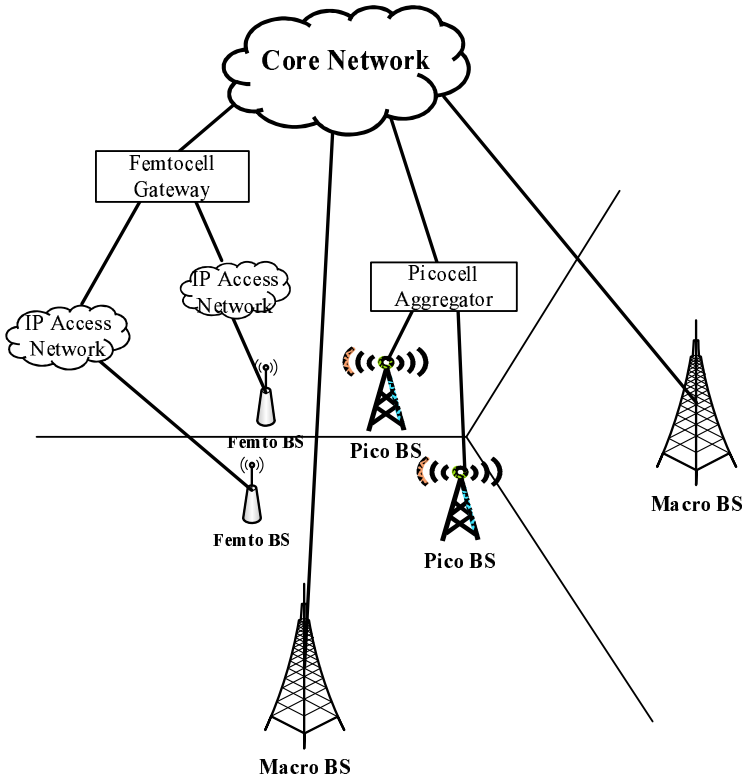

Figure 3.1: The base station locations and backhaul deployments of a 3-tier heterogeneous cellular network, comprising for example macro (tier 1), pico (tier 2) and femto (tier 3) BSs.

3.3.1 Overhead Message Interarrival Time

Assumption 8. The overhead arrival is assumed to be a stationary homogeneous arrival process with packet rate η, i.e. the packet interarrival times have the same distribution with $\mathbb{E}[\mathcal{T}] = 1/\eta$.

At its most general, we assume the interarrival time is gamma distributed with parameter M

$$\mathcal{T}^{(M)} \sim \text{Gamma}\left(M, \frac{1}{M\eta}\right). \tag{3.1}$$

For various values of M, the average interarrival time is still $\mathbb{E}\left[\mathcal{T}^{(M)}\right] = 1/\eta$. This model of $\mathcal{T}$ includes two widely used models on overhead arrivals as special cases: deterministic and Poisson arrivals.

Deterministic Overhead Arrivals. The interarrival time $\mathcal{T}$ can be a constant determined by BS_0 and BS_n based on standards or other agreements. An example is joint frequency allocation in LTE: base stations utilize certain preamble bits in each frame as their coordination message, to specify the frequency allocations for their users' data in this frame. Therefore the overhead message is generated in every 10 ms (i.e. each LTE frame) [60]. In (3.1), $M \to \infty$ gives constant interarrival time

$$\mathcal{T}^{(M)} \xrightarrow{d} \mathcal{T} = 1/\eta, \tag{3.2}$$

where $\xrightarrow{d}$ means convergence in distribution.

Poisson Overhead Arrivals. The interarrival time $\mathcal{T}$ can also be random, determined by the users or other cells rather than BS_0 and BS_n themselves. An example is user cell associations. As the users roam around, they choose their serving cells based on certain metrics including received power and congestion. Such choices will change the cell parameters (e.g. user scheduling and resource allocations) at BS_n, which means a new overhead message should

be generated and shared with BS_0. The overhead arrivals are thus random and often modelled as Poisson process with exponential interarrival time

$$\mathcal{T} \sim \exp(\eta). \tag{3.3}$$

It is known that exponential distribution is also a special case of (3.1) with $M = 1$.

These two special cases of practical interest provide insights into two opposite extremes since for a given rate, deterministic arrivals are the least random while Poisson arrivals are the most random (maximum entropy). An arbitrary overhead arrival model is therefore bounded by these two extreme cases (which also have practical significance).

3.3.2 Overhead Delay in Backhaul Signaling

When the overhead message is transmitted through the backhaul network[1], its delay generally comprises two parts: 1) processing latencies from switches, routers and gateways (generally termed *backhaul servers*) in the backhaul path; and 2) the transmission delay of the wire (e.g. fiber optic and copper wires) or wireless links (e.g. microwave). The latter kind of latency is quite small and often ignored, except that BSs are directly interconnected us-

[1]Backhaul is the intermediate link between operator's core network and base stations. Such a link can be either wired (e.g. fiber lines and copper wires) or wireless (microwave), and the backhaul is thus further categorized as wireline or wireless backhaul. It is important to clarify the fundamental differences of wireless backhaul and wireless overhead channel in the following subsection. In the former case, the overhead is transmitted to backhaul servers (e.g. routers and gateways) through microwave, and will be routed in the backhaul network. In the latter case, overhead is directly shared between BS_0 and BS_n without routing.

ing high-speed backbone without any intermediate backhaul servers [75]. For example, as the backhaul path between clustered picocells or co-located BSs contains few servers, the backhaul delay can be as low as 1 ms [2, 150, 154].

Assumption 9. We assume the backhaul servers have exponential service time, the i^{th} of which allocates service rate μ_i (bps) to overhead packets. According to Assumption 7, each backhaul server will drop overhead packet(s) in its system upon the arrival of new overhead

Note that the parameters $\{\mu_i\}$ in Assumption 9 are dependent on the scheduling policies of backhaul servers. In the following, we list a few common examples.

Example 1. (Pre-emptive Scheduling)*: In this case, servers recognize the extreme delay sensitivity of overhead packets and identify them as the highest priority traffic. Thus, overhead will be served before all other traffic in a pre-emptive way [155] and its allocated rate μ_i is indeed the total service rate μ_i^{total}.*

Example 2. (High Priority Scheduling)*: Servers identify overhead as a real-time flow with stringent delay and serve them before packets with an elastic delay requirement (e.g. non-real-time traffic such as web surfing) [130]. Suppose other real time traffic is Poisson with total rate ν^{rt}, the service rate experienced by overhead packets will be $\mu_i = \mu_i^{total} - \nu^{rt}$.*

Example 3. (Equal Priority Scheduling)*: All traffic is scheduled with equal priority at the servers. This is close to the worst case since the delay sensitivity*

of overhead traffic is ignored [130]. Suppose the data traffic are Poisson with rate ν^d, we then have $\mu_i = \mu_i^{total} - \nu^d$.

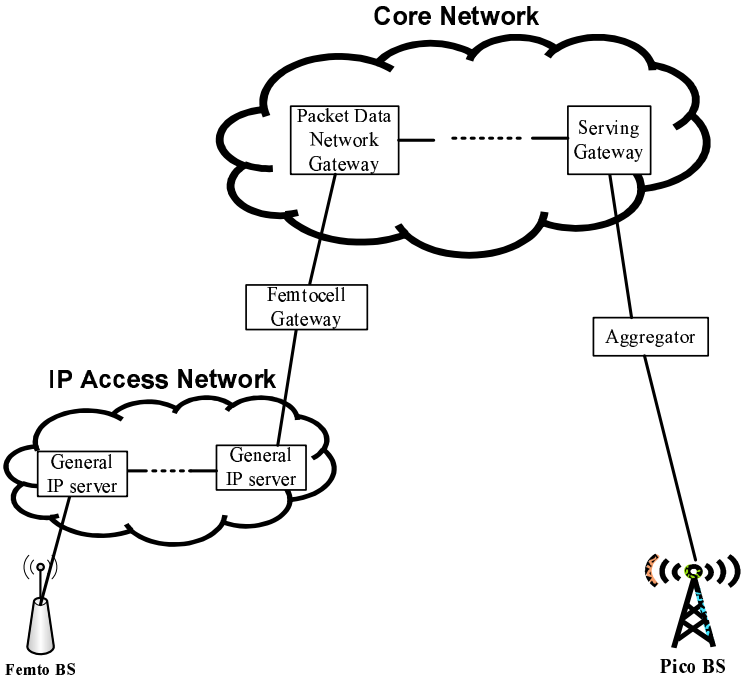

Figure 3.2: A diagram illustrating the backhaul connection between a femto and pico BSs. When overhead is shared between these two BSs through their backhaul, the overall delay consists of processing latencies from the backhaul servers (shown as rectangular boxes) and physical transmission latencies from the links among servers (e.g. fiber optic, dedicated wires and microwave).

Under Assumption 7 and 9, the overhead delay from the i^{th} backhaul server is

$$\mathcal{D}_i \sim \exp\left(\frac{\mu_i}{B}\right), \tag{3.4}$$

where μ_i is the effective service rate and $\frac{\mu_i}{B}$ is thus overhead packet rate per second. For overhead messages not dropped during transmission, the end-to-

end backhaul delay is

$$\mathcal{D} = \sum_{i=1}^{N} \mathcal{D}_i, \tag{3.5}$$

where N is the number of backhaul servers passed by overhead messages from BS_n to BS_0. The values of N and $\frac{\mu_i}{B}$ in (3.5) depend on the specific backhaul configurations between BS_n and BS_0. For the backhaul connection between macro BSs, N is typically around 10 to 20 and μ_i/B is thousands of packets per second [154]. In the most general case, the cumulative distribution function (CDF) of delay $\mathcal{D}$ is very complicated and still under investigation [13, 53]. Here, we consider a scenario of practical interest: $\mu_i \neq \mu_j$ for any $i \neq j$. The CDF is then [26]

$$\mathcal{F}(d, B, \{\mu_i\}|_{i=1}^{N}) \equiv \mathbb{P}(\mathcal{D} \leq d) = \sum_{i=1}^{N} a_i (1 - e^{-\mu_i d/B}), \tag{3.6}$$

where $a_i = \prod_{j \neq i} \frac{\mu_j}{\mu_j - \mu_i}$. Note that B and $\{\mu_i\}|_{i=1}^{N}$ in (3.6) are packet size (in bits) and backhaul servers' packet processing rates. We now derive an important property of $\{a_i\}$ in below, which will be frequently used in the sequel.

Property 1. $\sum_{i=1}^{N} a_i \frac{\mu_i}{\mu_i + x} = \prod_{i=1}^{N} \frac{\mu_i}{\mu_i + x}$, $\forall x \geq 0$. *In the special case of* $x = 0$, *we have* $\sum_{i=1}^{N} a_i = 1$.

Proof. See Appendix 3.7.1. □

In this subsection the overhead delay in backhaul signaling is modelled and its CDF $\mathcal{F}(\cdot)$ is also derived. In the following, we characterize wireless overhead delay by using our SIR results [81] in K-tier HCNs.

3.3.3 Overhead Delay in Wireless Overhead Channel

The wireless channel can be modelled as

$$h(x) = gL|x|^{-\alpha}, \tag{3.7}$$

where g is the short-term fading, L is the wall penetration loss (e.g. femtocells are usually deployed indoors), x is the Euclidean distance between transmitter and receiver, and α is the path loss exponent. We consider i.i.d. Rayleigh fading with unit mean power, i.e. $g \sim \exp(1)$. Denote P_k as the transmitting power of BSs in the k^{th} tier while α_k and L_k as path loss exponent and wall penetration of their channels to BS_0.

As the wireless overhead channel SIR depends on the spatial distributions of BS locations, we assume all tiers are independently distributed on the plane $\mathbb{R}^2$ and BSs in the k^{th} tier are distributed according to homogeneous Poisson Point Process (PPP) Φ_k with intensity λ_k. Previous studies on this PPP model show that, besides providing analytical tractability, the new model is as accurate as the hexagon-grid model in characterizing the SINR distribution [14, 48, 55]. Note that this assumption only affects the SIR CDF $q\{\cdot\}$ in Lemma 3.3.1, while our results on overhead signaling hold under various SINR distributions.

Under the cell selection policy that BS_n has the strongest long-term (i.e. with fading averaged out) power at BS_0, Lemma 3.3.1 below derives the SIR CDF of the overhead messages received at BS_0. See Lemma 1 and 3 and Theorem 1 in [81] for proof.

Lemma 3.3.1. *[81]* The probability that BS_n associates with k^{th} tier is

$$p_k \triangleq \mathbb{P}(\mathrm{BS}_n \textit{ is in the } k^{th} \textit{ tier}) = 2\pi\lambda_k \int_{x>0} x \exp\left(-\pi \sum_{j=1}^{K} \lambda_j \hat{P}_j^{2/\alpha_j} x^{2/\hat{\alpha}_j}\right) \mathrm{d}x. \tag{3.8}$$

where $\hat{P}_j = \frac{P_j L_j}{P_k L_k}$ and $\hat{\alpha}_j = \frac{\alpha_j}{\alpha_k}$. Under this condition, the probability density function $f_{R_{0,n}}(\cdot)$ of the distance $R_{0,n}$ between BS_0 and BS_n, and the cumulative distribution function $q_{k,r}\{\cdot\}$ of received SIR at BS_0 for an arbitrary distance $R_{0,n} = r$ are

$$f_{R_{0,n}}(r|\mathrm{BS}_n \in k^{th} \textit{ tier}) = \frac{2\pi\lambda_k r}{p_k} \exp\left(-\pi \sum_{j=1}^{K} \lambda_j \hat{P}_j^{\frac{2}{\alpha_j}} r^{\frac{2}{\hat{\alpha}_j}}\right) \tag{3.9}$$

$$\begin{aligned} q_{k,r}\{\beta\} &\triangleq \mathbb{P}(SIR \leq \beta|\mathrm{BS}_n \textit{ is in the } k^{th} \textit{ tier}, R_{0,n} = r) \\ &= 1 - \exp\left(-\pi \sum_{j=1}^{K} \lambda_j \hat{P}_j^{2/\alpha_j} \mathcal{Z}(\beta, \alpha_j) r^{2/\hat{\alpha}_j}\right) \end{aligned} \tag{3.10}$$

where

$$\mathcal{Z}(\beta, \alpha_j) = \beta^{\frac{2}{\alpha_j}} \int_{\beta^{-\frac{2}{\alpha_j}}}^{\infty} \frac{1}{1 + u^{\alpha_j/2}} \mathrm{d}u. \tag{3.11}$$

According to Assumption 7, BS_n can be reasonably assumed to drop existing overhead packets upon the arrival of new overhead, as backhaul servers in Assumption 9. The overhead packets, if not dropped during transmission, therefore experience delay given by

$$\mathcal{D} = \frac{B}{W \log(1 + \mathrm{SIR})}, \tag{3.12}$$

where B is the overhead packet size, W is the overhead channel bandwidth and the distribution of SIR is given in (3.10).

3.3.4 Fundamental Evaluation Metric

With overhead interarrival time $\mathcal{T}$ and delay $\mathcal{D}$ modeled, we here define overhead outage p_e.

Definition 4. An overhead message is successful if it arrives at the destination BS_0 before being outdated (i.e $\mathcal{D} \leq \mathcal{T}$, since an overhead is not outdated until a new one is generated) and before a hard deadline d (i.e. $\mathcal{D} \leq d$). Otherwise, it is defined as in outage.

The outage defined above is the probability that an overhead block is not fully received before a certain deadline specified by the coordination techniques. It is indeed the overhead block error, not including the effect of coding and complicated overhead transmission schemes [98]. Based on Definition 4, the fundamental evaluation metric of this work – the *overhead quality contour* is thus defined as

$$\mathcal{Q}_o \triangleq \{(\mathcal{T}, B, d, p_e) : \ p_e = 1 - \mathbb{P}(\mathcal{D} \leq \mathcal{T}, \mathcal{D} \leq d)\}, \tag{3.13}$$

where $\mathcal{T}$ is the overhead interarrival time, B is the overhead packet size, d is the required overhead deadline (i.e. maximal tolerable delay), and p_e is the corresponding outage probability. Note that the delay $\mathcal{D}$ is fully characterized by d and p_e, and thus is not explicitly included in $\mathcal{Q}_o$.

This metric above determines the feasible set of overhead parameters $\{\mathcal{T}, B, d, p_e\}$ as a function of overhead signaling configurations in HCNs (e.g.

overhead arrival process and channel parameters).As will be illustrated in Section III and IV, this framework can be used for the evaluation and design of coordination techniques and HCN overhead channel setups.

3.4 Overhead Quality Contour in Backhaul Signaling

This section presents the main results for backhaul overhead signaling. The *overhead quality contour* is quantified when BS_n and BS_0 share overhead through their dedicated backhaul. We consider the general scenario that the backhaul overhead delay is dominated by the processing latencies from backhaul servers, which is true for most backhaul network setups [123, 124, 154]. Of course, the analysis in this section does not apply to the case, for example, when macro BSs are directly interconnected with using high-speed backbone without any intermediate servers [75]. However the backhaul delay in these counter examples (which are not very common in HCNs) is often negligible [2, 150, 154]. In this section, denote the number of backhaul servers passed by overhead messages as N, and their overhead processing rates as $\{\mu_1/B, \ldots, \mu_N/B\}$.

3.4.1 General Case and Main Results

Theorem 3.4.1. For backhaul overhead signaling between BS_n and BS_0 with interarrival time $\mathcal{T} \sim \mathit{Gamma}\left(M, \frac{1}{M\eta}\right)$, the overhead quality contour is

$$\mathcal{Q}_o = \Bigg\{ (\mathcal{T}, B, d, p_e) : p_e = \sum_{i=1}^{N} a_i \Bigg[\left(1 - \frac{\gamma(M, M\eta d)}{\Gamma(M)}\right) e^{-\frac{\mu_i d}{B}} + \frac{\gamma\left(M, M\eta d + \frac{\mu_i d}{B}\right)}{\Gamma(M)} \left(\frac{M\eta}{M\eta + \frac{\mu_i}{B}}\right)^M \Bigg] \Bigg\}, \quad (3.14)$$

where $\{a_i\}$ are defined in (3.6), $\Gamma(\cdot)$ is the gamma function and $\gamma(M, x)$ is the lower incomplete gamma function given by

$$\gamma(M, x) = \int_0^x t^{M-1} e^{-t} \mathrm{d}t. \quad (3.15)$$

Proof. See Appendix 3.7.2. □

Theorem 3.4.1 quantifies all plausible overhead parameters that can be supported by given backhaul configurations. Since many coordination techniques often have additional requirements on several overhead parameters (e.g. requiring $p_e \leq 0.1$), their feasible overhead sets are strict subsets of $\mathcal{Q}_o$. In theory, these subsets can be determined from Theorem 3.4.1 by, for example, restricting $p_e \leq 0.1$ in (3.14). However, it is computationally hard in practice to derive feasible set of $(\mathcal{T}, B, d)$ under a given outage requirement. In the following, we derive simpler bounds on (3.14), which can be easily used to characterize the feasible set of several overhead parameters given others.

According to its definition and observations from Theorem 3.4.1, the outage probability p_e is an increasing function on the overhead rate η while a

decreasing function on the deadline requirement d. For example, the outage probability is zero when $\eta \to 0$ and $d \to \infty$ as shown in Theorem 3.4.1. Therefore, it has the following two lower bounds.

Lower Overhead Rate: By letting the overhead packet rate η go to zero, overhead packets have very long lifetimes (i.e. $\mathbb{E}[\mathcal{T}] = 1/\eta \to \infty$) and overhead outage only comes from the probability of not meeting the hard deadline (i.e. $\mathcal{D} > d$).

$$p_e \geq \sum_{i=1}^{N} a_i e^{-\mu_i d/B} = 1 - \mathcal{F}(d, B, \{\mu_i\}|_{i=1}^{N}) \stackrel{\triangle}{=} p_e^{lb,1}. \tag{3.16}$$

Relaxed Delay Deadline: By letting delay deadline d go to infinity, the overhead delay deadline is relaxed and outage only comes from the probability of being outdated during transmission (i.e. $\mathcal{D} > \mathcal{T}$).

$$p_e \geq \sum_{i=1}^{N} a_i \left(\frac{M\eta}{M\eta + \mu_i/B} \right)^M \stackrel{\triangle}{=} p_e^{lb,2}. \tag{3.17}$$

Remark 8. For backhaul signaling, a lower bound for overhead outage probability is

$$p_e \geq \max\left(p_e^{lb,1}, p_e^{lb,2}\right),$$

where $p_e^{lb,1}$ and $p_e^{lb,2}$ are given in (3.16) and (3.17) respectively.

Remark 8 can be used to estimate feasible overhead sets for various coordination techniques. For example, for coordination techniques requiring $p_e \leq 0.1$, we can estimate its feasible set of $(\mathcal{T}, B, d)$ by simply solving

$\max\left(p_e^{lb,1}, p_e^{lb,2}\right) \leq 0.1$. Such an estimation is fairly accurate, because numerical simulations in Section V show that the lower bound $\max\left(p_e^{lb,1}, p_e^{lb,2}\right)$ is reasonably tight under general overhead arrivals.

It is interesting to compare feasible overhead parameters $(\mathcal{T}, B, \mathcal{D})$ quantified by our framework with previous works. Previous models do not capture the randomness in overhead inter-arrival time $\mathcal{T}$, which is assumed to be the constant $1/\eta$ [165]. Overhead backhaul delay $\mathcal{D}$ in (3.5) is often neglected or simply assumed to be its averaged value [58, 59, 133, 138]

$$\mathcal{D} = \mathbb{E}\left[\sum_{i=1}^{N} \mathcal{D}_i\right] = \sum_{i=1}^{N} \frac{B}{\mu_i}. \tag{3.18}$$

Under the above simplified models, the *overhead quality contour* will reduce to

$$\mathcal{Q}_o = \left\{(\mathcal{T}, B, d, p_e) : p_e = 1 - \mathbf{1}\left(\sum_{i=1}^{N} \frac{B}{\mu_i} \leq \min(d, 1/\eta)\right)\right\}, \tag{3.19}$$

where $\mathbf{1}(\cdot)$ is the indicator function. Obviously the feasible overhead parameters defined in (3.19) are vastly different from (3.14). For example, under given backhaul servers' rates $\{\mu_i\}$, overhead outage in (3.19) can be zero under finite values of d and $1/\eta$. However, the lower bound in Remark 8 shows that $p_e = 0$ *iff* $d \to \infty$ *and* $1/\eta \to \infty$. Therefore the natural randomness in $\mathcal{T}$ and $\mathcal{D}$ crucially determines the feasible overhead signaling contours and will be discussed more in numerical simulations.

In general, the *overhead quality contour* $\mathcal{Q}_o$ can be used for the design and evaluation of coordination techniques in HCNs. For example, in below we

provide backhaul design guidelines to effectively support overhead signaling required by coordination techniques.

Corollary 3.4.2. For a given overhead requirement $(\mathcal{T}, B, d, p_e)$ from coordination techniques, the backhaul configuration, i.e. the values of N and $\{\mu_i\}$, must satisfy the following inequalities

$$\bar{\mu} \geq \frac{B}{d}\,\gamma^{-1}\left((1-p_e)(N-1)!, N\right)\,, \tag{3.20}$$

$$\bar{\mu} \geq \frac{M\eta B\,\sqrt[N]{1-p_e}}{\sqrt[N]{\binom{M+N-1}{N}} - \sqrt[N]{1-p_e}}\,, \tag{3.21}$$

where $\bar{\mu}$ is the average service rate $\bar{\mu} = \frac{\sum_{i=1}^{N}\mu_i}{N}$ and $\gamma^{-1}(x, N)$ is the inverse incomplete gamma function given by

$$x = \gamma(N, y) = \int_0^y t^{N-1}e^{-t}\mathrm{d}t \;\Leftrightarrow\; y = \gamma^{-1}(x, N). \tag{3.22}$$

Proof. See Appendix 3.7.3. □

The lower bounds in Corollary 3.4.2 are expected to be tight, since they are based on the tight bounds in Remark 8.

3.4.2 Special Cases: Deterministic and Poisson Overhead Arrivals

Corollary 3.4.3. For backhaul signaling under deterministic overhead arrivals, the overhead quality contour is

$$\mathcal{Q}_o = \left\{(\mathcal{T}, B, d, p_e) : p_e = 1 - \mathcal{F}\left(\min(d, 1/\eta), B, \{\mu_i\}|_{i=1}^{N}\right)\right\}. \tag{3.23}$$

Proof. Deterministic overhead arrival corresponds to the case of $M \to \infty$. Before we proceed to derive overhead rate and delay contours, we state two important results below.

$$\lim_{M\to\infty} \left(\frac{M\eta}{M\eta + x}\right)^M = \lim_{M\to\infty} \left(1 - \frac{x/\eta}{M + x/\eta}\right)^M = e^{-x/\eta}. \tag{3.24}$$

$$\lim_{M\to\infty} \frac{\gamma(M, Mx)}{\Gamma(M)} = \lim_{M\to\infty} \frac{\int_0^{Mx} u^{M-1}e^{-u}\,\mathrm{d}u}{\int_0^{\infty} u^{M-1}e^{-u}\,\mathrm{d}u} = \mathbf{1}(x \geq 1), \tag{3.25}$$

where $\mathbf{1}(\cdot)$ is the indicator function. Note that for a random variable $Y \sim$ Gamma $(M, 1)$, $\frac{\gamma(M,Mx)}{\Gamma(M)}$ is the probability that $Y \leq Mx$. By using Chebyshev's inequality on $\mathbb{P}(Y \leq Mx)$ and letting $M \to \infty$, the results in (3.25) follow. Based on the equations immediately above, the outage probability p_e below is derived by letting $M \to \infty$ in Theorem 3.4.1

$$\begin{aligned} p_e &= \sum_{i=1}^{N} a_i \left[(1 - \mathbf{1}(\eta d \geq 1))e^{-\mu_i d/B} + \mathbf{1}(\eta d \geq 1)e^{-\frac{\mu_i}{\eta B}}\right] \\ &= \sum_{i=1}^{N} a_i e^{-\mu_i \min(d,1/\eta)/B} \\ &\overset{(a)}{=} 1 - \sum_{i=1}^{N} a_i \left(1 - e^{-\mu_i \min(d,1/\eta)/B}\right) \\ &= 1 - \mathcal{F}\left(\min(d, 1/\eta), B, \{\mu_i\}|_{i=1}^{N}\right), \end{aligned} \tag{3.26}$$

where $\mathbf{1}(\cdot)$ is the indicator function, and (a) holds from Property 1 by letting $x = 0$. □

Under deterministic overhead arrivals, the lower bound $p_e^{lb,2}$ in (3.17) is

simplified as

$$p_e^{lb,2} = \lim_{M\to\infty} \sum_{i=1}^{N} a_i \left(\frac{M\eta}{M\eta + \mu_i/B}\right)^M$$
$$\stackrel{(a)}{=} \sum_{i=1}^{N} a_i e^{-\frac{\mu_i}{\eta B}} = 1 - \mathcal{F}(1/\eta, B, \{\mu_i\}|_{i=1}^N), \tag{3.27}$$

where (a) holds directly from (3.24). Combining the two lower bounds under deterministic overhead arrivals, i.e. (3.16) and (3.27), we have

$$\max\left(p_e^{lb,1}, p_e^{lb,2}\right) = 1 - \mathcal{F}(\min(d, 1/\eta), B, \{\mu_i\}|_{i=1}^N). \tag{3.28}$$

It is important to note that the lower bound above is *exactly* p_e given in Corollary 3.4.3.

Remark 9. Deterministic overhead arrivals minimize the outage probability, by achieving the lower bound in Remark 8.

The above remark implies that ignoring the randomness in the overhead arrival process will lead to an underestimation of overhead outage. Numerical results show that this lower bound is not tight.

Corollary 3.4.4. For backhaul signaling with Poisson overhead arrivals, the overhead quality contour is

$$\mathcal{Q}_o = \left\{(\mathcal{T}, B, d, p_e) : p_e = 1 - \left(\prod_{i=1}^{N} \frac{\mu_i}{\mu_i^{'}}\right) \mathcal{F}(d, B, \{\mu_i^{'}\}|_{i=1}^N)\right\}, \tag{3.29}$$

where $\mu_i^{'} = \mu_i + \eta B$.

Proof. Poisson overhead arrivals correspond to the special case of $M = 1$.

$$\begin{aligned}
p_e &\overset{(a)}{=} \sum_{i=1}^{N} a_i \left[e^{-\eta d - \mu_i d/B} + \left(1 - e^{-\eta d - \mu_i d/B}\right) \left(\frac{\eta}{\eta + \mu_i/B} \right) \right] \\
&\overset{(b)}{=} 1 - \sum_{i=1}^{N} a_i \left(1 - e^{-\eta d - \mu_i d/B}\right) \left(1 - \frac{\eta}{\eta + \mu_i/B} \right) \\
&= 1 - \sum_{i=1}^{N} \prod_{j \neq i} \frac{\mu_j}{\mu_j - \mu_i} \left(1 - e^{-\eta d - \mu_i d/B}\right) \left(\frac{\mu_i}{\eta B + \mu_i} \right) \\
&= 1 - \left(\prod_{i=1}^{N} \frac{\mu_i}{\mu_i + \eta B} \right) \sum_{i=1}^{N} \prod_{j \neq i} \frac{\mu_j + \eta B}{\mu_j - \mu_i} \left(1 - e^{-\eta d - \mu_i d/B}\right) \\
&= 1 - \left(\prod_{i=1}^{N} \frac{\mu_i}{\mu_i + \eta B} \right) \mathcal{F}(d, B, \{\mu_i + \eta B\}|_{i=1}^{N}). \qquad (3.30)
\end{aligned}$$

The equality (a) comes from the fact that $\gamma(1, x) = 1 - e^{-x}$ and $\Gamma(1) = 1$, while equality (b) holds from Property 1 (letting $x = 0$). See the proof of Property 1 for the last two steps. □

Given sum service rates $\sum_{i=1}^{N} \mu_i = C$, the delay CDF $\mathcal{F}(d, B, \{\mu_i\}|_{i=1}^{N})$ is maximized for any d and B *iff* all service rates are equal, i.e. $\mu_i = \bar{\mu} = C/N$ $(1 \leq i \leq N)$. Therefore equal rate allocation among backhaul servers minimizes the overhead outage under deterministic arrivals in Corollary 3.4.3. It is also the optimal choice for Poisson overhead arrivals because it simultaneously maximizes $\prod_{i=1}^{N} \frac{\mu_i}{\mu_i + \eta B}$ and $\mathcal{F}(d, B, \{\mu_i + \eta B\}|_{i=1}^{N})$ in Corollary 3.4.4. Such a conclusion in fact holds under general overhead arrivals. The maximized CDF implies that the delay $\mathcal{D}$ is stochastically minimized. The outage probability $p_e = 1 - \mathbb{P}(\mathcal{D} \leq \mathcal{T}, \mathcal{D} \leq d)$ is therefore minimized, independent on the overhead arrival process.

Remark 10. For a given sum of service rates, equal rate allocation among backhaul servers minimizes the overhead outage, independent on overhead arrival process.

Remark 9 and 10 together imply that the overhead outage is minimized when overhead arrivals are deterministic *and* backhaul servers have the same overhead processing rate $\bar{\mu}$.

In summary, in this section we have quantified the overhead quality contour – the feasible set of overhead parameters $(\mathcal{T}, B, d, p_e)$ – for backhaul signaling in general HCNs. We show that previous models – which ignore the inherent randomness in overhead inter-arrival time $\mathcal{T}$ and delay $\mathcal{D}$ – underestimate the overhead outage p_e and therefore are not accurate in quantifying the cost of overhead sharing. The derived overhead quality contour also provides design insights on backhaul network configurations, e.g. predicting the required overhead processing rates from backhaul servers and identifying the optimal rate allocation among them.

3.5 Overhead Quality Contour in Wireless Signaling

Dedicated wireless links (e.g. out-of-band GSM or to-be-defined overhead channels in LTE-A) are also used by coordination techniques to share overhead (e.g. CSI feedback). Since the radio environment in HCNs is very different from 1-tier macrocell case, the wireless overhead channels present new characteristics such as SINR distributions. In this section, we quantify

the *overhead quality contour* for wireless signaling in HCNs, assuming arbitrary tier index of BS_n (denoted as k) and distance between BS_0 and BS_n (denoted as r).

3.5.1 General Case and Main Results

Theorem 3.5.1. For wireless overhead signaling between BS_n and BS_0 with interarrival time $\mathcal{T} \sim \textit{Gamma}\left(M, \frac{1}{M\eta}\right)$, the overhead quality contour is

$$\mathcal{Q}_o = \Bigg\{(\mathcal{T}, B, d, p_e) : p_e = \left[1 - \frac{\gamma(M, M\eta d)}{\Gamma(M)}\right] q_{k,r}\{\beta(d)\} + \int_0^d q_{k,r}\{\beta(x)\} \frac{(M\eta x)^M e^{-M\eta x}}{x\Gamma(M)} \mathrm{d}x \Bigg\}, \tag{3.31}$$

where $\beta(x) = \exp\left(\frac{B\ln 2}{Wx}\right) - 1$ is the required SIR for overhead deadline x and the subscript k is the tier index of BS_n.

Proof. See Appendix 3.7.4. □

Theorem 3.5.1 quantifies the possible pairs of $(\mathcal{T}, B, d, p_e)$ for arbitrary wireless overhead channel setups. However, for the same reason stated below Theorem 3.4.1, we derive simpler bounds on $\mathcal{Q}_o$ in (3.31).

Remark 11. The overhead outage in Theorem 3.5.1 can be bounded as

$$p_e \begin{cases} \geq \max(q_{k,r}\{\beta(d)\}, \mathbb{E}[q_{k,r}\{\beta(\mathcal{T})\}]) \\ \leq \left[1 - \frac{\gamma(M, M\eta d)}{\Gamma(M)}\right] q_{k,r}\{\beta(d)\} + \frac{\gamma(M, M\eta d)}{\Gamma(M)} \end{cases} \tag{3.32}$$

Using the same argument in previous section, the lower bound on overhead outage can be achieved by letting $\eta \to 0$ or $d \to \infty$. The upper bound on

p_e can be found based on the fact that $q_{k,r}\{\cdot\} \leq 1$. By restricting several overhead parameters in (3.32) as required by coordination techniques, the bounds determine their feasible overhead sets in an easier way than Theorem 3.5.1.

Remark 11 shows the clear dependence between overhead outage p_e and the distribution of SINR ($q_{k,r}\{\cdot\}$ function) and $\mathcal{T}$ ($\gamma(\cdot)$ function). Therefore with appropriate models on SINR and overhead interarrival time $\mathcal{T}$, the *overhead quality contour* in Theorem 3.5.1 provides more accurate insights than previous works on feasible overhead parameters in HCNs.

Corollary 3.5.2. When BSs of all tiers have the same path loss exponent α, for a given overhead requirement $(\mathcal{T}, B, d, p_e)$ from coordination techniques, the bandwidth W of wireless overhead channel must satisfy following inequalities

$$W \geq \frac{B \ln 2}{d \log\left\{1 + \left(\frac{\log(1-p_e)}{\zeta(\alpha)} + \frac{\alpha}{2\pi}\sin(2\pi/\alpha)\right)^{\alpha/2}\right\}}, \tag{3.33}$$

where $\zeta(\alpha) = -\frac{2\pi^2}{\alpha}\csc\left(\frac{2\pi}{\alpha}\right)\left(\sum_{j=1}^{K}\lambda_j \hat{P}_j^{2/\alpha} r^2\right)$, *and* $\csc(x) = \sin^{-1}(x)$ *is the cosecant function.*

Proof. See Appendix 3.7.5. □

It is generally hard to provide design guidelines for wireless overhead channel (e.g. the bandwidth W) directly from the *overhead quality contour* or even its bounds. This is mainly because of the complicated expression of $q_k\{\cdot\}$ as in Lemma 3.3.1. In Corollary 3.5.2 we discuss it in a special case where $q_k\{\cdot\}$ can be simplified.

3.5.2 Special Cases: Deterministic and Poisson Overhead Arrivals

Corollary 3.5.3. For wireless signaling with deterministic overhead arrivals, the overhead quality contour is

$$\mathcal{Q}_o = \{(\mathcal{T}, B, d, p_e) : p_e = q_{k,r}\{\beta\left(\min(d, 1/\eta)\right)\}\}. \tag{3.34}$$

Proof. Based on the proof of Theorem 3.5.1, overhead outage under deterministic overhead arrival is

$$\begin{aligned} p_e &= 1 - \lim_{M\to\infty} \int_0^d \left[1 - \frac{\gamma(M, M\eta x)}{\Gamma(M)}\right] \mathrm{d}\mathbb{P}(\mathcal{D} \le x) \\ &= 1 - \int_0^d [1 - \mathbf{1}(\eta x \ge 1)] \mathrm{d}\mathbb{P}(\mathcal{D} \le x) \\ &= 1 - \mathbb{P}(\mathcal{D} \le \min(d, 1/\eta)) \\ &= q_{k,r}\{\beta(\min(d, 1/\eta))\}, \end{aligned} \tag{3.35}$$

where $\mathbf{1}(\cdot)$ is the indicator function. □

Corollary 3.5.4. For wireless signaling with Poisson overhead arrivals, the overhead quality contour is

$$\mathcal{Q}_o = \left\{(\mathcal{T}, B, d, p_e) : p_e = e^{-\eta d} q_{k,r}\{\beta(d)\} + \int_0^d q_{k,r}\{\beta(x)\}\eta e^{-\eta x} \mathrm{d}x \right\}. \tag{3.36}$$

Proof. The proof follows simply by replacing the general expression $\gamma(M, x)$ with $\gamma(1, x) = 1 - e^{-x}$. □

The results on *overhead quality contour* in Theorem 3.5.1 are greatly simplified in these special cases. Under deterministic arrivals, the lower bound

on p_e in Remark 11 reduces to

$$\begin{aligned}\max(q_{k,r}\{\beta(d)\}, \mathbb{E}[q_{k,r}\{\beta(\mathcal{T})\}]) &= \max(q_{k,r}\{\beta(d)\}, q_{k,r}\{\beta(1/\eta)\}) \\ &= q_{k,r}\{\beta\left(\min(d, 1/\eta)\right)\}. \end{aligned} \tag{3.37}$$

It is seen that, similar to backhaul signaling, deterministic arrivals are also optimal in wireless signaling. In other words, ignoring natural randomness in overhead arrivals leads to underestimation of wireless overhead delay and outage, which is non-trivial as shown through numerical results below.

In summary, in this section we have quantified the feasible set of overhead parameters $(\mathcal{T}, B, d, p_e)$ for wireless signaling in HCNs. The results are expressed as a function of $q\{\cdot\}$, which is the SIR distribution. Thus, they are applicable to various wireless overhead channels (e.g. in-band vs. out-band) and HCN models (e.g. grid model vs. PPP model for BS locations), by using the appropriate SIR distribution functions.

3.6 Numerical Results and Discussion

In this section, we consider a 3-tier heterogeneous network as shown in Fig. 3.1, comprising for example macro (tier 1), pico (tier 2) and femto (tier 3) BSs. Notation and system parameters are given in Table 3.1. Suppose BS_0 is a pico BS. According to the tier index of BS_n, the *overhead quality contour* is investigated in the following three scenarios.

Scenario I: BS_n belongs to 1^{st} tier. The backhaul path between pico and macro BSs includes backhaul servers from the core network and the

Table 3.1: Notation & Simulation Summary

Symbol	Description	Simulation Value
λ_1	Macro BS density	$5 \times 10^{-7}/m^2$ (average cell radius of 1 Km)
λ_2	Pico BS density	$5\times10^{-6}/m^2$ (average of 10 picos/macrocell)
λ_3	Femto BS density	$5\times10^{-5}/m^2$ (average of 100 femtos/macrocell)
P_1	Macro BS transmitting power	40 W
P_2	Pico BS transmitting power	1 W
P_3	Femto BS transmitting power	200 mW
α_1	Path loss exponent of Macro BSs	3.0
α_2	Path loss exponent of Pico BSs	3.5
α_3	Path loss exponent of Femto BSs	4.0
L_w	Wall penetration loss (femto BSs are indoor)	5 dB
k	The tier index of BS_n	k=1, 2 or 3
$R_{0,n}$	The distance between BS_0 and BS_n	40 m
W	Wireless channel bandwidth	Not Fixed
N_{IP}	Number of servers in IP access network (for femtocells)	10
N_{CN}	Number of servers in core network	10
N	Total number of servers in backhaul path	Not Fixed
$\bar{\mu}$	Backhaul servers' average rate (bps) for overhead packets	Not Fixed
B	Overhead packet size	30 bits
$\mathcal{T}$	Overhead packet interarrival time	Not Fixed
η	Average overhead packet rate, i.e. $\eta = 1/\mathbb{E}(\mathcal{T})$	Not Fixed
M	Parameter in the distribution of $\mathcal{T}$	$\mathcal{T} \sim$ Gamma $\left(M, \frac{1}{M\eta}\right)$
d	Overhead delay requirement	Not Fixed
$\beta(x)$	SIR target for a given overhead delay requirement x	$\frac{B}{W\log(1+\beta(x))} = x$

picocell aggregator, i.e. $N = N_{CN} + 1$.

Scenario II: BS_n belongs to 2^{nd} tier. Since nearby pico BSs are often clustered by sharing the same backhaul aggregator [119], the number of backhaul servers between BS_0 and its neighbour BS_n is $N = 1$.

Scenario III: BS_n belongs to 3^{rd} tier. The backhaul servers between pico and femto BSs consist of the picocell aggregator, the femtocell gateway, and those from the core network and femtocell's IP network, i.e. $N = 2 + N_{CN} + N_{IP}$.

In all three scenarios, we assume all backhaul servers have the same rate $\bar{\mu}$ for overhead packets, which is optimal per Remark 10.

3.6.1 Overhead Quality Contour in Backhaul Signaling

Ω_o vs. Backhaul Configurations. The *overhead quality contour* in various backhaul configurations (i.e. number of backhaul servers N and their rate $\bar{\mu}$) is shown in Fig. 3.3 and 3.4. Obviously, the overhead outage decreases as the number of servers decreases and/or their rate $\bar{\mu}$ increases. However two important observations are worth noting: 1) reducing the number of backhaul servers is critically important since the outage in scenarios II ($N = 1$) is way below the other two scenarios ($N > 10$); 2) it is difficult to ensure very small outage (e.g. $p_e \leq 0.1$) purely by increasing backhaul servers' rate $\bar{\mu}$, since the outage curve in Fig. 3.4 is almost flat in the region of $p_e \leq 0.1$. Under this circumstance, our conjecture is that appropriate retransmission schemes and certain level of coding should also be deployed for further outage reduction.

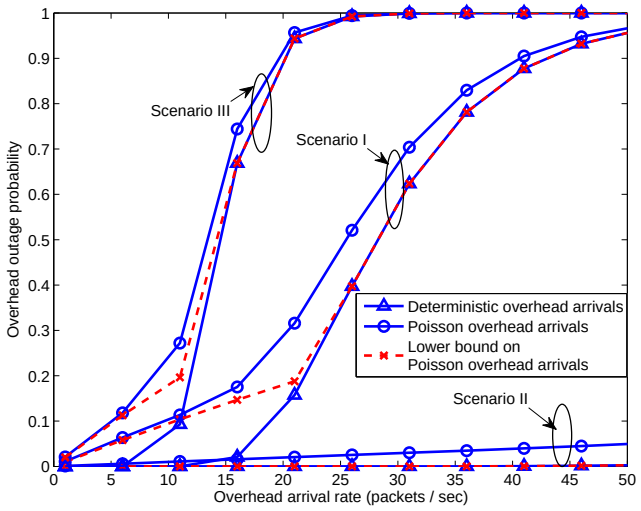

Figure 3.3: Overhead outage p_e vs. overhead arrival rate η in all three scenarios. The delay requirement d is $0.3\,\mathbb{E}[\mathcal{T}] = 0.3/\eta$, i.e. overhead signaling is allowed to occupy 30% time slots. The overhead service rate $\frac{\bar{\mu}}{B} = 1000$ packets/sec.

Insights on Backhaul Deployments. According to the specific overhead requirements, the minimum rate of backhaul servers is derived in Corollary 3.4.2 based on the lower bound in Remark 8. This bound is achieved under deterministic arrivals (as stated in Remark 9) but suspected to be loose under Poisson arrivals – the opposite extreme of deterministic. However Fig. 3.3 shows that it is fairly tight even for Poisson arrivals, especially in small outage region (i.e. $p_e \leq 0.1$) of practical interest. Therefore, the results in Corollary 3.4.2 provide accurate guidelines on the deployment of backhaul overhead channels in HCNs.

Comparison with Previous Models. Fig. 3.3 also shows the ap-

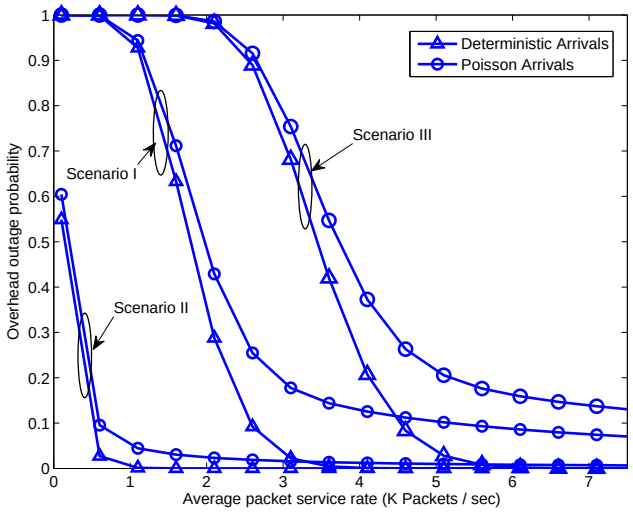

Figure 3.4: Overhead outage p_e vs. average packet service rate $\bar{\mu}/B$ in the three scenarios. The overhead rate $\eta = 50$ packets/sec, i.e. an overhead on average has lifetime $\mathbb{E}(\mathcal{T}) = 1/\eta = 20$ ms. The overhead delay requirement d is $0.3\,\mathbb{E}[\mathcal{T}] = 6$ ms.

preciable difference in overhead outage between Poisson and deterministic arrivals. For example, with the same overhead rate of 10 packets/sec in scenario III, deterministic arrivals incur 0.1 outage (usually an acceptable packet error percentage) while Poisson arrivals incur 0.3 outage (generally unacceptable). In other words, the randomness in overhead arrivals is an important factor for overhead signaling characterization but missed from previous works.

Fig. 3.5 shows the more comprehensive comparison of our results with previous simplified models in scenario II. It is seen that previous simplified models, ignoring the randomness in overhead arrivals *and* backhaul delay, are highly inaccurate even though their underlying assumption of low-latency

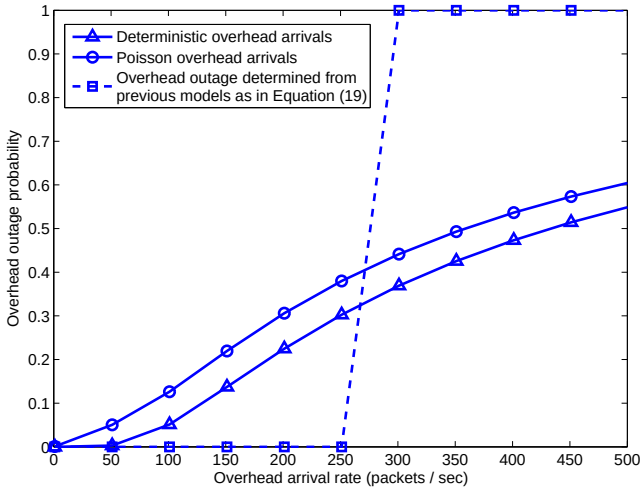

Figure 3.5: Overhead outage p_e vs. overhead arrival rate η in scenario II. The delay requirement d and overhead service rate $\frac{\bar{\mu}}{B}$ are the same as Fig. 3.3. Previous simplified models assume constant overhead delay $\mathcal{D} = \mathbb{E}(\mathcal{D}) = 1$ ms and constant overhead arrivals $\mathcal{T} = \mathbb{E}(\mathcal{T}) = 1/\eta$.

backhaul interface is satisfied in scenario II (mean delay is 1 ms). Under an outage requirement of, for example, $p_e \leq 0.1$, they predict that backhaul channel can support up to 250 packets/sec, which in fact is between 75 (Poisson arrivals) and 125 packets/sec (deterministic arrivals).

3.6.2 Overhead Quality Contour in Wireless Signaling

$\mathcal{Q}_o$ vs. Overhead Channel Configurations. Fig. 3.6 shows the overhead outage p_e in three scenarios, i.e. different types of BS_n. The overhead outage is significantly lower in scenario I, as the macro BSs have the large transmitting power and smaller path loss exponent. Fig. 3.6 also shows that the gap in overhead outage p_e increases as the overhead arrival rate goes up.

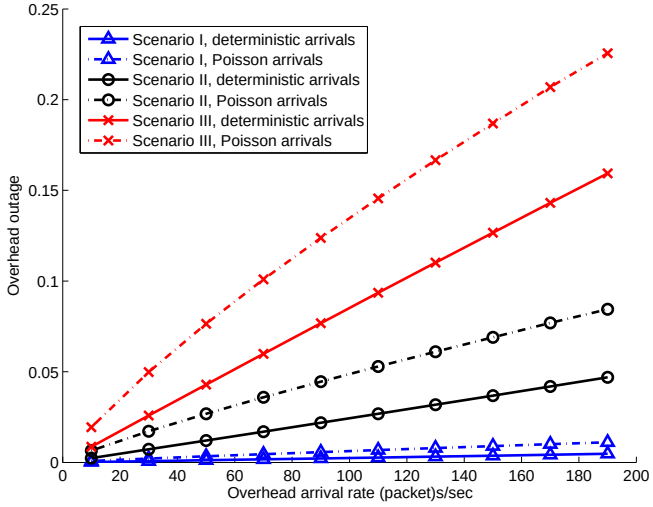

Figure 3.6: Overhead outage p_e vs. overhead arrival rate η for wireless signaling. The delay requirement d is $0.3\,\mathbb{E}[\mathcal{T}] = 0.3/\eta$. The overhead channel bandwidth is 50 KHz.

Fig. 3.7 illustrates the outage p_e vs. wireless overhead channel bandwidth W. The observation here is similar to Fig. 3.4: increasing bandwidth can easily reduce outage to about 0.1 but is not a cost-effective way for further outage reduction. Therefore, retransmission schemes, coding and diversity techniques will be useful in this situation.

Comparison with Previous Models. Two key differences from previous models contribute to our more accurate characterization of the overhead signaling in HCNs: 1) the consideration of overhead arrival dynamics, because Fig. 3.6 shows that Poisson overhead arrivals incur higher outage than deterministic arrivals (no randomness in $\mathcal{T}$ as assumed in previous models) by 0.05 to 0.1; 2) the appropriate spatial model on BS locations in HCNs, which

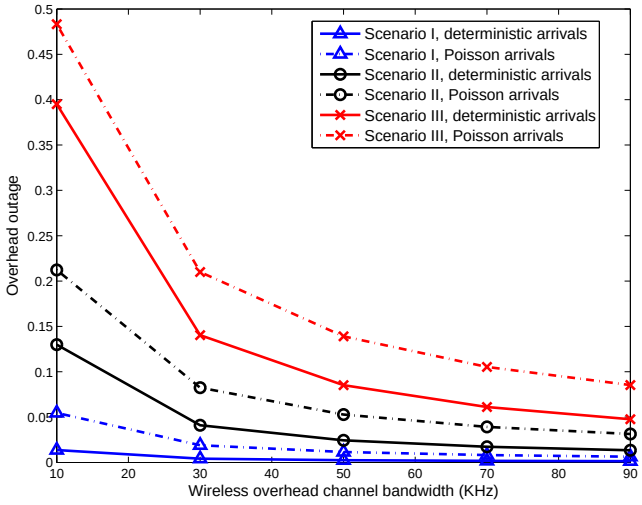

Figure 3.7: Overhead outage p_e vs. wireless overhead channel bandwidth W. The overhead rate $\eta = 100$ packets/sec, and the delay requirement d is $0.3\,\mathbb{E}[\mathcal{T}] = 0.3/\eta$.

is fundamental to spatial interference statistics and overhead channel SINR distribution $q_k\{\cdot\}$. The comparison of spatial models (our PPP based model vs. previous assumed grid model) is extensively discussed in [14, 48, 55].

3.6.3 The Optimal Overhead Signaling Method

Numerical results show that in all three scenarios, the optimal choices between backhaul vs. wireless signaling are determined by two important measures: 1) the overhead arrival rate η; and 2) the average overhead delay $\mathbb{E}[\mathcal{D}]$ derived from (3.5) and (3.12)

$$\mathbb{E}[\mathcal{D}] = \begin{cases} \sum_{i=1}^{N} \mathbb{E}[\mathcal{D}_i] = \frac{\bar{\mu}}{NB} & \text{backhaul channel} \\ \frac{W}{B}\mathbb{E}[\log(1+\text{SIR})] & \text{wireless channel} \end{cases} \tag{3.38}$$

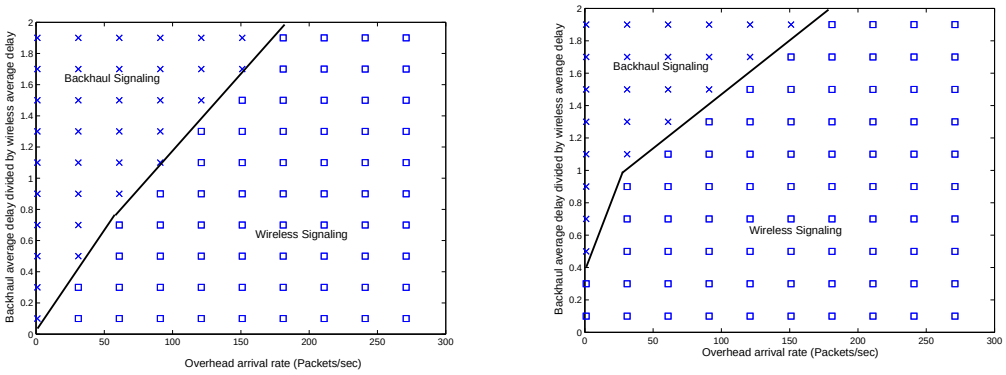

(a) Deterministic overhead arrivals

(b) Poisson overhead arrivals

Figure 3.8: Optimal overhead channel choice in Scenario I under deterministic and Poisson overhead arrivals. The wireless overhead channel bandwidth is 50 KHz and its overhead average delay $\mathbb{E}[\mathcal{D}] \doteq 2$ ms. The delay requirement d is $0.3\,\mathbb{E}[\mathcal{T}] = 0.3/\eta$. The mark "$\square$" means wireless signaling is preferred with lower outage, while "$\times$" means backhaul signaling is preferred.

Fig. 3.8 depicts the optimal choice in Scenario I under deterministic and Poisson arrivals. In general, the backhaul channel is preferred for slow overhead traffic, while the wireless channel is more preferred for fast overhead sharing. Comparing Fig. 3.8 (a) and (b), it is seen that as the randomness of overhead arrivals increases, wireless signaling becomes more preferable.

3.7 Appendix

3.7.1 Proof of Property 1

For $x = 0$, Property 1 obviously holds, since

$$\sum_{i=1}^{N} a_i = \sum_{i=1}^{N} a_i \lim_{d\to\infty}(1 - e^{-\mu_i d/B}) = \mathcal{F}(\infty, B, \{\mu_i\}|_{i=1}^{N}) = 1 \tag{3.39}$$

For $x > 0$, we have

$$\sum_{i=1}^{N} a_i \frac{\mu_i}{\mu_i + x} = \left(\prod_{i=1}^{N} \frac{\mu_i}{\mu_i + x}\right) \sum_{i=1}^{N} \prod_{j\neq i} \frac{\mu_j + x}{\mu_j - \mu_i} \overset{(a)}{=} \left(\prod_{i=1}^{N} \frac{\mu_i}{\mu_i + x}\right) \tag{3.40}$$

Note that $\{\prod_{j\neq i} \frac{\mu_j+x}{\mu_j-\mu_i}\}|_{i=1}^{N}$ is indeed the coefficient $\{a_i\}|_{i=1}^{N}$ in $\mathcal{F}(d, B, \{\mu_i + x\}|_{i=1}^{N})$. Thus the equality (a) holds from (3.39).

3.7.2 Proof of Theorem 3.4.1

According to its definition, the successful overhead will not be dropped by the backhaul servers. Therefore its delay is the sum latencies from all the backhaul servers as in (3.5). With the delay CDF given in (3.6), the overhead

outage is derived as

$$\begin{aligned}
p_e =& 1 - \int_0^d \mathbb{P}(\mathcal{T} \geq x)\, \mathrm{d}\mathcal{F}(x, B, \{\mu_i\}|_{i=1}^N) \\
=& 1 - \int_0^d \left[1 - \frac{\gamma(M, M\eta x)}{\Gamma(M)}\right] \mathrm{d}\mathcal{F}(x, B, \{\mu_i\}|_{i=1}^N) \\
=& \sum_{i=1}^N a_i \left[\int_0^d \int_0^{M\eta x} \frac{u^{M-1}e^{-u}}{\Gamma(M)} \mathrm{d}u\, \frac{\mu_i e^{-\mu_i x/B}}{B} \mathrm{d}x\right] + 1 - \mathcal{F}(d, B, \{\mu_i\}|_{i=1}^N) \\
\overset{(a)}{=}& \sum_{i=1}^N a_i \left[\frac{\gamma(M, M\eta d + \frac{\mu_i d}{B})}{\Gamma(M)} \left(\frac{M\eta}{M\eta + \frac{\mu_i}{B}}\right)^M - \frac{\gamma(M, M\eta d)}{\Gamma(M)} e^{-\frac{\mu_i d}{B}}\right] \\
& + 1 - \sum_{i=1}^N a_i \left(1 - e^{-\frac{\mu_i d}{B}}\right) \\
\overset{(b)}{=}& \sum_{i=1}^N a_i \left[\left(1 - \frac{\gamma(M, M\eta d)}{\Gamma(M)}\right) e^{-\frac{\mu_i d}{B}} + \frac{\gamma\left(M, M\eta d + \frac{\mu_i d}{B}\right)}{\Gamma(M)} \left(\frac{M\eta}{M\eta + \frac{\mu_i}{B}}\right)^M\right]
\end{aligned} \tag{3.41}$$

(a) holds from the definition of $\mathcal{F}(\cdot)$ in (3.6) and integration by parts. The equality (b) comes from the fact that $\sum_{i=1}^N a_i = 1$ (Property 1 by letting $x = 0$).

3.7.3 Proof of Corollary 3.4.2

As seen in Remark 10, equal rate allocation minimizes the overhead outage for a given sum rate. Under this backhaul setup, the CDF of delay $\mathcal{D}$ as in (3.5) is gamma distributed with CDF given as

$$\mathbb{P}(\mathcal{D} \leq d) = \frac{\gamma(N, \bar{\mu}d/B)}{\Gamma(N)}, \tag{3.42}$$

where $\bar{\mu} = \frac{\sum_{i=1}^{N} \mu_i}{N}$. Based on the proof of Theorem 3.4.1, we have

$$\begin{aligned} p_e &\geq 1 - \int_0^d \left[1 - \frac{\gamma(M, M\eta x)}{\Gamma(M)}\right] x^{N-1} \left(\frac{\bar{\mu}}{B}\right)^N \frac{e^{-\bar{\mu}x/B}}{\Gamma(N)} \mathrm{d}x \\ &= 1 - \frac{\bar{\mu}^N}{B^N (N-1)!} \sum_{k=0}^{M-1} \int_0^d \frac{(M\eta x)^k x^{N-1}}{k!} e^{-M\eta x - \bar{\mu}x/B} \mathrm{d}x \\ &\overset{(a)}{\geq} 1 - \min\left(\frac{\gamma(N, \bar{\mu}d/B)}{(N-1)!}, \sum_{k=0}^{M-1} \binom{k+N-1}{N-1} p^k (1-p)^N\right) \end{aligned}$$

where $p = \frac{M\eta}{M\eta + \bar{\mu}/B}$. Based on the argument in Remark 8, inequality (a) follows by letting $\eta = 0$ or $d = \infty$. For a given overhead requirement $(\mathfrak{T}, B, \mathfrak{D}, p_e)$, the value of $\bar{\mu}$ and N must satisfy

$$\begin{aligned} p_e &\geq 1 - \frac{\gamma(N, \bar{\mu}d/B)}{(N-1)!} \Rightarrow \bar{\mu} \geq \frac{B}{d} \gamma^{-1}\left((1-p_e)(N-1)!, N\right) \\ p_e &\geq 1 - \sum_{k=0}^{M-1} \binom{k+N-1}{N-1} p^k (1-p)^N \\ &\overset{(b)}{\geq} 1 - \binom{N+M-1}{N} (1-p)^N \\ &\overset{(c)}{\Rightarrow} \bar{\mu} \geq \frac{M\eta B \sqrt[N]{1-p_e}}{\sqrt[N]{\binom{M+N-1}{N}} - \sqrt[N]{1-p_e}} \end{aligned}$$

Inequality (b) follows from $p^k \leq 1$ and (c) holds by substituting back for p.

3.7.4 Proof of Theorem 3.5.1

The outage probability p_e in wireless signaling is

$$\begin{aligned} p_e &= 1 - \mathbb{P}(\mathcal{D} \leq d, \mathcal{D} \leq \mathcal{T}) \\ &= 1 - \int_0^d \mathbb{P}(\mathcal{T} \geq x) \mathrm{d}\mathbb{P}(\mathcal{D} \leq x) \\ &= 1 - \int_0^d \left[1 - \frac{\gamma(M, M\eta x)}{\Gamma(M)}\right] \mathrm{d}\mathbb{P}(\mathcal{D} \leq x) \\ &= \mathbb{P}(\mathcal{D} > d) + \frac{\gamma(M, M\eta d)}{\Gamma(M)} \mathbb{P}(\mathcal{D} \leq d) - \int_0^d \mathbb{P}(\mathcal{D} \leq x) \frac{1}{\Gamma(M)} \mathrm{d}\gamma(M, M\eta x) \end{aligned} \tag{3.43}$$

As BS_n belongs to the k^{th} tier, the wireless overhead delay is characterized as

$$\mathbb{P}(\mathcal{D} \leq x) = \mathbb{P}\left(\frac{B}{W \log(1 + \mathrm{SIR})} \leq x\right) = 1 - q_k(\beta(x))$$

where $\beta(x) = \exp\left(\frac{B \ln 2}{Wx}\right) - 1$. The outage probability p_e then follows.

3.7.5 Proof of Corollary 3.5.2

As shown in [81], the CDF $q_k\{\beta(d)\}$ is simplified under equal path loss exponents

$$q_{k,r}\{\beta(d)\} = 1 - \exp\left\{-\pi \left(\sum_{j=1}^{K} \lambda_j \hat{P}_j^{2/\alpha} r^2\right) \mathcal{Z}(\beta(d), \alpha)\right\},$$

where the function $\mathcal{Z}(\beta(d), \alpha)$ is

$$\begin{aligned} \mathcal{Z}(\beta(d), \alpha) &= [\beta(d)]^{\frac{2}{\alpha}} \int_{[\beta(d)]^{-\frac{2}{\alpha}}}^{\infty} \frac{1}{1 + u^{\frac{\alpha}{2}}} \mathrm{d}u \\ &\geq [\beta(d)]^{\frac{2}{\alpha}} \left[\int_0^{\infty} \frac{1}{1 + u^{\frac{\alpha}{2}}} \mathrm{d}u - \int_0^{[\beta(d)]^{-\frac{2}{\alpha}}} 1 \mathrm{d}u\right] \\ &= [\beta(d)]^{\frac{2}{\alpha}} \frac{2\pi}{\alpha} \csc \frac{2\pi}{\alpha} - 1. \end{aligned} \tag{3.44}$$

Using the bound immediately above in the lower bound of p_e, (3.33) follows.

Chapter 4

Downlink Coordinated Multi-Point With Overhead Modeling

To handle other-cell interference and improve the network capacity, one approach is coordinated multi-point communication, where multiple cells cooperate to improve the key quality-of-service metrics including network throughput (see [59] for an overview). Previous research studies the CoMP concept in conventional macrocell-only networks [30, 59, 70, 80, 133, 137]. However, two important aspects of existing works prevent their direct application to the new environment of HCNs.

The first one is the idealized assumption on overhead messaging among neighboring cells, i.e. assuming no inter-cell overhead delay. Not surprisingly, it results in promising predictions on CoMP performance such as multi-fold throughput gain [30, 58, 59, 70, 80, 133, 137]. However, inter-cell overhead delay is not trivial in typical cellular network [17, 20, 75, 114, 154], which leads to an irreducible performance bound in theory [98] and significant performance degradations in practice [17, 20, 75]. The importance of inter-cell overhead delay is further confirmed by latest industrial implementations, where the performance degradations are much smaller when inter-cell overhead channel

is particularly optimized (e.g. directly connecting base stations with gigabyte Ethernet) [20, 75]. Clearly, inter-cell overhead delay is an important performance limiting factor, and must be modelled and quantified in CoMP study [97]. However, this is not a trivial task in HCNs where different types of base stations (BSs) have very different backhaul capabilities and protocols [15, 20, 114, 154].

The second one is the SINR characterization. Previous works use the grid model or the Wyner model of base station locations to characterize the end-user's signal and other-cell interference in CoMP schemes. Unfortunately, neither model is suitable for HCNs because they assume base stations (BSs) are located on regular positions (e.g. locations form a hexagon [137, 166], a line [156] or a circle [80]) while small cells in HCNs have unplanned ad hoc locations. Besides, SINR characterization under these two models are inaccurate or intractable, or both. The Wyner model allows clean-form SINR results, to understand CoMP concept from information-theoretic perspective. However, this model is not accurate due to unrealistic assumptions on wireless channel and inter-cell interference [158]. On the other hand, the grid model of conventional macrocell networks is known to be intractable for SINR analysis [58]. In HCNs with additional tiers of overlaid small cells, the grid model becomes more complex and tractable SINR results are almost hopeless [48], not to mention a grid model for small cells is unlikely to be very realistic. In sum, previous models are incapable to capture the new characteristics of BS locations in HCNs, and new models are highly desired for accurate and

tractable SINR analysis.

4.1 Previous Work

Early theoretical literature completely ignores the impact of inter-cell overhead messaging in CoMP schemes, i.e. they assume that overhead messages have no quantization error and the overhead channel is delay-free with infinitely large capacity [30, 59, 70, 133, 137]. Such an ideal assumption is useful for the understanding of CoMP fundamentals, but obviously is far from reality in most practical cases. As a result, it causes highly over-optimistic predictions on the performance of CoMP schemes [17, 20, 75].

Practical issues of overhead messaging are considered in a few more recent works. The capacity limit of inter-cell overhead channel is considered especially in CoMP joint processing where user data is shared among cells [101, 131, 167]. The limited feedback model is widely used to characterize the quantization inaccuracy in overhead messages [78, 79, 96, 166]. However, the impact of overhead delay is either ignored or considered under a very simplified model – that is, a fixed delay model [9]. A more thorough review is presented in Chapter 3, which models overhead messaging in generic inter-cell coordination schemes. In short, appropriated modeling of overhead delay is still missing, to capture the imperfections of overhead channel such as congestion and hardware delays. In Chapter 3, various models on inter-cell overhead channels are proposed (e.g. backhaul and over-the-air overhead channels) and the respective delay distributions are derived. These modeling results are used

in this chapter to quantify the impact of overhead delay in CoMP performance.

Because the grid model and the Wyner model are obviously not suitable for SINR characterization in HCNs, several recent works focus on developing new models for BS locations [14, 48]. These works model the locations of BSs in HCNs as nodes in one or more spatial Poisson Point Processes (PPPs). Base station transceiver parameters (e.g. transmit power and path-loss exponent) become the mark of the respective node in the PPP. In this way, the PPP model characterizes the BS location randomness as well as the heterogeneity among different types of BSs. Previous studies on this PPP model show that, besides providing analytical tractability, the new model is at least as accurate as the hexagon-grid model in characterizing the SINR distribution [14, 25, 48, 142]. Therefore, some in industry have begun to use it for SINR characterization in HCNs [105].

4.2 Contributions

This paper evaluates downlink CoMP in HCNs, using appropriate models of inter-cell overhead delay and BS locations. We first develop a new analytical framework for the evaluation of a class of CoMP schemes without user data sharing among cells. This framework quantifies the impact of inter-cell overhead delay in HCNs by using our previous results on the delay distributions under various overhead channel configurations. Note that this framework includes previous CoMP analysis without overhead delay modeling as a special case. Therefore it can be used to explain the performance gaps between

previous analytical predictions and real implementations of CoMP.

To concretely illustrate the usage of this framework, we apple it to a specific scheme: downlink CoMP inter-cell interference cancellation (ICIC), where coordinated cells employ zero-forcing (ZF) precoders to cancel their mutual interference. CoMP ICIC has been studied in macrocell networks before [42, 79, 80, 166] and is attracting industrial implementation efforts [20]. We derive upper and lower bounds on the end-user SIR distribution for CoMP ICIC in HCNs, using the spatial PPP model to characterize other-cell interference from all BSs in the entire plane. These bounds are closed-form and show clear dependence on important parameters such as the overhead message bit size and the number of coordinated cells. Using this SIR characterization along with the CoMP evaluation framework, we quantify the downlink CoMP ICIC coverage and throughput as functions of overhead messaging configurations. Compared with previous work, our results provide new design insights for CoMP ICIC, for example, on the best number of coordinated cells and the appropriate configuration of overhead channels.

4.3 System Model

4.3.1 Downlink Heterogeneous Cellular Network Modeling

In a K-tier HCN, BSs of the k-th tier have transmit power P_k, number of antennas N_k, path loss exponent α_k and spatial density λ_k BSs per unit area. For example, compared with macrocells, femtocells typically have much lower transmit power, fewer antennas and eventually a much higher spatial

density as tens to hundreds of femtocells will often be deployed in the area of a macrocell [15].

We consider a typical end-user equipped with a single antenna. In the following, we simply call this typical user *the end-user* for convenience. We denote its location as the origin and the locations of BSs as $\{X_{i,k}, k = 1, 2 \ldots, K,\ i \in \mathbb{N}\}$, where $X_{i,k}$ is the location of the i^{th} closest BS to the origin in the k^{th} tier. The same as Chapter 3, we assume all tiers are independently distributed on the plane $\mathbb{R}^2$ and BSs in the k^{th} tier are distributed according to homogeneous Poisson Point Process (PPP) Φ_k with intensity λ_k.

For the purpose of cell association, the end-user will listen to the downlink pilot signals from different BSs, and measure their long-term average powers. With short-term fading averaged out, the end-user will associate with the BS from whom it receives the strongest average power $\max\limits_{k=1,2\ldots,K, i\in\mathbb{N}} \{P_k |X_{i,k}|^{-\alpha_k}\}$. The index of the selected serving BS is

$$\{i^\star, k^\star\} = \arg \max_{k=1,2,\ldots K,\ i\in\mathbb{N}} \{P_k |X_{i,k}|^{-\alpha_k}\} = \arg \max_{k=1,2,\ldots,K} \{i^\star = 1, P_k |X_{1,k}|^{-\alpha_k}\}. \tag{4.1}$$

Therefore, we denote the selected serving BS as $\mathrm{BS}_{1,k^\star}$. In CoMP ICIC, suppose $\mathrm{BS}_{1,k^\star}$ cancels its interference to $L_{1,k^\star}$ other cells. Denote the set of these $L_{1,k^\star}$ cells as $\mathcal{S}_{1,k^\star}$, which we call *the coordination set of* $\mathrm{BS}_{1,k^\star}$. In this work, we consider a pair-wise fair coordination strategy, that is, $\mathrm{BS}_{1,k^\star}$ cancels its interference to another base station $\mathrm{BS}_{i,k}$, if and only if $\mathrm{BS}_{i,k}$ cancels its interference to $\mathrm{BS}_{1,k^\star}$ as well [67, 92]. Therefore, all the $L_{1,k^\star}$ cells in $\mathcal{S}_{1,k^\star}$ cancel

their interference to $\mathrm{BS}_{1,k^\star}$. Previous work usually assumes that, besides cancelling their interference to $\mathrm{BS}_{1,k^\star}$, all the $L_{1,k^\star}$ cells in $\mathcal{S}_{1,k^\star}$ cancel their mutual interference as well [11, 71, 166]. We do not have such a restrictive assumption in our analysis.

To make the following analysis general, we do not specify how $\mathrm{BS}_{1,k^\star}$ selects its coordination set $\mathcal{S}_{1,k^\star}$. Its selection criterion can be based on various considerations (possibly distinct from others), such as the interference powers or locations of other cells [11, 71, 79, 166], or game theory related concerns [67, 92]. However, there is one feasibility constraint for CoMP ICIC on the value of $L_{1,k^\star}$ [10, 11]

$$L_{1,k^\star} < N_{k^\star}, \tag{4.2}$$

where $N_{k^\star}$ is the number of antennas at $\mathrm{BS}_{1,k^\star}$.

4.3.2 Overhead Messaging in CoMP Schemes

In this chapter, we investigate the impact of realistic inter-cell overhead signaling on a class of CoMP schemes, where an end-user is served by only one BS without user data sharing among coordinated cells. To cooperate with the serving cell, a coordinated BS $\mathrm{BS}_{i,k} \in \mathcal{S}_{1,k^\star}$ needs to be updated with certain key parameters in that cell. The choices of these cooperation-dependent parameters are different among various CoMP schemes, with common examples being user channel states and user scheduling information. These parameters naturally fluctuate over time because of the dynamics in network environment and user mobility.

Assumption 10. (i.i.d. block model) We assume the cooperation-dependent parameters stay constant for a time $\mathcal{T}_{i,k}$ (which can be either *deterministic* or *random*) and then change to a new i.i.d. value. We denote $\eta_{i,k} = 1/\mathbb{E}[\mathcal{T}_{i,k}]$ as the average change rate.

This assumption is true for parameters such as user scheduling information, which are determined by BSs and stays constant per transmission time interval (TTI). On the other hand, parameters such as channel fading may change continuously. However, the i.i.d. block fading model on channel fading (named *block fading* model in other literature) is fairly accurate and widely used [96, 148].

We assume a general gamma distribution on $\mathcal{T}_{i,k}$ in Assumption 10

$$\mathcal{T}_{i,k} \sim \text{Gamma}\left(M, \frac{1}{M\eta_{i,k}}\right), \tag{4.3}$$

where M is the parameter. See Chapter 3 for justification and more details about this model. Note that $\mathbb{E}[\mathcal{T}_{i,k}] = \frac{1}{\eta_{i,k}}$ is unchanged under various values of M. This general distribution with different values of M can model different scenarios from deterministic process (i.e. $\mathcal{T}_{i,k}$ becomes deterministic as $M \to \infty$) to Poisson process (i.e. $\mathcal{T}_{i,k}$ is exponentially distributed for $M = 1$).

Because of the dynamics of these cooperation-dependent parameters, the end-user or its serving cell needs to detect the changes in their values. Several parameters like user scheduling information are determined by the BS and their values are thus known on real-time basis. For other parameters such

as channel fading, the end-user can constantly measure their values through frequent pilot signals. Once the values of the parameters change, an overhead message will then be generated and sent. In this way, the overhead message will be updated every $\mathcal{T}_{i,k}$, a sufficient frequency without unnecessary burden on the overhead channel.

After being generated by the serving base station $\mathrm{BS}_{1,k^\star}$, an overhead message is transmitted to $\mathrm{BS}_{i,k}$ through inter-cell overhead channel. The overhead channel incurs delay denoted as $\mathcal{D}_{i,k}$. With this updating overhead message, $\mathrm{BS}_{i,k}$ can take the appropriate cooperation strategy accordingly. Note that each overhead message only has a lifetime of $\mathcal{T}_{i,k}$, because the parameters change after $\mathcal{T}_{i,k}$ and a new overhead message is generated.

We now consider overhead design in CoMP ICIC, where coordinated neighboring BSs use zero-forcing precoders to null their mutual interference [59, 79, 166]. Therefore, the cooperation-dependent parameter in CoMP ICIC is the channel direction information (CDI)

$$\tilde{\mathbf{h}}_{i,k} \triangleq \frac{\mathbf{h}_{i,k}}{\|\mathbf{h}_{i,k}\|}, \tag{4.4}$$

where $\mathbf{h}_{i,k}$ is the $N_k \times 1$ fading vector between $\mathrm{BS}_{i,k}$ and the end-user. We assume uncorrelated Rayleigh fading, i.e. each component of $\mathbf{h}_{i,k}$ is i.i.d. complex Gaussian $\mathcal{CN}(0,1)$. According to Assumption 10, the fading $\mathbf{h}_{i,k}$ stays constant for a time $\mathcal{T}_{i,k}$ and then changes independently, i.e. block fading [148]. In this specific example, $\mathcal{T}_{i,k}$ is the channel coherence time.

In the beginning of each fading block, the end-user observes the new

fading value $\mathbf{h}_{i,k}$. It searches through a codebook $\mathcal{C}_{i,k}$ known by both itself and $\mathrm{BS}_{i,k}$, which consists of $2^{B_{i,k}}$ codewords. From the codebook $\mathcal{C}_{i,k}$, the end-user will choose the codeword $\mathbf{c}_{i,k}$ closest to current fading direction $\tilde{\mathbf{h}}_{i,k}$ such that $|\tilde{\mathbf{h}}_{i,k}\mathbf{c}_{i,k}|$ is maximized. The index of this selected codeword $\mathbf{c}_{i,k}$ is fed back to $\mathrm{BS}_{1,k^\star}$ using $B_{i,k}$ bits. For $\mathrm{BS}_{1,k^\star}$, the overhead messages form an arrival process with inter-arrival time $\mathcal{T}_{i,k}$. The serving BS $\mathrm{BS}_{1,k^\star}$ then transmits these overhead messages to $\mathrm{BS}_{i,k}$ through an inter-cell overhead channel. Based on the received overhead, $\mathrm{BS}_{i,k}$ chooses a zero-forcing precoding vector $\mathbf{f}_{i,k}$ such that $|\mathbf{f}_{i,k}\,\mathbf{c}_{i,k}|^2 = 0$. See Fig. 4.1 for a conceptual plot of overhead messaging in CoMP ICIC.

4.3.3 The Impact of Overhead Delay

Realistic overhead messaging has two major imperfections – delay and quantization inaccuracy. To make the discussion more concrete, we describe the impact of overhead delay in the context of CoMP ICIC, while the situations in other CoMP schemes are similar. The delay $\mathcal{D}_{i,k}$ of an overhead message is defined as the time between when that overhead is generated (i.e. the beginning of the respective fading block) and when it is received by $\mathrm{BS}_{i,k}$. It is caused by unavoidable propagation time and the imperfections of the overhead channel such as congestion and hardware delays. We call this time window the *overhead messaging phase*. If the overhead delay $\mathcal{D}_{i,k}$ is smaller than the fading block length $\mathcal{T}_{i,k}$, we call the rest time $\mathcal{T}_{i,k} - \mathcal{D}_{i,k}$ in that fading block the *cooperation phase*. Note that the cooperation phase may not exist in a

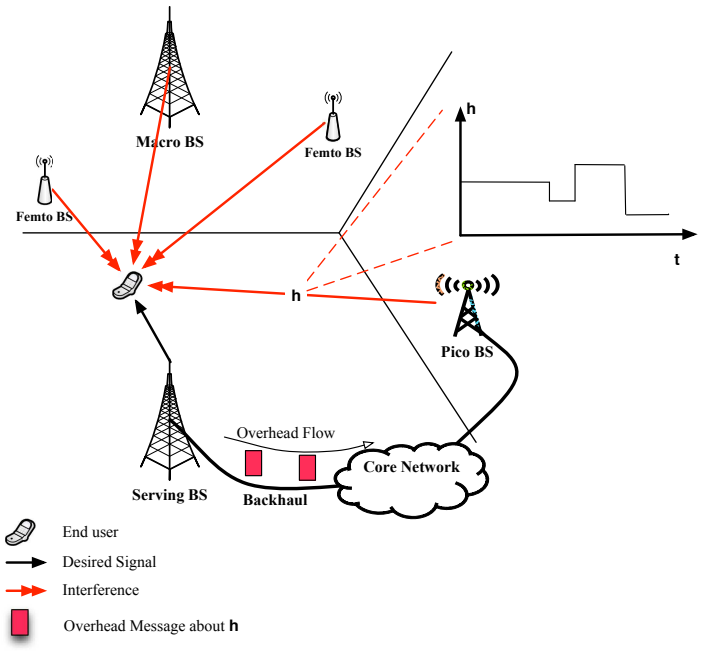

Figure 4.1: A conceptual plot of CoMP ICIC in a heterogeneous cellular network. The end-user's serving BS coordinates with a pico BS, which requires frequent overhead messaging between them regarding current fading value $\mathbf{h}$.

fading block if the overhead delay $\mathcal{D}_{i,k}$ is larger than $\mathcal{T}_{i,k}$. See Fig. 4.2 for an example.

The interference from $\text{BS}_{i,k}$ is different between these two phases. In the overhead messaging phase, the channel fading $\mathbf{h}_{i,k}$ has already changed but $\text{BS}_{i,k}$ does not know its value yet. Therefore the zero-forcing precoder $\mathbf{f}_{i,k}$ is still determined from previously received overhead message. According to Assumption 10, the current fading state $\mathbf{h}_{i,k}$ is independent of the previous fading block and thus the precoder $\mathbf{f}_{i,k}$ based on it. Therefore, statistically the interference $|\mathbf{f}_{i,k}\mathbf{h}_{i,k}|^2$ is not reduced in the overhead message phase, which is

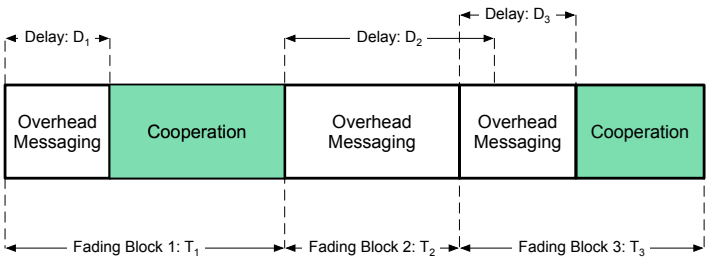

Figure 4.2: Overhead messaging phases and cooperation phases of a coordinated BS in CoMP ICIC. The overhead message phase starts from the beginning of each fading block and has a time length of overhead delay $\mathcal{D}$. In a fading block, the coordinated BS will have cooperation phase only if the overhead delay $\mathcal{D}$ is smaller than the fading block length $\mathcal{T}$.

the worst-case interference scenario [78, 96].

On the other hand, $\text{BS}_{i,k}$ receives the new overhead message in the cooperation phase and adjusts its zero-forcing precoder $\mathbf{f}_{i,k}$ accordingly. Because of Assumption 10, the fading value $\mathbf{h}_{i,k}$ is assumed to keep unchanged during this block. Therefore the new overhead message remains accurate (minus quantization errors) in the cooperation phase and the selected precoder $\mathbf{f}_{i,k}$ minimizes the interference $|\mathbf{f}_{i,k}\mathbf{h}_{i,k}|^2$ for the entire phase [78, 96]. This is the best-case interference scenario.

It is seen that Assumption 10 simplifies the impact of overhead delay into two opposite extreme cases: the interference to $\text{BS}_{i,k}$ is either not reduced in the overhead messaging phase or maximally reduced in the cooperation phase. In practice, the channel fading $\mathbf{h}_{i,k}$ continuously changes with temporal correlation, instead of the i.i.d. block fading model in Assumption 10. Therefore, the interference from $\text{BS}_{i,k}$ should gradually change over time and

is in fact bounded by the two extreme cases. However, it is hard to quantify mathematically. We use Assumption 10 because it is tractable for analysis, widely used in previous literature on MIMO systems [96,148] and allows a first-order analysis on the impact of overhead delay. Future work should consider more complicated models on channel fading, such as discrete time Markov models in [9, 76, 153].

4.3.4 The Impact of Overhead Quantization Error

Another concern of realistic overhead messaging is the finite overhead quantization bits $B_{i,k}$. Larger $\mathrm{B}_{i,k}$ usually translates into smaller quantization error and thus higher cooperation gains. However, the exact impact of $\mathrm{B}_{i,k}$ depends on the specific CoMP scheme and the overhead codebook $\mathcal{C}_{i,k}$. See [96] for an overview. We now discuss its impact in the context of CoMP ICIC.

The end-user's SIR γ in CoMP ICIC can be generally expressed as[1]

$$\gamma = \frac{P_{k^\star}|X_{1,k^\star}|^{-\alpha_{k^\star}}|\mathbf{f}_{1,k^\star}\mathbf{h}_{1,k^\star}|^2}{\sum_{X_{i,k}\in\bigcup_{k=1}^{K}\Phi_k\setminus\{X_{1,k^\star}\}} P_k|X_{i,k}|^{-\alpha_k}|\mathbf{f}_{i,k}\mathbf{h}_{i,k}|^2}, \tag{4.5}$$

where the value of $|\mathbf{f}_{i,k}\mathbf{h}_{i,k}|$ is elaborated on in the following.

1. The end-user's serving BS $\mathrm{BS}_{1,k^\star}$ needs to null its interference to the $L_{1,k^\star}$ coordinated cells. Meanwhile it also wants to maximize the signal power

[1] In modern cellular networks, thermal noise is not an important consideration either in cell interior where the signal power is strong or in cell edge where interference is usually much larger. Interference is more dominant especially in HCNs because of additional overlaid cells with high spatial densities. We therefore neglect thermal noise and consider SIR.

$|\mathbf{f}_{1,k^\star}\mathbf{h}_{1,k^\star}|^2$ to the end-user. Thus its precoder $\mathbf{f}_{1,k^\star}$ is chosen such that $|\mathbf{f}_{1,k^\star}\mathbf{h}_{1,k^\star}|^2 \sim \chi^2_{2N_{k^\star}-2L_{1,k^\star}}$ [79, 166].

2. A coordinated BS $\mathrm{BS}_{i,k} \in \mathcal{S}_{1,k^\star}$ cannot null its interference during the overhead messaging phase, because its zero-forcing precoder $\mathbf{f}_{i,k}$ is independent of $\tilde{\mathbf{h}}_{i,k}$ and we have $|\mathbf{f}_{i,k}\mathbf{h}_{i,k}|^2 \sim \chi^2_2$. In the cooperation phase, $\mathrm{BS}_{i,k}$ receives the updated overhead indicating the codeword $\mathbf{c}_{i,k} = \arg\max_{\mathbf{c}\in\mathcal{C}_{i,k}} |\tilde{\mathbf{h}}_{i,k}\mathbf{c}|$ and chooses $\mathbf{f}_{i,k}$ such that $|\mathbf{f}_{i,k}\,\mathbf{c}_{i,k}|^2 = 0$. However, because $\mathbf{c}_{i,k}$ is not the exact CDI $\tilde{\mathbf{h}}_{i,k}$, the value of $|\mathbf{f}_{i,k}\mathbf{h}_{i,k}|^2$ is still positive and dependent on the design of overhead codebook $\mathcal{C}_{i,k}$. In this chapter, we assume random vector quantization (RVQ) codebook $\mathcal{C}_{i,k}$, which is commonly used in previous CoMP ICIC [78, 79, 96, 166]. Under this assumption, we then have $|\mathbf{f}_{i,k}\mathbf{h}_{i,k}|^2 \sim 2^{-\frac{B_{i,k}}{N_k-1}}$ for $\mathrm{BS}_{i,k}$ in the cooperation phase.

3. A non-coordinated BS $\mathrm{BS}_{i,k} \notin \mathcal{S}_{1,k^\star}$ chooses the precoder independent of its interference to the end-user, and will have $|\mathbf{f}_{i,k}\,\mathbf{h}_{i,k}|^2 \sim \chi^2_2$.

Based on the derivations above, the end-user SIR can be expressed as

$$\gamma = \frac{P_{k^\star} S_{1,k^\star} |X_{1,k^\star}|^{-\alpha_{k^\star}}}{\sum_{X_{i,k}\in \bigcup_{k=1}^{K} \Phi_k \setminus \{X_{1,k^\star}\}} P_k \rho_{i,k} S_{i,k} |X_{i,k}|^{-\alpha_k}} \tag{4.6}$$

where $S_{1,k^\star} \sim \chi^2(2N_{k^\star} - 2L_{1,k^\star})$, $S_{i,k} \sim \chi^2_2$, and $\rho_{i,k}$ is the *interference cancellation factor* for $\mathrm{BS}_{i,k}$

$$\rho_{i,k} = \begin{cases} 1 & \text{For } \mathrm{BS}_{i,k} \notin \mathcal{S}_{1,k^\star} \\ 1 & \text{For } \mathrm{BS}_{i,k} \in \mathcal{S}_{1,k^\star} \text{ during the overhead messaging phase} \\ 2^{-\frac{B_{i,k}}{N_k-1}} & \text{For } \mathrm{BS}_{i,k} \in \mathcal{S}_{1,k^\star} \text{ during the cooperation phase} \end{cases} \tag{4.7}$$

4.4 CoMP Throughput Evaluation With Imperfect Overhead Messaging

In this section, we present a throughput evaluation framework for a class of downlink CoMP schemes, where inter-cell overhead messaging does not include user data. Common examples in this category include CoMP beamforming [42, 79, 166] and interference alignment [30]. The general framework considers the practical issues from overhead messaging but is also analytically tractable.

Lemma 4.4.1. *The long-term time fraction $\tau_{i,k}$ that a coordinated BS $\mathrm{BS}_{i,k}$ is in the cooperation phase is*

$$\tau_{i,k} = p(\mathcal{T}_{i,k}, \infty) - \eta_{i,k} \int_0^\infty \{p(\mathcal{T}_{i,k}, \infty) - p(\mathcal{T}_{i,k}, s)\} \, \mathrm{d}s, \tag{4.8}$$

where $p(\mathcal{T}_{i,k}, s) \triangleq \mathbb{P}(\mathcal{D}_{i,k} \leq \mathcal{T}_{i,k}, \mathcal{D}_{i,k} \leq d)$ is overhead delay distribution.

Proof. See Appendix 4.9.1. □

In Chapter 3, we provide general models on overhead messaging delay for both backhaul and over-the-air inter-cell overhead channels. We then derive the delay distribution $p(\cdot)$ as an explicit function of inter-cell overhead channel parameters (e.g. over-the-air overhead channel bandwidth). Note that our overhead delay models only affect the characterization of $p(\cdot)$, while the result in Lemma 4.4.1 holds under various forms of delay distribution $p(\cdot)$.

In previous literature, no overhead delay is considered, i.e. delay $\mathcal{D}_{i,k} = 0$ and thus $p(\mathcal{T}_{i,k}, s) = 1$ for any s and $\mathcal{T}_{i,k}$. Under this condition, $\tau_{i,k}$ in

(4.8) becomes 1 as well, which means $\mathrm{BS}_{i,k}$ is always in the cooperation phase with interference maximally reduced. This is obviously an over-optimistic prediction on the interference.

Theorem 4.4.2. *For CoMP schemes without user data sharing, the end-user's long-term throughput is*

$$\mathcal{R} = \sum_{\mathcal{S} \subset \mathcal{S}_{1,k^\star}} p_{\mathcal{S}} R(\gamma_{\mathcal{S}}), \tag{4.9}$$

where the summation is over all possible subset $\mathcal{S} \subset \mathcal{S}_{1,k^\star}$, $\gamma_{\mathcal{S}}$ is the end-user SIR when BSs $\in \mathcal{S}$ are in the cooperation phase and BSs $\in \mathcal{S}_{1,k^\star} \setminus \mathcal{S}$ are in the overhead messaging phase, $R(\cdot)$ is the SIR-rate mapping function, and

$$p_{\mathcal{S}} = \left(\prod_{\mathrm{BS}_{i,k} \in \mathcal{S}} \tau_{i,k} \prod_{\mathrm{BS}_{i,k} \in \mathcal{S}_{1,k^\star} \setminus \mathcal{S}} (1 - \tau_{i,k}) \right), \tag{4.10}$$

Proof. Due to the overhead messaging delay, each coordinated BS $\mathrm{BS}_{i,k} \in \mathcal{S}_{1,k^\star}$ now has two states: 1) the overhead messaging phase (with probability $1 - \tau_{i,k}$) when the overhead message at $\mathrm{BS}_{i,k}$ is already outdated and the updated overhead has not been received yet; and 2) the cooperation phase (with probability $\tau_{i,k}$) when $\mathrm{BS}_{i,k}$ receives the updated overhead message. $\mathrm{BS}_{i,k}$ has different cooperation performance between these two states, for example, as shown in (4.7) for CoMP ICIC. Therefore, we use a subset $\mathcal{S} \subset \mathcal{S}_{1,k^\star}$ to denote the scenario that only BSs $\in \mathcal{S}$ are in the cooperation phase. The probability of this scenario is

$$p_{\mathcal{S}} = \left(\prod_{\mathrm{BS}_{i,k} \in \mathcal{S}} \tau_{i,k} \prod_{\mathrm{BS}_{i,k} \in \mathcal{S}_{1,k^\star} \setminus \mathcal{S}} (1 - \tau_{i,k}) \right). \tag{4.11}$$

Each subset $\mathcal{S} \subset \mathcal{S}_{1,k^\star}$ corresponds to a possible scenario regarding which coordinated BSs are in the cooperation phase. The end-user's long-term is the average rate over all possible scenarios. □

As shown in (4.9), the CoMP throughput evaluation framework explicitly quantifies the impact of overhead delay through the time fraction $\tau_{i,k}$ and probability distribution $p_{\mathcal{S}}$. It also includes the impact of finite overhead bit size because the end-user SIR $\gamma_{\mathcal{S}}$ is affected by overhead quantization error, for example, as shown in (4.7) for CoMP ICIC. In this way, the framework considers the imperfections in the overhead messaging. Combined with the SIR characterizations, it can be used to quantify the throughput and coverage of different CoMP schemes.

As we mentioned before, previous work does not fully consider practical issues in inter-cell overhead messaging. In particular, they ignore the overhead delay, which is in fact non-trivial in most network environments [17,20,154]. To show the importance of modeling and analysing overhead delay in CoMP evaluation, we compare the result in Theorem 4.4.2 with previous work. Without overhead delay, the coordinated BSs always have the updated overhead and stay in the cooperation phase. Obviously, this is an idealized special case of Theorem 4.4.2.

Corollary 4.4.3. *Under the assumption of delay-free overhead messaging, the long-term CoMP throughput is*

$$\mathcal{R} = R(\gamma_{\mathcal{S}_{1,k^\star}}), \tag{4.12}$$

where $\gamma_{\mathcal{S}_{1,k^\star}}$ is defined in Theorem 4.4.2.

Proof. When overhead messaging has no delay, all coordinated BSs will always be in the cooperation phase, i.e. $\tau_{i,k} = 1$ for each $\text{BS}_{i,k} \in \mathcal{S}_{1,k^\star}$. Therefore we have $p_{\mathcal{S}} = 1$ if $\mathcal{S} = \mathcal{S}_{1,k^\star}$ and $p_{\mathcal{S}} = 0$ otherwise. The end-user's rate is then $\mathcal{R} = R(\gamma_{\mathcal{S}_{1,k^\star}})$. □

As shown in Corollary 4.4.3, assuming no overhead delay significantly simplifies the analysis of CoMP schemes. However, as we elaborated before and will be shown in the numerical simulations, this assumption is far from the reality and causes the wide gaps between analytical predictions and realistic implementations.

4.5 CoMP Inter-cell Interference Cancellation Throughput Analysis

In this section, we derives the distribution of the end-user's SIR $\gamma_{\mathcal{S}}$ for CoMP ICIC, which will be used with the evaluation framework in Theorem 4.4.2 to quantify the CoMP ICIC throughput. We first derive the SIR CDF in 1-tier cellular networks in Theorem 4.5.1, and then extend it to the general HCN scenario in Theorem 4.5.2.

For now, we simplify the notation for 1-tier cellular networks by dropping the tier index k. Specifically in 1-tier networks, the BSs have the same transmit power P, number of antennas N and path loss exponent α. Their locations $\{X_i, i \in \mathbb{N}\}$ form a PPP Φ with intensity λ. Therefore the serving BS

is simply BS_1, the nearest BS to the end user. In CoMP ICIC, we denote its coordination set as $\mathcal{S}_1$ and the number of these coordinated cells as $L_1 = |\mathcal{S}_1|$. Similarly, we now use notation ρ_i and B_i as simplified versions of $\rho_{i,k}$ and $B_{i,k}$ in (4.7).

In 1-tier networks, the end-user SIR $\gamma_{\mathcal{S}}$ in (4.9) can be simplified as

$$\gamma_{\mathcal{S}} = \frac{PS_1|X_1|^{-\alpha}}{\sum\limits_{X_i \in \Phi \setminus \{X_1\}} P\rho_i S_i |X_i|^{-\alpha}} = \frac{S_1|X_1|^{-\alpha}}{\sum\limits_{X_i \in \Phi \setminus \{X_1\}} \rho_i S_i |X_i|^{-\alpha}}. \tag{4.13}$$

where $\rho_i = 2^{\frac{B_i}{N-1}}$ for $\mathrm{BS}_i \in \mathcal{S}$ and $\rho_i = 1$ otherwise.

Theorem 4.5.1. *In 1-tier cellular networks, the CDF of the end-user SIR $\gamma_{\mathcal{S}}$ in (4.9) is bounded as*

$$\mathbb{P}(\gamma_{\mathcal{S}} \leq \beta) \begin{cases} \leq \frac{\beta}{N-L_1-1} \sum\limits_{i=2}^{\infty} \rho_i \frac{\Gamma\left(1+\frac{\alpha}{2}\right)(i-1)!}{\Gamma\left(i+\frac{\alpha}{2}\right)} \\ \geq 1 - \exp\left\{ -\Gamma(1+2/\alpha) \left[\frac{(N-L_1)\Gamma(1-\alpha/2)}{\beta[3^{-\alpha}\rho_{\min} + (2l+3)^{-\alpha}(1-\rho_{\min})]} \right]^{-2/\alpha} \right\} \end{cases} \tag{4.14}$$

where $l = |\mathcal{S}|$ is the cardinality of the set $\mathcal{S}$, $\rho_{\min} = \min\limits_{\mathrm{BS}_i \in \mathcal{S}} \{\rho_i\}$, and

$$\rho_i = \begin{cases} 1 & \mathrm{BS}_i \notin \mathcal{S} \\ 2^{-\frac{B_i}{N-1}} & \mathrm{BS}_i \in \mathcal{S} \end{cases} \tag{4.15}$$

Proof. We denote the normalized interference (normalized by P) as

$$I_{\mathcal{S}} \stackrel{\triangle}{=} \sum_{X_i \in \Phi \setminus \{X_1\}} \rho_i S_i |X_i|^{-\alpha} = \sum_{\mathrm{BS}_i \in \mathcal{S}} \rho_i S_i |X_i|^{-\alpha} + \sum_{X_i \in \Phi \setminus \{X_1 \bigcup \mathcal{S}\}} S_i |X_i|^{-\alpha}. \tag{4.16}$$

The last equality comes from the definition of $\mathcal{S}$.

Upper Bound: For a PPP $\Phi = \{X_1, X_2, \ldots\}$ in $\mathbb{R}^2$ with an arbitrary density λ, $\{|X_1|^2, |X_2|^2, \ldots\}$ form a one dimensional PPP with intensity $\pi\lambda$. We thus have

$$\mathbb{E}\left[\frac{|X_1|^\alpha}{|X_i|^\alpha}\right] = \mathbb{E}\left[\left(\frac{|X_1|^2}{|X_i|^2}\right)^{\alpha/2}\right] = \frac{\Gamma\left(1+\frac{\alpha}{2}\right)(i+1)!}{\Gamma\left(i+\frac{\alpha}{2}\right)}, \tag{4.17}$$

where the last equality holds from Appendix 4.9.2. The rest of the proof is similar to Theorem 1 in [10], and thus omitted here.

Lower Bound: Let $I_{(m)} = \sum_{X_i \in \Phi \setminus \{X_1,\ldots,X_m\}} S_i |X_i|^{-\alpha}$. In other words, $I_{(m)}$ is the sum interference experienced by the end-user, if the nearest m BSs (including the serving BS) are removed or turned off. Note that $I_{(0)}$ means that the end-user is not associated with any BS, and experiences interference from all the BSs in the PPP Φ. Denote $l = |\mathcal{S}|$ as the cardinality of $\mathcal{S}$ and $\rho_{\min} = \min_{\mathrm{BS}_i \in \mathcal{S}}\{\rho_i\}$. The actual interference $I_{\mathcal{S}}$ can be expressed as a function of $I_{(m)}$

$$\begin{aligned}
I_{\mathcal{S}} &\geq \sum_{\mathrm{BS}_i \in \mathcal{S}} \rho_{\min} S_i |X_i|^{-\alpha} + \sum_{X_i \in \Phi \setminus \{X_1 \bigcup \mathcal{S}\}} S_i |X_i|^{-\alpha} \\
&\overset{(b)}{\succeq} \sum_{\mathrm{BS}_i \in \{\mathrm{BS}_2,\ldots,\mathrm{BS}_{l+1}\}} \rho_{\min} S_i |X_i|^{-\alpha} + \sum_{X_i \in \Phi \setminus \{X_1,\ldots,X_{l+1}\}} S_i |X_i|^{-\alpha} \\
&= \rho_{\min} \sum_{X_i \in \Phi \setminus \{X_1\}} S_i |X_i|^{-\alpha} + (1-\rho_{\min}) \sum_{X_i \in \Phi \setminus \{X_1,\ldots,X_{l+1}\}} S_i |X_i|^{-\alpha} \\
&= \rho_{\min} I_{(1)} + (1-\rho_{\min}) I_{(l+1)} \\
&\overset{(c)}{\succeq} \left[3^{-\alpha}\rho_{\min} + (2l+3)^{-\alpha}(1-\rho_{\min})\right] I_{(0)}
\end{aligned} \tag{4.18}$$

where $\succeq$ means stochastic dominance. In the right hand side of (b), we assume the strongest l interfering BSs are cancelling their interference, instead of the

l BSs in the set of $\mathcal{S}$. Therefore it is a lower bound on the interference $I_{\mathcal{S}}$. (c) holds from Appendix 4.9.3 deriving the lower bound of an arbitrary $I_{(m)}$.

Based on the lower bound on interference I, the SIR CDF can be lower bounded as follows

$$\mathbb{P}\left(\gamma = \frac{S_1|X_1|^{-\alpha}}{I_{\mathcal{S}}} \leq \beta\right) \geq \mathbb{P}\left(\frac{S_1|X_1|^{-\alpha}}{\left[3^{-\alpha}\rho_{\min} + (2l+3)^{-\alpha}(1-\rho_{\min})\right] I_{(0)}} \leq \beta\right)$$
$$\overset{(d)}{\geq} 1 - \mathbb{E}\left[e^{-A(Z)}\right] \tag{4.19}$$

where $Z \triangleq \frac{S_1|X_1|^{-\alpha}}{\beta[3^{-\alpha}\rho_{\min}+(2l+3)^{-\alpha}(1-\rho_{\min})]}$, $A(Z) = \pi\lambda\Gamma(1+\frac{2}{\alpha})Z^{-\frac{2}{\alpha}}$, and (d) holds from Theorem 1 in [94]. The CDF lower bound is then derived as

$$\begin{aligned}\mathbb{P}(\gamma_{\mathcal{S}} \leq \beta) &\geq 1 - \mathbb{E}\left[e^{-A(Z)}\right] \\ &\overset{(e)}{\geq} 1 - \exp\left\{-\pi\lambda\Gamma(1+2/\alpha)(\mathbb{E}[Z])^{-\frac{2}{\alpha}}\right\} \\ &= 1 - \exp\left\{-\Gamma(1+2/\alpha)\left[\frac{(N-L_1)\Gamma(1-\alpha/2)}{\beta\left[3^{-\alpha}\rho_{\min} + (2l+3)^{-\alpha}(1-\rho_{\min})\right]}\right]^{-2/\alpha}\right\},\end{aligned} \tag{4.20}$$

where (e) holds from Jensen's inequality. □

Based on the results in Theorem 4.5.1 for the 1-tier networks, we now characterize the end-user's SIR $\gamma_{\mathcal{S}}$ in a general K-tier HCN.

Theorem 4.5.2. *In a general K-tier heterogeneous cellular network, the CDF*

of the end-user SIR $\gamma_{\mathcal{S}}$ in (4.9) is bounded as

$$\mathbb{P}\left[\gamma_{\mathcal{S}} \leq \beta\right] \begin{cases} \leq \frac{\beta}{N_{k^\star}-L_{1,k^\star}-1}\left[\sum\limits_{i=2}^{\infty}\rho_{i,k^\star}\frac{\Gamma\left(1+\frac{\alpha_{k^\star}}{2}\right)(i-1)!}{\Gamma\left(i+\frac{\alpha_{k^\star}}{2}\right)}+\sum\limits_{\substack{k=1\\k\neq k^\star}}^{K}\frac{P_k}{P_{k^\star}}\sum\limits_{i=1}^{\infty}\rho_{i,k}\frac{(\lambda_{k^\star}\pi)^{-\frac{\alpha_{k^\star}}{2}}\Gamma\left(1+\frac{\alpha_{k^\star}}{2}\right)(i-1)!}{(\lambda_k\pi)^{\frac{-\alpha_k}{2}}\Gamma\left(i+\frac{\alpha_k}{2}\right)}\right] \\ \geq 1-\exp\left[-\left(\pi\hat{\lambda}\right)^{1-\frac{\alpha_{k^\star}}{\alpha_{\max}}}\Gamma\left(1+\frac{2}{\alpha_{\max}}\right)\left(\frac{(N_{k^\star}-L_{1,k^\star})\Gamma\left(1-\frac{\alpha_{k^\star}}{2}\right)}{\beta[3^{-\alpha_{\max}}\rho_{\min}+(2l+3)^{-\alpha_{\max}}(1-\rho_{\min})]}\right)^{-\frac{2}{\alpha_{\max}}}\right] \end{cases} \tag{4.21}$$

where $l = |\mathcal{S}|$, $\hat{\lambda} = \sum\limits_{k=1}^{K}\lambda_k\left(P_k/P_{k^\star}\right)^{\frac{2}{\alpha_k}}$, $\alpha_{\max} \triangleq \max\{\alpha_1,\ldots,\alpha_K\}$, $\rho_{\min} = \min\limits_{\mathrm{BS}_{i,k}\in\mathcal{S}}\{\rho_{i,k}\}$, *and*

$$\rho_{i,k} = \begin{cases} 1 & \mathrm{BS}_{i,k}\notin\mathcal{S} \\ 2^{-\frac{B_{i,k}}{N_k-1}} & \mathrm{BS}_{i,k}\in\mathcal{S} \end{cases} \tag{4.22}$$

Proof. In the K-tier HCN, the normalized interference $I_{\mathcal{S}}$ can be written as

$$I \triangleq \sum_{k=1}^{K}\sum_{X_{i,k}\in\Phi_k\setminus\{X_{1,k^\star}\}}\frac{P_k}{P_{k^\star}}\rho_{i,k}S_{i,k}|X_{i,k}|^{-\alpha_k}, \tag{4.23}$$

where $\rho_{i,k} = 2^{\frac{B_{i,k}}{N_k-1}}$ for $\mathrm{BS}_{i,k}\in\mathcal{S}_{1,k^\star}$ and $\rho_{i,k}=1$ otherwise.

Upper Bound. Similar to the proof for the 1-tier case, the upper bound of SIR CDF is

$$\begin{aligned}&\mathbb{P}\left(\gamma=\frac{S_{1,k^\star}|X_{1,k^\star}|^{-\alpha_{k^\star}}}{I_{\mathcal{S}}}\leq\beta\right)\\ \leq&\frac{\beta}{N_{k^\star}-L_{1,k^\star}-1}\left[\sum_{i=2}^{\infty}\rho_{i,k}\mathbb{E}\left[\frac{|X_{1,k^\star}|^{\alpha_{k^\star}}}{|X_{i,k^\star}|^{\alpha_k^\star}}\right]+\sum_{\substack{k=1\\k\neq k^\star}}^{K}\sum_{i=1}^{\infty}\frac{P_k}{P_{k^\star}}\rho_{i,k}\mathbb{E}\left[\frac{|X_{1,k^\star}|^{\alpha_{k^\star}}}{|X_{i,k}|^{\alpha_k}}\right]\right].\end{aligned} \tag{4.24}$$

Following the same steps in Appendix 4.9.2 we have

$$\mathbb{E}\left[\frac{|X_{1,k^\star}|^{\alpha_{k^\star}}}{|X_{i,k^\star}|^{\alpha_{k^\star}}}\right]=\frac{\Gamma\left(1+\frac{\alpha_{k^\star}}{2}\right)(i-1)!}{\Gamma\left(i+\frac{\alpha_{k^\star}}{2}\right)} \tag{4.25}$$

For $k \neq k^\star$, $X_{i,k}$ and $X_{1,k^\star}$ belong to two independent PPPs. Therefore we have

$$\mathbb{E}\left[\frac{|X_{1,k^\star}|^{\alpha_{k^\star}}}{|X_{i,k}|^{\alpha_k}}\right] = \frac{\mathbb{E}\left[|X_{1,k^\star}|^{\alpha_{k^\star}}\right]}{\mathbb{E}\left[|X_{i,k}|^{\alpha_k}\right]} = \frac{\left(\lambda_{k^\star}\pi\right)^{-\frac{\alpha_{k^\star}}{2}}\Gamma\left(1+\frac{\alpha_{k^\star}}{2}\right)(i-1)!}{\left(\lambda_k\pi\right)^{\frac{-\alpha_k}{2}}\Gamma\left(i+\frac{\alpha_k}{2}\right)} \tag{4.26}$$

Therefore the upper bound in Theorem 4.5.2 is proven.

Lower Bound. The key idea of this proof is converting the interference from K tiers to that of a single tier. Then we apply the lower bound from Theorem 4.5.1. Comparing (4.23) with (4.16), it is seen that the K-tier case is different from the 1-tier case in two important aspects: 1) BSs from different tiers have different powers; and 2) BSs from different tiers have different path loss exponents.

We first present the way of eliminating the power differences. The interference from the k^{th} tier is

$$\begin{aligned} I_k &= \sum_{X_{i,k}\in\Phi_k} P_k \rho_{i,k} S_{i,k} |X_{i,k}|^{-\alpha_k} \\ &= \sum_{X_{i,k}\in\Phi_k} P_k^\star \rho_{i,k} S_{i,k} \left|\frac{X_{i,k}}{\left(P_k/P_{k^\star}\right)^{\frac{1}{\alpha_k}}}\right|^{-\alpha_k} \\ &= \sum_{Y_{i,k}\in\hat{\Phi}_k} P_k^\star \rho_{i,k} S_{i,k} \left|Y_{i,k}\right|^{-\alpha_k} \end{aligned} \tag{4.27}$$

where $Y_{i,k} \triangleq \frac{X_{i,k}}{\left(P_k/P_{k^\star}\right)^{\frac{1}{\alpha_k}}}$. The conservation property in [94, 140] states that $\{Y_{i,k}, i \in \mathbb{N}\}$ form a new PPP $\hat{\Phi}_k$ with intensity $\hat{\lambda}_k = \lambda_k \left(P_k/P_{k^\star}\right)^{\frac{2}{\alpha_k}}$. Therefore the interference can be viewed as generated from the K new tiers $\{\hat{\Phi}_1, \ldots, \hat{\Phi}_K\}$ with the same transmitting power $P_{k^\star}$. Therefore, the normalized interference

in (4.23) can be rewritten as

$$I_{\mathbb{S}} \stackrel{d.}{=} \sum_{k=1}^{K} \sum_{Y_{i,k} \in \hat{\Phi}_k \setminus \{Y_{1,k^\star}\}} \rho_{i,k} S_{i,k} |Y_{i,k}|^{-\alpha_k}, \tag{4.28}$$

where $\stackrel{d.}{=}$ means equivalence in distribution.

We then set all the path loss exponents to a common value $\alpha_{\max} \stackrel{\triangle}{=} \max(\alpha_1, \ldots, \alpha_K)$, which is the best case since the interference attenuates faster. The normalized interference in (4.23) can be lower bounded as

$$I_{\mathbb{S}} \geq \sum_{k=1}^{K} \sum_{Y_{i,k} \in \hat{\Phi}_k \setminus \{Y_{1,k^\star}\}} \rho_{i,k} S_{i,k} |Y_{i,k}|^{-\alpha_{\max}} \stackrel{\triangle}{=} I_{\mathbb{S}}^{lb}. \tag{4.29}$$

Denote $\hat{\Phi} = \bigcup_{k=1}^{K} \hat{\Phi}_k$. Because $\{\hat{\Phi}_1, \ldots, \hat{\Phi}_K\}$ are independent PPPs, $\hat{\Phi}$ is also a PPP with intensity $\hat{\lambda} = \sum_{k=1}^{K} \hat{\lambda}_k$. The interference lower bound $I_{\mathbb{S}}^{lb}$ can be viewed as generated from a single tier where 1) the BS locations forms a PPP $\hat{\Phi}$ with intensity $\hat{\lambda}$; 2) BSs have the same transmitting power $P_{k^\star}$; and 3) BSs have the same path loss exponent $\alpha_{\max}$. Therefore, $I_{\mathbb{S}}^{lb}$ can be rewritten as

$$\begin{aligned} I_{\mathbb{S}}^{lb} &= \sum_{X_{i,k} \in \hat{\Phi} \setminus \{X_{1,k^\star}\}} \rho_{i,k} S_{i,k} |Y_{i,k}|^{-\alpha_{\max}} \\ &= \sum_{\mathrm{BS}_{i,k} \in \mathbb{S}} \rho_{i,k} S_{i,k} |Y_{i,k}|^{-\alpha_{\max}} + \sum_{\mathrm{BS}_{i,k} \in \hat{\Phi} \setminus \{\mathrm{BS}_{1,k^\star} \bigcup \mathbb{S}\}} S_{i,k} |Y_{i,k}|^{-\alpha_{\max}}. \end{aligned} \tag{4.30}$$

It is obvious now that $I_{\mathbb{S}}^{lb}$ is in the same form as $I_{\mathbb{S}}$ in (4.16).

Applying (4.19) and (4.20), we have the lower bound on the end-user

SIR

$$\mathbb{P}\left(\gamma = \frac{S_{1,k^\star}|X_{1,k^\star}|^{-\alpha_{k^\star}}}{I_{\mathcal{S}}} \leq \beta\right) \geq \mathbb{P}\left(\frac{S_{1,k^\star}|X_{1,k^\star}|^{-\alpha_{k^\star}}}{I_{\mathcal{S}}^{lb}} \leq \beta\right)$$
$$\geq 1 - \exp\left[-\pi\hat{\lambda}\Gamma\left(1+\frac{2}{\alpha_{\max}}\right)(\mathbb{E}[\hat{Z}])^{-\frac{2}{\alpha_{\max}}}\right], \tag{4.31}$$

where $\hat{Z} = \frac{S_{1,k^\star}|X_{1,k^\star}|^{-\alpha_{k^\star}}}{\beta[3^{-\alpha_{\max}}\rho_{\min}+(2l+3)^{-\alpha_{\max}}(1-\rho_{\min})]}$, $l = |\mathcal{S}|$, and $\rho_{\min} = \min_{\mathrm{BS}_{i,k}\in\mathcal{S}}\{\rho_{i,k}\}$. From Lemma 1 and 3 in [81], we have $\mathbb{E}[|X_{1,k^\star}|^{-\alpha_{k^\star}}] = (\pi\hat{\lambda})^{-\alpha_{k^\star}}\Gamma(1-\alpha_{k^\star}/2)$, which gives

$$\mathbb{E}[\hat{Z}] = \frac{(N_{k^\star} - L_{1,k^\star})(\pi\hat{\lambda})^{\frac{\alpha_{k^\star}}{2}}\Gamma\left(1-\frac{\alpha_{k^\star}}{2}\right)}{\beta[3^{-\alpha_{\max}}\rho_{\min} + (2l+3)^{-\alpha_{\max}}(1-\rho_{\min})]}. \tag{4.32}$$

Therefore the lower bound in Theorem 4.5.2 follows. □

The bounds in Theorem 4.5.1 and 4.5.2 are insightful as they show clear dependence on important parameters such as the number of BS antennas N, the path loss exponent α and the number of coordinated neighbouring BSs $L_{1,k^\star}$. On the other hand, the bounds in 1-tier network case are independent of the BS spatial density λ. This is often called *scale-invariance* which is a known property of interference-limited cellular networks [14, 48, 81]. These bounds on the end-user SIR $\gamma_{\mathcal{S}}$ can be used with the throughput evaluation framework in Theorem 4.4.2 to derive the bounds on the end-user throughput.

4.6 Numerical Results and Discussion

In the analysis, we do not specify how the serving base station $\mathrm{BS}_{1,k^\star}$ selects its coordination set $\mathcal{S}_{1,k^\star}$. In the numerical simulation, we consider

three different scenarios.

Table 4.1: Notation & Simulation Summary

notation	Description	Simulation Value
K	The number of tiers in the HCN	3
k	The tier index	k=1 (macro), 2 (pico), 3 (femto)
$k^\star$	The tier index of the serving BS	1 (macro)
P_k	Transmitting powers of k^{th}-th tier	$P_1 = 40W$, $P_2 = 2W$, $P_3 = 0.2W$
λ_k	Spatial density of k^{th} tier	$\lambda_1 = 10^{-6}/m^2$, $\lambda_2 = 10^{-5}/m^2$, $\lambda_3 = 10^{-4}/m^2$
α_k	Path loss exponent of k^{th} tier	$\alpha_1 = 4.0$, $\alpha_2 = 3.5$, $\alpha_3 = 3.0$
N_k	The number of BS antennas in the k-th tier	$N_1 = 8$, $N_2 = 4$, $N_3 = 2$
$\mathcal{D}_{i,k}$	Overhead delay	Not fixed
$\tau_{i,k}$	Time fraction of $\text{BS}_{i,k}$ in cooperation phase	Not fixed
$\mathcal{T}_{i,k}$	Channel fading block length of $\text{BS}_{i,k}$	Fixed length of 80 ms
$B_{i,k}$	Overhead message quantization bits for $\text{BS}_{i,k}$	Not fixed
$\mathcal{S}_{1,k^\star}$	The coordination set of $\text{BS}_{1,k^\star}$	Not fixed
$L_{1,k^\star}$	The number of cells coordinating with $\text{BS}_{1,k^\star}$	$L_{1,k^\star} = \lvert\mathcal{S}_{1,k^\star}\rvert$
γ_{target}	The target SIR used in (4.33)	3 dB
G	The Shannon gap used in (4.34)	3 dB

Optimal Coordination Scenario. In this scenario, $\text{BS}_{1,k^\star}$ coordinates $L_{1,k^\star}$ other cells who cause strongest interference to the end-user. It is the optimal scenario because the user's interference is maximally cancelled. Note that this optimal scenario may not be feasible, because some of these presumed coordination cells probably do not have available antenna dimensions

for interference cancellation [11].

Best-effort Coordination Scenario. In this scenario, $\mathrm{BS}_{1,k^\star}$ selects to coordinate with $L_{1,k^\star}$ other cells who cause strongest interference to its user *and accept its coordination request*. A selected cell $\mathrm{BS}_{i,k}$ can decide if it accepts the coordination request from $\mathrm{BS}_{1,k^\star}$ based on its own criterion. Here we suppose it accepts the coordination request if the total number of its received coordination requests $M_{i,k}$ is less than its number of antennas N_k. Otherwise, we suppose it accepts the request with probability $(N_k - 1)/M_{i,k}$. This is called the best-effort coordination scenario because $\mathrm{BS}_{i,k}$ can at most coordinate with $N_k - 1$ other cells in CoMP ICIC.

Intra-tier Coordination Scenario. In practice, cross-tier coordination may be restricted in HCNs and only intra-tier coordination is allowed. For example, the end-user installed femtocells are controlled by their owners, and may not be allowed to or capable of coordinating with macrocells [15]. The selection on coordinated cells is the same as the best-effort coordination scenario, except that $\mathrm{BS}_{1,k^\star}$ now selects cells only inside its own tier.

We consider a 3-tier heterogeneous cellular network comprising macro (tier 1), pico (tier 2) and femto (tier 3) BSs. We simulate the scenario that the serving BS is a macrocell BS, i.e. $k^\star = 1$. Notation and system parameters are given in Table 4.1. Regarding inter-cell overhead channels, we consider the scenario that the overhead messages are shared through the BSs' backhaul. As shown in Chapter 3, the backhaul connection between two coordinated BSs is modelled as a tandem queue network consisting of several

servers (e.g. switches, routers and gateways), each of which has exponential processing time. The limited processing rate from the backhaul servers inevitably introduces overhead delay, whose distribution $p(\mathcal{T}_{i,k}, d)$ is derived in Chapter 3 and used in the simulations.

4.6.1 Evaluation Metrics

Two main performance metrics for CoMP schemes (including CoMP ICIC) are their improvements on network coverage and capacity. We simulate both performance metrics, by considering the different types of SIR-rate mapping functions $R(\cdot)$ in Theorem 4.4.2.

1. (Coverage under CoMP ICIC) If the end-user only requires a fixed target rate $\mathcal{R}_{\text{target}}$ (e.g. a voice user), its SIR-rate mapping function $R(\cdot)$ is

$$R(\gamma) = \begin{cases} \mathcal{R}_{\text{target}} & \gamma \geq \gamma_{\text{target}} \\ 0 & \gamma < \gamma_{\text{target}} \end{cases}. \tag{4.33}$$

   The throughput quantified in Theorem 4.4.2 is then simply the user's target rate times its probability of being in coverage (i.e. with SIR γ larger than the target SIR γ_{target}). Therefore, we can quantify the coverage improvement from CoMP ICIC by normalizing the derived throughput by $\mathcal{R}_{\text{target}}$. We use $\gamma_{\text{target}} = 3$ dB in the simulations.

2. (Throughput under CoMP ICIC) If the end-user is a data-greedy user, its SIR-rate mapping function $R(\cdot)$ is

$$R(\gamma) = \log_2\left(1 + \frac{\gamma}{G}\right) \quad \text{bps/Hz}, \tag{4.34}$$

where G is the Shannon gap, which is 3 dB in our simulations. Quantifying the rate of users of this kind will show the throughput improvement from CoMP ICIC.

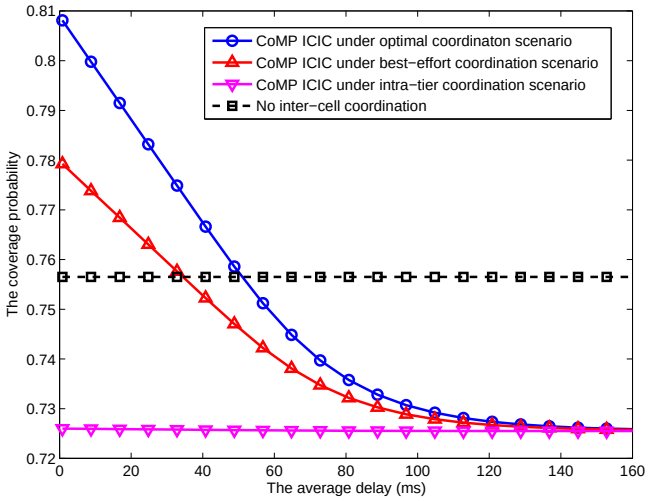

Figure 4.3: Downlink CoMP ICIC coverage probability vs. the average overhead delay. The overhead bit size is $B_{i,k} = 3(N_k - 1)$, which gives $\rho_{i,k} = 12.5\%$ (i.e. a coordinated $\mathrm{BS}_{i,k}$ can cancel 87.5% of its interference once receiving the updated overhead). For the three coordination scenarios, we consider $L_{1,k^\star} = 1$, i.e. $\mathrm{BS}_{1,k^\star}$ only coordinates with one other cell.

4.6.2 The Impact of Overhead Delay

Fig. 4.3 and 4.4 show the overhead delay impacts on CoMP ICIC coverage and throughput, respectively. As the average delay grows from zero (i.e. delay-free overhead channel as assumed in previous literature), CoMP ICIC coverage and throughput fall significantly in the optimal and best-effort coordination scenarios. In the intra-tier coordination scenario, the performance of

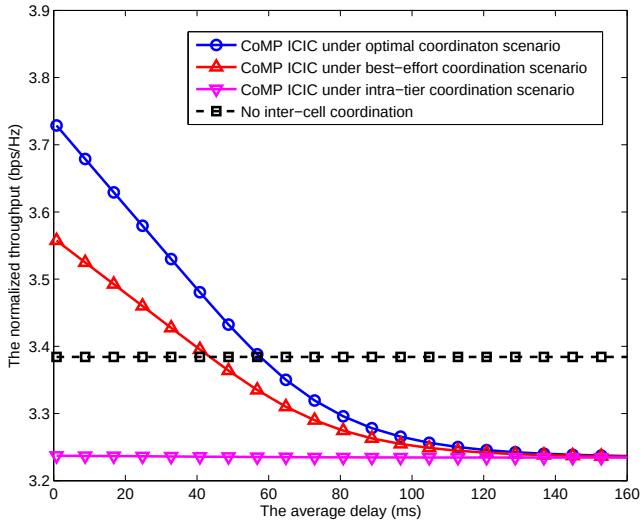

Figure 4.4: Downlink CoMP ICIC throughput vs. the average overhead channel delay. The coordination set $\mathcal{S}_{1,k^\star}$ and $B_{i,k}$ are the same as Fig. 4.3.

CoMP ICIC is severely constrained by this sub-optimal coordination strategy and thus only falls slightly as delay goes larger. When the overhead channel delay is larger than 60% of the fading coherence time $\mathcal{T}_{i,k}$, CoMP ICIC does not bring any coverage or throughput gain, no matter how the coordinated cells are selected. The key takeaway from these two plot is, the gain of CoMP ICIC depends heavily on the overhead delay and can easily become negative even under the optimal coordination scenario. This observation diverges significantly from previous optimistic performance predictions which ignore the overhead delay. It also provides a rule of thumb for the overhead channel configurations for CoMP ICIC.

4.6.3 Choosing Coordinated Cells

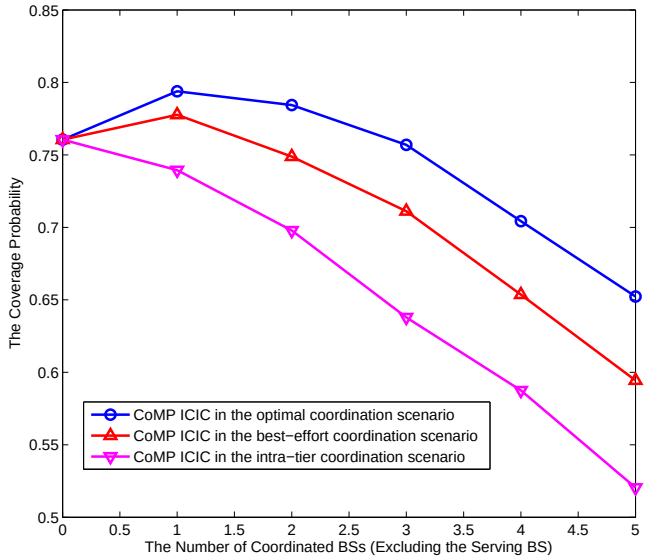

Figure 4.5: CoMP ICIC coverage vs. $L_{1,k^\star}$. We use $B_{i,k} = 3(N_k - 1)$ to give $\rho_{i,k} = 12.5\%$, i.e. a coordinated BS $\mathrm{BS}_{i,k}$ can cancel 87.5% of its interference once receiving the overhead. For the overhead delay $\mathcal{D}_{i,k}$ between the serving cell and $\mathrm{BS}_{i,k}$, we adjust the servers' processing rates in their backhaul path, to make sure that the average overhead delay $\mathbb{E}[\mathcal{D}_{i,k}] = 20$ ms.

A fundamental design question for CoMP ICIC is how many and which neighbouring cells should be selected for coordination. Coordinating more cells may translates into less interference from other cells, but also weaker signal power for the end-user and heavier overhead messaging burden. Therefore, there is a best number of coordinated cells, which is of great interest in the design of CoMP ICIC.

Fig. 4.5 and 4.6 show CoMP ICIC coverage and throughput vs. the

number of coordinated cells $L_{1,k^\star}$ in the three coordination scenarios. In the intra-tier coordination scenario, CoMP ICIC does not bring any coverage or throughput rate gain, because $L_{1.k^\star} = 0$ (no coordination among cells) is optimal. For the other two scenarios, coordinating with only one other cell (i.e $L_{1,k^\star} = 1$) is nearly optimal for a serving base station $\mathrm{BS}_{i,k^\star}$ with eight antennas. This observation is quite different from previous work in conventional macrocell networks.

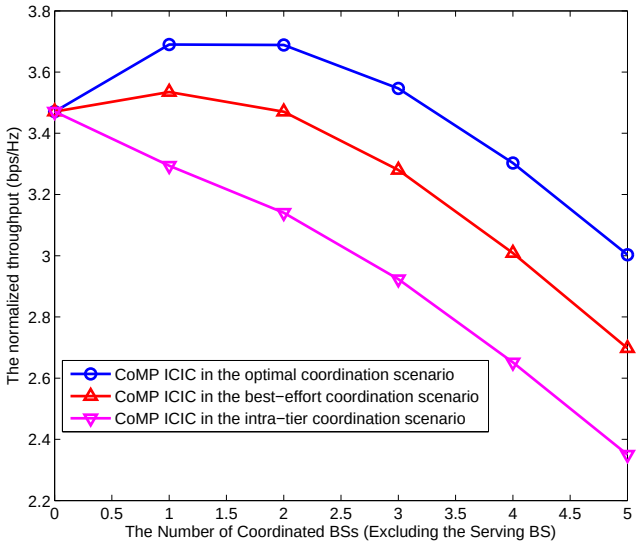

Figure 4.6: CoMP ICIC throughput vs. $L_{1,k^\star}$. The configurations on $B_{i,k}$ and the backhaul channel are the same as Fig. 4.5 (i.e. $B_{i,k} = 3(N_k - 1)$ and $\mathbb{E}[\mathcal{D}_{i,k}] = 20$ ms).

Because the observation from Fig. 4.5 and 4.6 is possibly contingent on our overhead model (we consider 20 ms average delay and finite quantization bits there), we examine the impact of different overhead models in Fig. 4.7

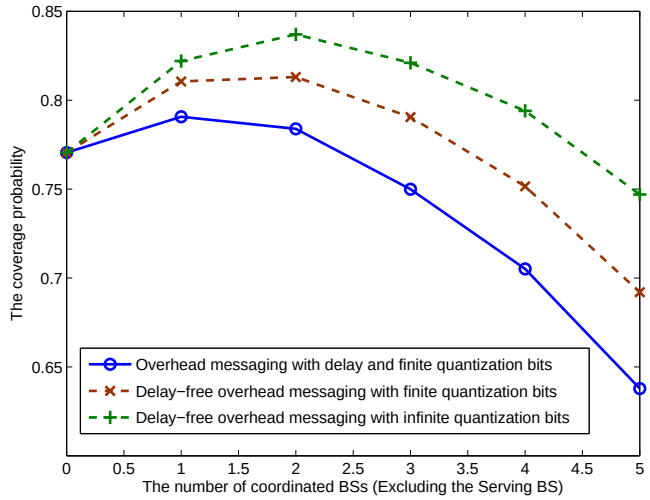

Figure 4.7: CoMP ZFBF coverage probability vs. $L_{1,k^\star}$ in the optimal coordination scenario. We consider three overhead models here. The top dash curve is the ideal overhead messaging (delay-free and infinite quantization bits), the dash curve in the middle is the limited feedback overhead messaging (delay-free but finite quantization bits $B_{i,k} = 3(N_k - 1)$), and the solid curve is our overhead model (considering overhead delay and finite quantization bits, with configurations elaborated in Fig. 4.5).

and 4.8. These two plots consider the optimal coordination scenario and show the best number of coordinated cells $L_{1,k^\star}$ under different overhead models including the ideal overhead model (i.e. infinite quantization bits and no delay) and limited feedback overhead model (i.e. no delay but finite quantization bits). It is seen that the optimum value of $L_{1,k^\star}$ is still small (less than 4), even when the overhead messaging is perfect without delay or quantization errors. A main takeaway from the four figures in this subsection is that dominant interference comes from only a few neighboring cells in HCNs and thus the number of coordinated cells should be kept fairly small in CoMP ICIC.

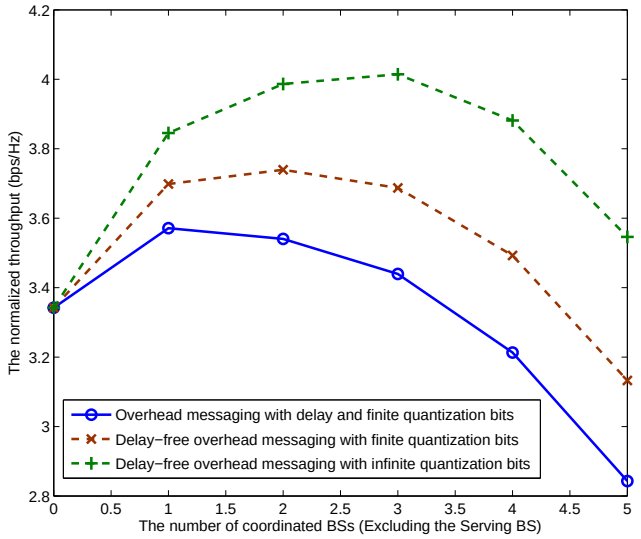

Figure 4.8: CoMP ICIC throughput (bps/Hz) vs. $L_{1,k^\star}$ in the optimal coordination scenario. The overhead models are the same as Fig. 4.7.

4.7 Discussion on Model Limitations

As observed from numerical results above, the performance of CoMP ICIC is not very promising in general. Note that such an observation/conclusion is possibly contingent on the analytical models we use, apart from the inherent shortcomings of CoMP ICIC itself [59, 79, 166]. In the following, we discuss the model limitations and their impact on the CoMP ICIC performance.

Fading Model. We use the i.i.d. block fading model for channel dynamics for reasons elaborated in Section 4.3. This model reduces the interference in the overhead messaging and cooperation states into two extreme cases: 1) no current channel information and thus no interference cancellation in the overhead messaging state, which is the worst-case scenario; and

2) accurate channel information (minus quantization errors) and thus maximum interference cancellation in the cooperation state, which is the best-case scenario. The end-user's long-term rate is then the time average of its rates under these two opposite extremes. In practice, fading changes continuously with temporal correlation. Temporal correlation means coordinated cells will have partial channel information from old overhead message in the overhead messaging state, and since the fading changes continuously, the channel information in the new overhead message cannot remain accurate over the entire period of the cooperation state. Thus, the end-user's rate will be higher in the overhead messaging state but lower in the cooperation state. Overall it is not clear if the user's long-term rate will increase, decrease or remain the same. Careful investigations under more sophisticated fading models are needed, for example discrete time models in previous works [8, 9, 76, 153, 165].

Overhead Codebook Model. In this chapter, we suppose the interfering channels from different cells are separately quantized using different RVQ codebooks known by the end-user and the respective cells. For example, the interfering channel $\mathbf{h}_{i,k}$ of $\mathrm{BS}_{i,k}$ is quantized according to codebook $\mathcal{C}_{i,k}$ with sizes $B_{i,k}$. Although optimum codebooks are unknown for CoMP techniques [21], several more sophisticated codebooks are potential candidates for CoMP performance improvements. First, different interfering channels can be jointly quantized based on their interfering powers, which is an active topic of ongoing research [23]. When quantizing interference channels separately, codebooks from the limited feedback literature can be exploited [96]. For ex-

ample, the optimal or near-optimal codebook design using Grassmannian line packing [95, 96] and vector quantization techniques [129, 169] has been intensively studied for single cell feedback, which can be used for the interfering channel quantization as well. Besides, the adaptive selection on codebook size $B_{i,k}$ is shown to be important [11, 21], based on the relative strengths of interference from different cells. Predictive codebooks (considering overhead delay in codebook design) are also relevant [74].

Poisson Point Process Model. In this chapter, we use the Poisson Point Process to model the spatial distribution of BSs in HCNs. Compared with previous grid or Wyner models, it is more difficult to define cell-edge in this model, because the locations of BSs are uncertain and the cell sizes are random. Therefore, existing works (including our work) study the performance of a typical end-user in this model, without distinguishing if it is an interior and cell-edge user. In other words, the results are averaged among all users in the entire network. However, many CoMP schemes are primarily used and expect significant gains only for cell-edge users who suffer strong inter-cell interference. We suspect that it is part of the reason why the performance of CoMP ICIC is not very promising in this chapter. In the future, it is important to study CoMP schemes for a cell-edge user, instead of a typical user. One possible approach is quantifying the user's SINR conditioned on the ratio of its distance to the serving BS over the serving cell radius.

4.8 Review of Other Downlink CoMP Schemes

In this chapter, we study downlink CoMP ICIC with single user antenna. In the following, we review and discuss other downlink CoMP approaches comparable to CoMP ICIC. For the sake of discussion, we suppose each mobile user requires only one data stream. Therefore, the received signal of the end-user is

$$y_{1,k^\star} = \mathbf{w}_{1,k^\star}\left[\sqrt{|X_{1,k^\star}|^{-\alpha_{1,k^\star}}}\mathbf{h}_{1,k^\star}\mathbf{f}_{1,k^\star}s_{1,k^\star} + \sum_{\mathrm{BS}_{i,k}\neq\mathrm{BS}_{1,k^\star}}\sqrt{|X_{i,k}|^{-\alpha_{i,k}}}\mathbf{h}_{i,k}\mathbf{f}_{i,k}s_{i,k}\right] + n_{1,k^\star}, \tag{4.35}$$

where $\mathbf{w}_{1,k^\star}$ is the end-user's receive vector (if multiple user antennas), $s_{i,k}$ and $\mathbf{f}_{i,k}$ are the transmit symbol and transmit precoding vector at $\mathrm{BS}_{i,k}$, and $n_{1,k^\star}$ is thermal noise. The general formulation (4.35) includes many CoMP techniques such as CoMP beamforming, CoMP ICIC, and interference alignment. For example, in CoMP ICIC, $\mathbf{f}_{i,k}$ is a zero-forcing precoder such that

$$\mathbf{h}_{i,k}\mathbf{f}_{i,k} = 0, \quad \forall\, \mathrm{BS}_{i,k} \in \text{ coordination set } \mathcal{S}_{1,k^\star}. \tag{4.36}$$

4.8.1 CoMP Schemes with Optimal Transceiver Design

From the information theory perspective, previous work investigates optimal transceiver vectors $\{\mathbf{w}, \mathbf{f}\}$ that achieve the rate tuples on the Pareto boundary of the rate region. However, this problem is non-convex and NP hard, even in the single user antenna case [32]. Therefore except in the two-cell multi-input-single-output (MISO) case [83, 93], it is very difficult to derive all Pareto-optimal vectors and achieve the whole Pareto boundary of the rate

region [24, 32]. Optimal or near-optimal vectors can be found by different searching algorithms, which usually require iterations and may not converge [122, 134, 168]. Besides Pareto optimum, there are other considerations in the design of $\{\mathbf{w}, \mathbf{f}\}$. In the following, we briefly discuss various designs of CoMP schemes, in both scenarios of single and multiple user antennas.

4.8.2 CoMP Schemes with Single User Antenna

In this subsection, we review downlink CoMP techniques which can work in single user antenna networks, i.e. MISO channels. To distinguish them from other CoMP schemes requiring multiple user antennas (e.g. interference alignment), we call them *MISO CoMP schemes*. For example, the CoMP ICIC studied in this chapter is a type of MISO CoMP. In MISO CoMP, the receive vector $\mathbf{w}$ is a scalar and thus the design challenge boils down to finding appropriate transmit vector $\mathbf{f}$. MISO CoMP using zero-forcing (i.e. CoMP ICIC in this chapter) and MMSE precoders are perhaps most widely studied, because these two precoders have closed-form expressions and scale with dirty-paper-coding (DPC) in the high SNR regime [80, 163]. A major drawback of these precoders is that the BS needs to sacrifice L antenna dimensions for interference cancellation when coordinating with L other cells. This means a significantly reduced power gain of its intended user and that the number of coordination cells L must be less than its number of antennas [11, 67, 71, 79, 92, 166]. Besides, noise enhancement effect exists for the zero-forcing precoding [163].

More sophisticated designs of transmit vectors $\mathbf{f}$ are proposed and investigated for other MISO CoMP schemes. The transmit vector $\mathbf{f}$ can be optimized for various design goals, such as transmit power minimization given SINR constraints [42,125], (weighted) sum rate maximization [22,151] and network utility maximization [66]. Compared with the ZF and MMSE precoders, these precoders can bring appreciable performance gains. However, they usually do not have closed-form expressions and iterative searching algorithms are thus needed.

4.8.3 CoMP Schemes with Multiple User Antennas

When mobile users have multiple antennas, both the receiver vector $\mathbf{w}$ and the transmit vector $\mathbf{f}$ can be optimized. One way of using multiple receiver antennas is to improve the performance of MISO CoMP schemes described in the previous subsection, simply by combining their transmit vectors $\mathbf{f}$ with common types of multi-antenna receivers [43, 79]. Take CoMP ICIC for example. With a single user antenna, its performance is not very promising as shown in this chapter. Besides our model limitations and the overhead impacts, one inherent reason is that the user signal power is reduced for the purpose of interference cancellation. From the numerical results in this chapter, this power loss is quite significant when the end-user has only a single antenna. On the other hand, this power loss can be greatly mitigated with the help of multi-antenna receivers. For example, CoMP ICIC with maximum ratio combining (MRC) receivers achieves large throughput gains [33, 67].

Besides enhancing MISO CoMP schemes, multiple receiver antennas open many new dimensions of CoMP designs as well. For instance, the transceiver vectors $\{\mathbf{w}, \mathbf{f}\}$ can be jointly optimized for purposes such as interference cancellation, i.e. jointly selecting $\{\mathbf{w}, \mathbf{f}\}$ as in [52, 112] such that

$$\mathbf{w}_{1,k^\star}\mathbf{h}_{i,k}\mathbf{f}_{i,k} = 0, \quad \forall\, \mathrm{BS}_{i,k} \in \text{ coordination set } \mathcal{S}_{1,k^\star}. \tag{4.37}$$

It is interesting to compare interference cancellation in (4.37) with (4.36). With a single user antenna, interference cancellation purely relies on the transmit vector $\mathbf{f}_{i,k}$ and therefore a BS cannot cancel more inter-cell interference than its number of antennas. Multi-antenna receivers can help cancel inter-cell interference and relax this stringent constraint. One problem, however, is that the joint optimization of $\{\mathbf{w}, \mathbf{f}\}$ is hard in general, even for the simple goal of interference cancellation [52, 72, 112, 152].

MIMO interference alignment (IA) is another prime example showing the benefits of multiple user antennas. Different from conventional interference cancellation where coordinated BSs try to null their mutual interference, BSs in IA align interference to create interference-free subspaces for their users. IA can be done in time, frequency or vector space. Recent research efforts are motivated by the seminal result in [30], which shows that IA can maximizing the achievable degrees of freedom (DoF), with the total DoF growing linearly with the number of users. However, this result critically depends on the *infinite* channel diversity assumption (i.e. an unbounded amount of independently faded parallel channels in time, frequency and/or vector spaces).

Many important issues still remain in practical scenarios with *finite* channel diversity. In the following, I discuss them in the context of MIMO IA, where interference is aligned in the vector space of each other. Of course, it requires multiple user antennas in the downlink. See [99] for an overview of different types of interference alignments.

A majority of previous literature considers constant MIMO channels $\{\mathbf{H}_{i,k}\}$ and focuses on designing the precoding vector $\mathbf{f}$ to achieve the maximum DoF. However, the maximum DoF achievable through IA is generally unknown for an arbitrary system (e.g. arbitrary numbers of users, transmit/receiver antennas and streams per user) [27, 127, 147, 161]. As seen from several special cases, the achievable DoF depends heavily on the amount of channel diversity [28,126]. For example, it is much less and severely limited by the transmit and receiver antennas in narrow-band constant channels (i.e. no time/frequency diversity) [126]. Besides, analytical results on the precoding vector $\mathbf{f}$ are unknown in general. Therefore, numerous algorithms are proposed to find the precoding vector $\mathbf{f}$ and the maximum DoF [62, 120, 121, 132].

Except the constant channels, other types of MIMO channels are also considered for interference alignment. [63] derives bounds on the achievable DoF through IA in fast fading MIMO channels. One practical concern for fading channels is the channel state information at the transmitter (CSIT), which can be obtained through channel reciprocity or feedback from the receivers (digital [143] [88] or analog feedback [18]). In either cases, it is not perfect in terms of delay and accuracy [18]. Several works study the per-

formance of MIMO IA with imperfect CSIT [109, 145, 149] or even without CSIT [69, 77, 171]. Moving beyond a single IA cluster, [110, 144, 146] study MIMO IA performance in large-scale networks and provide design insights on, for example, the appropriate size of the IA cluster.

4.9 Appendix

4.9.1 Proof of Lemma 4.4.1

The cooperation phase only occurs in fading blocks for which the overhead messaging delay $\mathcal{D}$ is smaller than $\mathcal{T}$. Here I omit the subscripts of delay $\mathcal{D}$ and block length $\mathcal{T}$ to keep the proof general. The percentage of these fading blocks is

$$\mathbb{P}(\mathcal{D} \leq \mathcal{T}) = \mathbb{P}(\mathcal{D} \leq \mathcal{T}, \mathcal{D} \leq \infty) = p(\mathcal{T}, \infty), \tag{4.38}$$

where the last equality holds by definition. In these fading blocks, the overhead messaging phase will have a time length $\mathbb{E}[\mathcal{D}|\mathcal{D} < \mathcal{T}]$

$$\mathbb{E}[\mathcal{D}|\mathcal{D} < \mathcal{T}] = \int_0^\infty \{1 - \mathbb{P}(\mathcal{D} \leq s|\mathcal{D} \leq \mathcal{T})\}\mathrm{d}s. \tag{4.39}$$

Thus the average duration of the cooperation phase is $\mathbb{E}[\mathcal{T}] - \mathbb{E}[\mathcal{D}|\mathcal{D} \leq \mathcal{T}]$.

In sum, the long-term time fraction of the cooperation phase is

$$\begin{aligned}\eta &= p(\mathcal{T},\infty) \times \left(\frac{\mathbb{E}[\mathcal{T}] - \mathbb{E}[\mathcal{D}|\mathcal{D}\leq\mathcal{T}]}{\mathbb{E}[\mathcal{T}]}\right) \\ &= p(\mathcal{T},\infty) - \frac{p(\mathcal{T},\infty)}{\mathbb{E}[\mathcal{T}]}\int_0^\infty \{1-\mathbb{P}(\mathcal{D}\leq s|\mathcal{D}\leq\mathcal{T})\}\mathrm{d}s \\ &\overset{(a)}{=} p(\mathcal{T},\infty) - \frac{1}{\mathbb{E}[\mathcal{T}]}\int_0^\infty \{p(\mathcal{T},\infty) - p(\mathcal{T},s)\}\,\mathrm{d}s. \end{aligned} \tag{4.40}$$

By definition, $p(\mathcal{T},\infty) = \mathbb{P}(\mathcal{D}\leq\mathcal{T},\mathcal{D}\leq\infty) = \mathbb{P}(\mathcal{D}\leq\mathcal{T})$. Therefore (a) follows.

4.9.2 Auxiliary Result for the CDF Upper Bound in Theorem 4.5.1

Consider a one-dimensional PPP $\Phi = \{Y_1, Y_2, \ldots\}$ with intensity λ, we have

$$Y_i = \sum_{j=1}^{i} \Delta_j \tag{4.41}$$

where $\Delta_j \sim \exp(\lambda)$. For an arbitrary positive number ν, the following equality holds

$$\begin{aligned}\mathbb{E}\left[\frac{Y_1^\nu}{Y_i^\nu}\right] &= \mathbb{E}\left[\left(\frac{\Delta_1}{\Delta_1+\Delta_2+\ldots\Delta_i}\right)^\nu\right] \\ &= \mathbb{E}\left\{\mathbb{E}\left[\left(\frac{\Delta_1}{\Delta_1+\Delta_2+\ldots\Delta_i}\right)^\nu \middle| \Delta_1+\ldots\Delta_i = x\right]\right\} \\ &= \mathbb{E}\left\{\frac{\Gamma(1+\nu)(i-1)!}{\Gamma(i+\nu)}\right\} \\ &= \frac{\Gamma(1+\nu)(i-1)!}{\Gamma(i+\nu)} \end{aligned} \tag{4.42}$$

4.9.3 Auxiliary Result for the CDF Lower Bound in Theorem 4.5.1

For an arbitrary m, $I_{(m)}$ can be expressed as

$$\begin{aligned}
I_{(m)} &= \sum_{X_i \in \Phi \setminus \{X_1,\ldots,X_m\}} S_i |X_i|^{-\alpha} \\
&= \sum_{X_i \in \Phi \setminus \{X_1,\ldots,X_m\}} S_i \left(|X_i| - |X_m| + |X_m|\right)^{-\alpha} \\
&= \sum_{X_i \in \Phi \setminus \{X_1,\ldots,X_m\}} \left(1 + \frac{|X_m|}{|X_i| - |X_m|}\right)^{-\alpha} S_i (|X_i| - |X_m|)^{-\alpha} \\
&\geq \sum_{X_i \in \Phi \setminus \{X_1,\ldots,X_m\}} \left(1 + \frac{|X_m|}{|X_{m+1}| - |X_m|}\right)^{-\alpha} S_i (|X_i| - |X_m|)^{-\alpha} \\
&= \left(1 + \frac{|X_m|}{|X_{m+1}| - |X_m|}\right)^{-\alpha} \sum_{X_i \in \Phi \setminus \{X_1,\ldots,X_m\}} S_i (|X_i| - |X_m|)^{-\alpha} \qquad (4.43)
\end{aligned}$$

Since the above inequality holds for any realization of $|X_m|$ and $|X_{m+1}|$, we have

$$\begin{aligned}
I_{(m)} &\overset{a.s.}{\geq} \left(1 + \frac{\mathbb{E}[|X_m|]}{\mathbb{E}[|X_{m+1}|] - \mathbb{E}[|X_m|]}\right)^{-\alpha} \sum_{X_i \in \Phi \setminus \{X_1,\ldots,X_m\}} S_i (|X_i| - |X_m|)^{-\alpha} \\
&\overset{(a)}{=} (1 + 2m)^{-\alpha} \sum_{X_i \in \Phi \setminus \{X_1,\ldots,X_m\}} S_i (|X_i| - |X_m|)^{-\alpha}, \qquad (4.44)
\end{aligned}$$

where (a) follows because we have $\mathbb{E}[|X_m|] = (\lambda\pi)^{-0.5} \frac{\Gamma(m+0.5)}{(m-1)!}$.

Now we define another point process $\tilde{\Phi}_m \overset{\triangle}{=} \{Y_j \in \mathbb{R}^2 : \text{ for any, } Y_j = X_i - \frac{X_i}{|X_i|}|X_m|, j = i-m\}$, i.e. $\tilde{\Phi}$ is formed by moving $\{X_{m+1}, X_{m+2}, \ldots\}$ in the PPP Φ toward the origin by distance $|X_m|$. Note that $\tilde{\Phi}$ is also a spatial Poisson Point Process, but non-homogeneous with a larger density than the original Φ (because when moving points toward the origin, we actually compress the

space in $\mathbb{R}^2$). Therefore the sum interference from $\tilde{\Phi}_m$ is larger than that from the original Φ, i.e. larger than $I_{(0)}$.

$$\begin{aligned} I_{(m)} &\overset{a.s.}{\geq} (1+2m)^{-\alpha} \sum_{X_i \in \Phi \setminus \{X_1,\ldots,X_m\}} S_i (|X_i| - |X_m|)^{-\alpha} \\ &= (1+2m)^{-\alpha} \sum_{Y_i \in \tilde{\Phi}} S_i |Y_i|^{-\alpha} \\ &\succeq (1+2m)^{-\alpha} I_{(0)}. \end{aligned} \tag{4.45}$$

Chapter 5

Conclusion

In this dissertation, we have studied both decentralized and coordinated interference management techniques in the new paradigm of heterogeneous cellular networks. We summarize the main results in this chapter and point out possible directions for future research.

5.1 Summary of Main Results

5.1.1 Uplink Access Control in Uncoordinated Femtocell Networks

In Chapter 2, we provide an analytical framework to study femtocell access schemes in co-spectrum uncoordinated two-tier femtocell networks. The framework quantifies femtocell-site-specific "loud neighbour" interfering effects and can be used to compare other techniques such as power control and spectrum allocation. Interference reduction from femtocell open access is dominantly important in non-orthogonal uplink multiple access (CDMA), whereas not much in orthogonal uplink multiple access (TDMA or OFDMA) depending on many other factors such as femtocell locations, user density and handoff policies. Note that these conclusions are possibly contingent on our analysis assumptions, among which the following two may be the most critical: 1) the

assumption of no inter-BS coordination both among and cross the two tiers; 2) the assumption on handoff policy. More sophisticated handoff policy may further improve the performance of open access [38]. Investigations on the impact of these assumptions are important related topics for future research.

5.1.2 Fundamentals of Overhead Signaling in Inter-cell Coordination

In Chapter 3, we develop various models of overhead messaging in HCNs and quantify the respective delay distributions as functions of overhead rate and plausible HCN deployments. Note that these models and results are independent on specific spatial distributions of BS locations. They can be used in the evaluation of inter-cell coordination schemes, to determine their performance gains for any given overhead messaging setups. For example, they are used in Chapter 4 for coordinated multi-point communications. Besides, they also provide design guidelines on appropriate overhead messaging configurations (for both backhaul and wireless) to accommodate specific coordination techniques and maximize their gains. Future extensions can include quantifying the delay distribution under sophisticated overhead retransmission schemes or proposing models of overhead messaging between multiple (more than two) cells. Investigations and testing of these overhead models would also be useful.

5.1.3 Downlink Coordinated Multi-Point Communications

In Chapter 4, we present a novel approach to evaluate downlink CoMP schemes in HCNs, by developing a new throughput evaluation framework with overhead modeling (based on results in Chapter 3) and using PPP model in end-user SINR characterization. It can be used for a class of CoMP schemes, and is applied to CoMP ZFBF in Chapter 4 as an example. Compared with previous works where results are either inaccurate or not in closed form, our approach provides clean-form results showing clear dependence on important parameters such as the overhead delay and the number of coordinated cells. These results align with the findings from several industrial implementations [17, 20, 75], and provide insights very different from previous works ignoring overhead modeling. For example, we show that CoMP ZFBF does not bring any throughput gain when the overhead delay is larger than 60% of the channel coherence time. We also find that, in most cases, coordinating with only one or two other cells is already optimum for downlink CoMP ZFBF.

5.2 Future Work

The first research topic closely related to this dissertation is studying CoMP schemes under more sophisticated models. We make several simplifying assumptions such as the full buffer assumption and the i.i.d. block model of the cooperation-dependent parameters (e.g. channel fading). As discussed in the end of Chapter 4, these assumptions may cause inaccurate evaluation on CoMP schemes and should be modified or removed in the future. For example,

using discrete-time Markov models to capture channel temporal correlation is highly desirable for CoMP study [9, 76, 153]. Besides evaluating the gains of CoMP schemes, their optimizations are also relevant, for example, by designing better overhead codebooks as we discussed in the end of Chapter 4.

As we mentioned in Chapter 1, a HCN contains base stations with vastly different backhaul and processing capabilities. In this dissertation, we have studied 1) access control which requires no overhead traffic and is thus suitable for BSs with very slow backhaul, and 2) coordinated multi-points which in general requires intense overhead sharing and is therefore suitable for BSs with superior backhaul connections. Interference management techniques with other levels of overhead traffic are highly desirable as well, because there is a spectrum of other cases between these two extreme cases depending on network deployment strategies. For example, enhanced inter-cell interference coordination (eICIC) with low overhead traffic (termed *loose coordination* in [20, 44]) are now under active research and standardization, with examples being semi-static and dynamic resource partition among neighboring cells. Of course, the gains of these techniques must be quantified and optimized vs. overhead quality and quantity required. The gains here can be metrics like users per tier, sum throughput, or SINR distribution.

Heterogeneous cellular networks are much more dynamic than conventional macrocell networks in terms of network topology, traffic and load. Small cells may be temporarily added for special events and removed later. Besides, they are usually not fully loaded and thus not transmitting (causing interfer-

ence) all the time [47]. In particular, femtocells can be turned on or off by the end-users at any time without prior warning. Under range extension, small cell ranges are adjusted based on the number of end-users in their owner cells and neighboring cells [20, 44, 89]. Considering the overwhelming number of small cells in future HCNs, manually tuning them are impossible. Therefore, future research should consider interference management techniques automatically adapting to neighboring environments [4–6]. For example, the adaptive selections on the number of coordinated cells and overhead bits as functions of instantaneous other-cell interference can potentially bring more CoMP gains.

Bibliography

[1] 3GPP TR25.8200 v1.0.0 release 8. November 2007.

[2] 3GPP TR 36.814 v9.0.0: Further advancements for E-UTRA physical layer aspects (release 9). March 2010.

[3] 3GPP TS 25.467 v9.3.0: Utran architecture for 3G Home NodeB (HNB) (release 9). June 2010.

[4] 3GPP TS 32.500: telecommunication management; self-organizing networks (SON); concepts and requirements (release 11). 2011.

[5] 3GPP TS 36.300: Evolved universal terrestrial radio access (E-UTRA) and evolved universal terrestrial radio access network (E-UTRAN). 2011.

[6] 3GPP TS 36.902: self-configuring and self-optimizing network use cases and solutions. 2011.

[7] 3GPP. Overview of 3GPP release 11. September 2012.

[8] A. Abdi and M. Kaveh. A space-time correlation model for multielement antenna systems in mobile fading channels. *IEEE J. Selected Areas in Communications*, 20(3):550–560, 2002.

[9] S. Akoum and Robert W. Heath. Limited feedback for temporally correlated MIMO channels with other cell interference. *IEEE Trans. Signal Processing*, 58(10):5219 –5232, Oct. 2010.

[10] S. Akoum, M. Kountouris, M. Debbah, and Robert W. Heath. Spatial interference mitigation for multiple input multiple output ad hoc networks: MISO gains. In *Proc. IEEE Asilomar Conference on Signals, Systems, and Computers*, pages 708–712, 2011.

[11] Salam Akoum and Robert W. Heath. Interference coordination: Random clustering and adaptive limited feedback. *arXiv preprint arXiv:1210.6095*, October 2012.

[12] M. S. Alouini and A. J. Goldsmith. Area spectral efficiency of cellular radio systems. *IEEE Trans. Veh. Technol.*, 48(4):1047–66, July 1999.

[13] Suprasad V. Amari and Ravindra B. Misra. Closed-form expression for distribution of the sum of independent exponential random variables. *IEEE Trans. Reliability*, 46(4):519 – 522, December 1997.

[14] J. G. Andrews, F. Baccelli, and R. K. Ganti. A tractable approach to coverage and rate in cellular networks. *IEEE Transactions on Communications*, 59(11):3122 – 3134, Nov. 2011.

[15] J. G. Andrews, H. Claussen, M. Dohler, S. Rangan, and M. C. Reed. Femtocells: Past, present, and future. *IEEE J. Selected Areas in Communications*, 30(3):497 – 508, April 2012.

[16] Jeff Andrews. The 7 ways hetnets are changing wireless communications forever. *Invited talk, IEEE Communication Theory Workshop*, May 2012, [Online]: http://www.ieee-ctw.org/2012/HetNetsParadigmShift_CTW2012.pdf.

[17] S. Annapureddy, A. Barbieri, S. Geirhofer, S. Mallik, and A. Gorokhov. Coordinated joint transmission in WWAN. *Invited talk, IEEE Communication Theory Workshop*, May 2010, [Online]: http://www.ieee-ctw.org/2010/mon/Gorokhov.pdf.

[18] O. E. Ayach and Robert W. Heath. Interference alignment with analog channel state feedback. *IEEE Trans. Wireless Commun.*, 11(2):626–636, 2012.

[19] S. Barbarossa, A. Carfagna, S. Sardellitti, M. Omilipo, and L. Pescosolido. Optimal radio access in femtocell networks based on markov modeling of interferers' activity. In *Proc. of the IEEE Int. Conf. on Acoustics, Speech, and Signal Proc.*, pages 3212 –3215, May 2011.

[20] A. Barbieri, P. Gaal, S. Geirhofer, T. Ji, D. Malladi, Y. Wei, and F. Xue. Coordinated downlink multi-point communications in heterogeneous cellular networks. In *Information Theory and Applications Workshop*, Feb. 2012.

[21] R. Bhagavatula and Robert W. Heath. Adaptive bit partitioning for multicell intercell interference nulling with delayed limited feedback. *IEEE Trans. Signal Processing*, 59(8):3824–3836, 2011.

[22] R. Bhagavatula and Robert W. Heath. Adaptive limited feedback for sum-rate maximizing beamforming in cooperative multicell systems. *IEEE Trans. Signal Processing*, 59(2):800–811, 2011.

[23] R. Bhagavatula, Robert W. Heath, and B. Rao. Limited feedback with joint CSI quantization for multicell cooperative generalized eigenvector beamforming. In *IEEE International Conference on Acoustics Speech and Signal Processing (ICASSP)*, pages 2838–2841, 2010.

[24] E. Bjornson, M. Bengtsson, and B. Ottersten. Pareto characterization of the multicell MIMO performance region with simple receivers. *Signal Processing, IEEE Transactions on*, 60(8):4464–4469, 2012.

[25] B. Blaszczyszyn, M.K. Karray, and H.P. Keeler. Using Poisson processes to model lattice cellular networks. *arXiv preprint arXiv:1207.7208*, 2012.

[26] Gunter Bolch, Stefan Greiner, Hermann de Meer, and Kishor S. Trivedi. *Queueing Networks and Markov Chains: Modeling and Performance Evaluation With Computer Science Applications*. Wiley-Interscience, 1998.

[27] G. Bresler, D. Cartwright, and D. Tse. Settling the feasibility of interference alignment for the MIMO interference channel: the symmetric square case. *arXiv preprint arXiv:1104.0888*, 2011.

[28] G. Bresler and D.N.C. Tse. 3 user interference channel: Degrees of freedom as a function of channel diversity. In *Allerton Conference on Commun., Control, and Computing*, pages 265–271, 2009.

[29] D. Cabric, M. S. W. Chen, D. A. Sobel, S. Wang, J. Yang, and R. W. Brodersen. Novel radio architectures for UWB, 60 GHz, and cognitive wireless systems. *EURASIP Journal on Wireless Communications and Networking*, 2006:1 – 18, 2006.

[30] V. R. Cadambe and S. A. Jafar. Interference alignment and degrees of freedom of the K-user interference channel. *IEEE Trans. Inform. Theory*, 54(8):3425 –3441, August 2008.

[31] G. Caire, N. Jindal, M. Kobayashi, and N. Ravindran. Multiuser MIMO achievable rates with downlink training and channel state feedback. *IEEE Trans. Inform. Theory*, 56(6):2845–2866, 2010.

[32] P. Cao, E. Jorswieck, and S. Shi. On the pareto boundary for the two-user single-beam MIMO interference channel. *arXiv preprint arXiv:1202.5474*, 2012.

[33] Chan-Byoung Chae, Insoo Hwang, Robert W. Heath, and V. Tarokh. Interference aware-coordinated beamforming in a multi-cell system. *IEEE Trans. Wireless Commun.*, 11(10):3692 –3703, October 2012.

[34] V. Chandrasekhar and J. G. Andrews. Spectrum allocation in tiered cellular networks. *IEEE Trans. Commun.*, 57(10):3059 – 3068, October

2009.

[35] V. Chandrasekhar and J. G. Andrews. Uplink capacity and interference avoidance for two-tier femtocell networks. *IEEE Trans. Wireless Commun.*, 8(7):3498–3509, July 2009.

[36] V. Chandrasekhar, J. G. Andrews, and A. Gatherer. Femtocell networks: a survey. *IEEE Commun. Mag.*, 46(9):59–67, September 2008.

[37] Vikram Chandrasekhar, Jeffrey G. Andrews, Tarik Muharemovic, Zukang Shen, and Alan Gatherer. Power control in two-tier femtocell networks. *IEEE Trans. Wireless Commun.*, 8(8):4316 – 4328, August 2009.

[38] Y. Chen, J. Zhang, and Q. Zhang. Utility-aware refunding framework for hybrid access femtocell network. *IEEE Trans. Wireless Commun.*, 11(5):1688 –1697, May 2012.

[39] W.C. Cheung, T.Q.S. Quek, and M. Kountouris. Access control and cell association in two-tier femtocell networks. In *Proc. IEEE Wireless Commun. Networking Conf.*, pages 893–897, 2012.

[40] W.C. Cheung, T.Q.S. Quek, and M. Kountouris. Throughput optimization, spectrum allocation, and access control in two-tier femtocell networks. *IEEE J. Selected Areas in Communications*, 30(3):561–574, 2012.

[41] D. Choi, P. Monajemi, Shinjae Kang, and J. Villasenor. Dealing with loud neighbors: The benefits and tradeoffs of adaptive femtocell access.

In *Proc. IEEE Global Telecommunications Conference*, pages 1 –5, Dec. 2008.

[42] H. Dahrouj and Wei Yu. Coordinated beamforming for the multi-cell multi-antenna wireless system. *IEEE Trans. Wireless Commun.*, 9(5):1748 –1759, May 2010.

[43] H. Dai, A.F. Molisch, and H.V. Poor. Downlink capacity of interference-limited MIMO systems with joint detection. *Wireless Communications, IEEE Transactions on*, 3(2):442–453, 2004.

[44] A. Damnjanovic, J. Montojo, Yongbin Wei, Tingfang Ji, Tao Luo, M. Vajapeyam, Taesang Yoo, Osok Song, and D. Malladi. A survey on 3GPP heterogeneous networks. *IEEE Wireless Communications*, 18(3):10 –21, June 2011.

[45] R. C. Daniels and R. W. Heath. 60 GHz wireless communications: emerging requirements and design recommendations. *IEEE Vehicular Technology Magazine*, 2(3):41–50, 2007.

[46] Guillaume de la Roche, Alvaro Valcarce, David López-Pérez, and Jie Zhang. Access control mechanisms for femtocells. *IEEE Commun. Mag.*, 48(1):33 – 39, January 2010.

[47] H. S. Dhillon, R. K. Ganti, and J. G. Andrews. Load-aware modeling and analysis of heterogeneous cellular networks. *submitted, IEEE. Trans. Wireless Comm.*, April 2012, arXiv preprint arXiv:1204.1091.

[48] H. S. Dhillon, R. K. Ganti, F. Baccelli, and J. G. Andrews. Modeling and analysis of K-tier downlink heterogeneous cellular networks. *IEEE J. Selected Areas in Communications*, 30(3):550 – 560, April 2012.

[49] C. H. Doan, S. Emami, D. A. Sobel, A. M. Niknejad, and R. W. Brodersen. Design considerations for 60 GHz CMOS radios. *IEEE Commun. Mag.*, 42(12):132–140, 2004.

[50] M. Dohler, R. W. Heath, A. Lozano, C. B. Papadias, and R. A. Valenzuela. Is the PHY layer dead? *IEEE Commun. Mag.*, 49(4):159 –165, April 2011.

[51] T. Elkourdi and O. Simeone. Outage and diversity-multiplexing tradeoff analysis of closed and open-access femtocells. In *Proc. IEEE Global Telecommunications Conference*, Dec. 2010.

[52] B. Farhang-Boroujeny, Q. Spencer, and L. Swindlehurst. Layering techniques for space-time communication in multi-user networks. In *Proc. IEEE Veh. Technol. Conf.*, volume 2, pages 1339–1343, 2003.

[53] Stefano Favaro and Stephen G. Walker. On the distribution of sums of independent exponential random variables via Wilks' integral representation. *Acta Applicandae Mathematicae*, 109(3):1035–1042, March 2010.

[54] M. Feng, D. Chen, Z. Wang, T. Jiang, and D. Qu. Throughput improvement for OFDMA femtocell networks through spectrum allocation

and access control strategy. In *Computing, Communications and Applications Conference (ComComAp)*, pages 387–391, 2012.

[55] Philip J. Fleming, Alexander L. Stolyar, and Burt Simon. Closed-form expressions for other-cell interference in cellular CDMA. *Technical Report, University of Colorado at Denver*, December 1997.

[56] UMTS forum Report 37. Magic mobile future 2010-2020. April 2005.

[57] UMTS forum Report 44. Mobile traffic forecasts 2010-2020 report. January 2011.

[58] G. J. Foschini, K. Karakayali, and R. A. Valenzuela. Coordinating multiple antenna cellular networks to achieve enormous spectral efficiency. *IEE Proceedings Communications*, 153(4):548 – 555, August 2006.

[59] David Gesbert, Stephen Hanly, Howard Huang, Shlomo Shamai, Osvaldo Simeone, and Wei Yu. Multi-cell MIMO cooperative networks: A new look at interference. *IEEE J. Selected Areas in Communications*, 28(9):1380 – 1408, December 2010.

[60] A. Ghosh, J. Zhang, J. G. Andrews, and R. Muhamed. *Fundamentals of LTE*. Englewood Cliffs, New Jersey, 2010.

[61] A. Golaup, M. Mustapha, and L.B. Patanapongpibul. Femtocell access control strategy in UMTS and LTE. *IEEE Commun. Mag.*, 47(9):117 –123, September 2009.

[62] K. Gomadam, V.R. Cadambe, and S.A. Jafar. Approaching the capacity of wireless networks through distributed interference alignment. In *Proc. IEEE Global Telecommunications Conference*, pages 1–6, 2008.

[63] Tiangao Gou and S. A. Jafar. Degrees of freedom of the K user M × N MIMO interference channel. *IEEE Trans. Inform. Theory*, 56(12):6040 –6057, Dec. 2010.

[64] N. Guo, R. C. Qiu, S. S. Mo, and K. Takahashi. 60-GHz millimeter-wave radio: Principle, technology, and new results. *EURASIP Journal on Wireless Communications and Networking*, 2007:1– 8, 2007.

[65] S. Guruacharya, D. Niyato, and D.I. Kim. Access control via coalitional power game. In *Proc. IEEE Wireless Commun. Networking Conf.*, pages 2824–2828, 2012.

[66] N. Hassanpour, J. Smee, J. Hou, and J. Soriaga. Distributed beamforming based on signal-to-caused-interference ratio. In *Proc. IEEE International Symposium on Spread Spectrum Techniques and Applications (ISSSTA)*, volume 8, pages 405–410.

[67] Z.K.M. Ho and D. Gesbert. Balancing egoism and altruism on interference channel: The MIMO case. In *Proc. IEEE Int. Conf. Commun.*, pages 1–5, 2010.

[68] J. Hoydis, S. Ten Brink, and M. Debbah. Massive MIMO: How many antennas do we need? In *Allerton Conference on Commun., Control,*

and Computing, pages 545–550, 2011.

[69] C. Huang, S. A. Jafar, S. Shamai, and S. Vishwanath. On degrees of freedom region of MIMO networks without channel state information at transmitters. *IEEE Trans. Inform. Theory*, 58(2):849–857, 2012.

[70] H. Huang and Sivarama Venkatesan. Asymptotic downlink capacity of coordinated cellular networks. In *Proc. IEEE Asilomar Conference on Signals, Systems, and Computers*, pages 850 – 855, Nov. 2004.

[71] K. Huang and Jeffrey G. Andrews. A closer look at multi-cell cooperation via stochastic geometry and large deviations. *submitted, IEEE Trans. Inform. Theory*, April 2012, arXiv preprint arXiv:1204.3167.

[72] K. Huang and R. Zhang. Cooperative precoding with limited feedback for MIMO interference channels. *IEEE Trans. Wireless Commun.*, 11(3):1012–1021, 2012.

[73] Pierre Humblet, Balaji Raghothaman, Anand Srinivas, Srinivasan Balasubramanian, Chirag Patel, and Mehmet Yavuz. System design of cdma2000 femtocells. *IEEE Commun. Mag.*, 47(9):92 – 100, September 2009.

[74] T. Inoue and Robert W. Heath. Grassmannian predictive coding for delayed limited feedback MIMO systems. In *Allerton Conference on Commun., Control, and Computing*, pages 783–788, 2009.

[75] Ralf Irmer, Heinz Droste, Patrick Marsch, Michael Grieger, Gerhard Fettweis, Stefan Brueck, Hans-Peter Mayer, Lars Thiele, and Volker Jungnickel. Coordinated multipoint: Concepts, performance, and field trial results. *IEEE Commun. Mag.*, 49:102 – 111, Feburary 2011.

[76] Y. Isukapalli and B. D. Rao. Finite rate feedback for spatially and temporally correlated MISO channels in the presence of estimation errors and feedback delay. In *Proc. IEEE Global Telecommunications Conference*, pages 2791 –2795, Nov. 2007.

[77] S.A. Jafar. Blind interference alignment. *IEEE J. Selected Topics in Signal Processing*, 6(3):216–227, 2012.

[78] N. Jindal. MIMO broadcast channels with finite-rate feedback. *IEEE Trans. Inform. Theory*, 52(11):5045 –5060, November 2006.

[79] N. Jindal, J. G. Andrews, and S. Weber. Multi-antenna communication in ad hoc networks: Achieving MIMO gains with SIMO transmission. *IEEE Trans. Commun.*, 59(2):529 –540, February 2011.

[80] Sheng Jing, David N. C. Tse, Joseph B. Soriaga, Jilei Hou, John E. Smee, and Roberto Padovani. Multicell downlink capacity with coordinated processing. *EURASIP Journal on Wireless Communications and Networking*, 2008:1 – 19, 2008.

[81] H.-S. Jo, Y. J. Sang, P. Xia, and J. G. Andrews. Heterogeneous cellular networks with flexible cell association: a comprehensive downlink SINR

analysis. *accepted, IEEE Trans. Wireless Commun.*, 2012.

[82] H. S. Jo, P. Xia, and J.G. Andrews. Downlink femtocell networks: Open or closed? In *Proc. IEEE Int. Conf. Commun.*, pages 1–5, 2011.

[83] E.A. Jorswieck, E.G. Larsson, and D. Danev. Complete characterization of the pareto boundary for the MISO interference channel. *IEEE Trans. Signal Processing*, 56(10):5292–5296, 2008.

[84] S. Joshi, R. Cheung, P. Monajemi, and J. D. Villasenor. Traffic-based study of femtoce policy impacts on HSPA service quality. In *Proc. IEEE Global Telecommunications Conference*, pages 1 – 6, Nov. 2009.

[85] Aamod Khandekar, Naga Bhushan, Ji Tingfang, and Vieri Vanghi. LTE advanced: Heterogeneous networks. In *European Wireless Conference*, pages 978 – 982, June 2010.

[86] Douglas N. Knisely and Frank Favichia. Standardization of femtocells in 3GPP2. *IEEE Commun. Mag.*, 47(9):76 – 82, September 2009.

[87] Douglas N. Knisely, Takahito Yoshizawa, and Frank Favichia. Standardization of femtocells in 3GPP. *IEEE Commun. Mag.*, 47(9):68 – 75, September 2009.

[88] R.T. Krishnamachari and M.K. Varanasi. Interference alignment under limited feedback for MIMO interference channels. In *Proc. IEEE Int. Symp. Information Theory*, pages 619–623. IEEE, 2010.

[89] D. López-Pérez, Xiaoli Chu, and İ. Güvenc. On the expanded region of picocells in heterogeneous networks. *IEEE J. Selected Topics in Signal Processing*, 6(3):281 –294, June 2012.

[90] David López-Pérez, A. Valcarce, G. De La Roche, Enjie Liu, and Jie Zhang. Access methods to WiMAX femtocells: A downlink system-level case study. In *IEEE Singapore Internation Conferece*, pages 1657 –1662, Nov. 2008.

[91] David López-Pérez, Alvaro Valcarce, Ákos Ladányi, Guillaume de la Roche, and Jie Zhang. Intracell handover for interference and handover mitigation in OFDMA two-tier macrocell-femtocell networks. *EURASIP Journal of Wireless Communications and Networking*, 2010 (2010), 16 pages.

[92] E. Larsson and E. Jorswieck. Competition versus cooperation on the MISO interference channel. *IEEE J. Selected Areas in Communications*, 26(7):1059–1069, 2008.

[93] J. Lindblom, E. Karipidis, and E.G. Larsson. Closed-form parameterization of the pareto boundary for the two-user MISO interference channel. In *IEEE International Conference on Acoustics, Speech and Signal Processing (ICASSP)*, pages 3372–3375, 2011.

[94] C.-H. Liu and J. G. Andrews. Distributed SIR-aware scheduling in large-scale wireless networks. *arXiv preprint arXiv:1107.1731*, 2011.

[95] D. J. Love, Robert W. Heath, and T. Strohmer. Grassmannian beamforming for multiple-input multiple-output wireless systems. *IEEE Trans. Inform. Theory*, 49(10):2735–2747, 2003.

[96] David J. Love, Robert W. Heath, Vincent K. N. Lau, David Gesbert, Bhaskar D. Rao, and Matthew Andrews. An overview of limited feedback in wireless communication systems. *IEEE J. Selected Areas in Communications*, 26(8):1341–1365, October 2008.

[97] Angel Lozano, Robert W. Heath, and Jeffrey G. Andrews. Fundamental limits of cooperation. *submitted, IEEE Trans. Inform. Theory*, March 2012, arXiv preprint arXiv:1204.0011.

[98] Mohammad Ali Maddah-Ali and David Tse. Completely stale transmitter channel state information is still very useful. In *Allerton Conference on Commun., Control, and Computing*, pages 1188 – 1195, September 2010.

[99] Behrang Nosrat Makouei. Designing MIMO interference alignment networks. *Ph.D. dissertation, The University of Texas at Austin*, 2012.

[100] Durga Malladi. Heterogeneous networks 3G and 4G. *Invited talk, IEEE Communication Theory Workshop*, May 2012, [Online]: http://www.ieee-ctw.org/2012/HetNets3Gand4GIEEECTW2012.pdf.

[101] P. Marsch and G. Fettweis. A framework for optimizing the uplink performance of distributed antenna systems under a constrained backhaul.

In *Proc. IEEE Int. Conf. Commun.*, pages 975 –979, June 2007.

[102] T. L. Marzetta. Noncooperative cellular wireless with unlimited numbers of base station antennas. *IEEE Trans. Wireless Commun.*, 9(11):3590–3600, 2010.

[103] S. Mukherjee. Analysis of UE outage probability and macrocellular traffic offloading for WCDMA macro network with femto overlay under closed and open access. In *Proc. IEEE Int. Conf. Commun.*, June 2011.

[104] S. Mukherjee. UE coverage in LTE macro network with mixed CSG and open access femto overlay. In *Proc. IEEE Int. Conf. Commun.*, June 2011.

[105] S. Mukherjee. Distribution of downlink SINR in heterogeneous cellular networks. *IEEE J. Selected Areas in Communications*, 30(3):575 – 585, April 2012.

[106] Nokia Siemens Networks. Initial Home NodeB coexistence simulation results. *3GPP Document Reference R4-070902, 3GPP TSG-RAN WG4 Meeting*, June 2007.

[107] A. Niknejad. Siliconization of 60 GHz. *IEEE Microwave Magazine*, 11(1):78–85, 2010.

[108] Nortel and Vodafone. Open and closed access for home NodeBs. *3GPP document Reference R4-071231, 3GPP TSG-RAN WG4 Meeting 44*, August 2007.

[109] B. Nosrat-Makouei, Jeffrey G. Andrews, and Robert W. Heath. MIMO interference alignment over correlated channels with imperfect CSI. *IEEE Trans. Signal Processing*, 59(6):2783–2794, 2011.

[110] B. Nosrat-Makouei, Jeffrey G. Andrews, Robert W. Heath, and R. K. Ganti. MIMO interference alignment in random access networks. In *Proc. IEEE Asilomar Conference on Signals, Systems, and Computers*, pages 641–645. IEEE, 2011.

[111] T. D. Novlan, R. K. Ganti, A. Ghosh, and J. G. Andrews. Analytical evaluation of fractional frequency reuse for heterogeneous cellular networks. *IEEE Trans. Commun.*, 60(7):2029–2039, 2012.

[112] Z. Pan, K.K. Wong, and T.S. Ng. Generalized multiuser orthogonal space-division multiplexing. *IEEE Trans. Wireless Commun.*, 3(6):1969–1973, 2004.

[113] F. Pantisano, M. Bennis, W. Saad, and M. Debbah. Spectrum leasing as an incentive towards uplink macrocell and femtocell cooperation. *IEEE J. Selected Areas in Communications*.

[114] F. Pantisano, M. Bennis, W. Saad, M. Debbah, and M. Latva-aho. On the impact of heterogeneous backhauls on coordinated multipoint trans-

mission in femtocell networks. In *Proc. IEEE Int. Conf. Commun.*, June 2012.

[115] CISCO White Paper. Cisco visual networking index: Global mobile data traffic forecast update, 2010 - 2015. February 2011.

[116] CISCO White Paper. Cisco visual networking index: Global mobile data traffic forecast update, 2011 - 2016. February 2012.

[117] Ericsson White Paper. Traffic and market data report. Feb. 2012.

[118] Signals Research Group White Paper. Femto forum femtocell business case whitepaper. June 2009.

[119] Tropos Network White Paper. Picocell mesh: Bringing low-cost coverage, capacity and symmetry to mobile WiMAX. March 2007.

[120] S. W. Peters and Robert W. Heath. Interference alignment via alternating minimization. In *Proc. IEEE International Conference on Acoustics, Speech and Signal Processing (ICASSP)*, pages 2445–2448, 2009.

[121] S. W. Peters and Robert W. Heath. Cooperative algorithms for MIMO interference channels. *IEEE Trans. Veh. Technol.*, 60(1):206–218, 2011.

[122] J. Qiu, R. Zhang, Z.Q. Luo, and S. Cui. Optimal distributed beamforming for MISO interference channels. *IEEE Trans. Signal Processing*, 59(11):5638–5643, 2011.

[123] S. Ramprashad and G. Caire. Cellular vs. network MIMO: A comparison including the channel state information overhead. In *Proc. of the IEEE Int. Symp. on Personal Indoor and Mobile Radio Comm.*, September 2009.

[124] S. Ramprashad, G. Caire, and H. Papadopoulos. Cellular and network MIMO architectures: MU-MIMO spectral efficiency and costs of channel state information. In *Proc. IEEE Asilomar Conference on Signals, Systems, and Computers*, November 2009.

[125] F. Rashid-Farrokhi, K.J.R. Liu, and L. Tassiulas. Transmit beamforming and power control for cellular wireless systems. *IEEE J. Selected Areas in Communications*, 16(8):1437–1450, 1998.

[126] M. Razaviyayn, G. Lyubeznik, and Z.Q. Luo. On the degrees of freedom achievable through interference alignment in a MIMO interference channel. *Signal Processing, IEEE Transactions on*, 60(2):812–821, 2012.

[127] M. Razaviyayn, M. Sanjabi, and Z.Q. Luo. Linear transceiver design for interference alignment: Complexity and computation. *IEEE Trans. Inform. Theory*, 58(5):2896–2910, 2012.

[128] The Economist Special Report. Personal technology: Beyond the PC. October 8 2011.

[129] J.C. Roh and B.D. Rao. Transmit beamforming in multiple-antenna systems with finite rate feedback: a VQ-based approach. *IEEE Trans.*

Inform. Theory, 52(3):1101–1112, 2006.

[130] Bilal Sadiq, Ritesh Madan, and Ashwin Sampath. Downlink scheduling for multiclass traffic in LTE. *EURASIP Journal on Wireless Communications and Networking*, July 2009.

[131] A. Sanderovich, O. Somekh, H. V. Poor, and S. Shamai. Uplink macro diversity of limited backhaul cellular network. *IEEE Trans. Inform. Theory*, 55(8):3457 –3478, August 2009.

[132] D.A. Schmidt, C. Shi, R.A. Berry, M.L. Honig, and W. Utschick. Minimum mean squared error interference alignment. In *Proc. IEEE Asilomar Conference on Signals, Systems, and Computers*, pages 1106–1110, 2009.

[133] S. Shamai and B. M. Zaidel. Enhancing the cellular downlink capacity via co-processing at the transmitting end. In *Proc. IEEE Veh. Technol. Conf.*, volume 3, pages 1745 –1749, 2001.

[134] Q. Shi, M. Razaviyayn, Z.Q. Luo, and C. He. An iteratively weighted MMSE approach to distributed sum-utility maximization for a MIMO interfering broadcast channel. *IEEE Trans. Signal Processing*, 59(9):4331–4340, 2011.

[135] O. Simeone, E. Erkip, and S. Shamai. Robust communication against femtocell access failures. In *Information Theory Workshop*, pages 263 –267, Oct. 2009.

[136] H. Singh, J. Oh, C. Kweon, X. Qin, H. R. Shao, and C. Ngo. A 60 GHz wireless network for enabling uncompressed video communication. *IEEE Commun. Mag.*, 46(12):71–78, 2008.

[137] O. Somekh and S. Shamai. Shannon-theoretic approach to a Gaussian cellular multiple-access channel with fading. *IEEE Trans. Inform. Theory*, 46(4):1401 –1425, July 2000.

[138] O. Somekh, B. M. Zaidel, and S. Shamai. Sum rate characterization of joint multiple cell-site processing. *IEEE Trans. Inform. Theory*, 53(12):4473 – 4497, Decemeber 2007.

[139] Oren Somekh, Osvaldo Simeone, Amichai Sanderovich, Benjamin M. Zaidel, and Shlomo Shamai. On the impact of limited-capacity backhaul and inter-users links in cooperative multicell networks. In *42nd Annual Conference on Information Sciences and Systems*, 2008.

[140] D. Stoyan, W. Kendall, and J. Mecke. *Stochastic Geometry and Its Applications*. John Wiley and Sons, Inc., 2 edition, 1996.

[141] P. Tarasak, T.Q.S. Quek, and F. Chin. Uplink timing misalignment in open and closed access OFDMA femtocell networks. *IEEE Communications Letters*, 15(9):926 –928, september 2011.

[142] D.B. Taylor, H.S. Dhillon, T.D. Novlan, and J.G. Andrews. Pairwise interaction processes for modeling cellular network topology. In *Proc. IEEE Global Telecommunications Conference*, 2012.

[143] J. Thukral and H. Bolcskei. Interference alignment with limited feedback. In *Proc. IEEE Int. Symp. Information Theory*, pages 1759–1763, 2009.

[144] R. Tresch, G. Alfano, and M. Guillaud. Interference alignment in clustered ad hoc networks: High reliability regime and per-cluster aloha. In *IEEE International Conference on Acoustics, Speech and Signal Processing (ICASSP)*, pages 3348 –3351, May 2011.

[145] R. Tresch and M. Guillaud. Cellular interference alignment with imperfect channel knowledge. In *Proc. IEEE Int. Conf. Commun.*, pages 1–5, 2009.

[146] R. Tresch and M. Guillaud. Clustered interference alignment in large cellular networks. In *Proc. of the IEEE Int. Symp. on Personal Indoor and Mobile Radio Comm.*, pages 1024–1028. IEEE, 2009.

[147] R. Tresch, M. Guillaud, and E. Riegler. On the achievability of interference alignment in the K-user constant MIMO interference channel. In *IEEE Workshop on Statistical Signal Processing*, pages 277–280, 2009.

[148] D. Tse and Pramod Viswanath. *Fundamentals of Wireless Communication*. Cambridge University Press, 1 edition, 2005.

[149] C.S. Vaze and M.K. Varanasi. The degrees of freedom regions of two-user and certain three-user MIMO broadcast channels with delayed CSIT. *arXiv preprint arXiv:1101.0306*, 2010.

[150] G. K. Venkatesan and K. Kulkarni. Wireless backhaul for LTE - requirements, challenges and options. In *IEEE International Symposium on Advanced Networks and Telecommunication Systems*, Decemeber 2008.

[151] L. Venturino, N. Prasad, and X. Wang. Coordinated linear beamforming in downlink multi-cell wireless networks. *IEEE Trans. Wireless Commun.*, 9(4):1451–1461, 2010.

[152] H. Wang, Y. Huang, K.K. Wong, and L. Yang. Asymptotic performance of two-user interference channels using coordinated zero-forcing. *IEEE Communications Letters*, 16(5):608–611, 2012.

[153] Hong Shen Wang and N. Moayeri. Finite-state Markov channel – a useful model for radio communication channels. *IEEE Trans. Veh. Technol.*, 44(1):163 –171, Feb. 1995.

[154] Du Wei. Leading edge–LTE requirements for bearer networks. *Huawei Communicate*, pages 49 –51, June 2009.

[155] M. Wernersson, S. Wänstedt, and P. Synnergren. Effects of QoS scheduling strategies on performance of mixed services over LTE. In *Proc. of the IEEE Int. Symp. on Personal Indoor and Mobile Radio Comm.*, 2007.

[156] A. D. Wyner. Shannon-theoretic approach to a gaussian cellular multiaccess channel. *IEEE Trans. Inform. Theory*, pages 1713 – 1727, Nov. 1994.

[157] Z. Xiao, P. Wang, X. Zhang, S. Mahato, L. Chen, and J. Zhang. Incentive mechanism for uplink interference avoidance in two-tier macro-femto networks. In *Proc. IEEE Veh. Technol. Conf.*, pages 1–6, 2012.

[158] Jiaming Xu, Jun Zhang, and J. G. Andrews. On the accuracy of the Wyner model in cellular networks. *IEEE Trans. Wireless Commun.*, 10(9):3098 –3109, September 2011.

[159] Mehmet Yavuz, Farhad Meshkati, Sanjiv Nanda, Akhilesh Pokhariyal, Nick Johnson, Balaji Raghothaman, and Andy Richardson. Interference management and performance analysis of UMTS/HSPA+ femtocells. *IEEE Commun. Mag.*, 47(9):102 – 109, September 2009.

[160] Qiaoyang Ye, Beiyu Rong, Yudong Chen, Mazin Al-Shalash, Constantine Caramanis, and Jeffrey G. Andrews. User association for load balancing in heterogeneous cellular networks. *submitted, IEEE Trans. Wireless Commun.*, 2012, arXiv preprint arXiv:1205.2833.

[161] C.M. Yetis, T. Gou, S.A. Jafar, and A.H. Kayran. On feasibility of interference alignment in MIMO interference networks. *IEEE Trans. Signal Processing*, 58(9):4771–4782, 2010.

[162] Seyoung Yun, Yung Yi, Dong-Ho Cho, and Jeonghoon Mo. Open or close: On the sharing of femtocells. In *Proc. IEEE INFOCOM*, pages 116 –120, April 2011.

[163] H. Zhang and H. Dai. Cochannel interference mitigation and cooperative processing in downlink multicell multiuser MIMO networks. *EURASIP Journal on Wireless Communications and Networking*, 2004(2):222–235, 2004.

[164] J. Zhang and J. G. Andrews. Distributed antenna systems with randomness. *IEEE Trans. Wireless Commun.*, 7(9):3636–46, September 2008.

[165] J. Zhang, M. Kountouris, J. G. Andrews, and Robert W. Heath. Multimode transmission for the MIMO broadcast channel with imperfect channel state information. *IEEE Transactions on Communications*, 59(3):803–814, March 2011.

[166] Jun Zhang and J. G. Andrews. Adaptive spatial intercell interference cancellation in multicell wireless networks. *IEEE J. Selected Areas in Communications*, 28(9):1455 –1468, December 2010.

[167] Jun Zhang, Runhua Chen, J. G. Andrews, and Robert W. Heath. Networked MIMO with clustered linear precoding. *IEEE Trans. Wireless Commun.*, 8(4):1910 –1921, April 2009.

[168] R. Zhang and S. Cui. Cooperative interference management with MISO beamforming. *IEEE Trans. Signal Processing*, 58(10):5450–5458, 2010.

[169] J. Zheng, E.R. Duni, and B.D. Rao. Analysis of multiple-antenna systems with finite-rate feedback using high-resolution quantization theory.

IEEE Trans. Signal Processing, 55(4):1461–1476, 2007.

[170] Y. Zhong and W. Zhang. Multi-channel hybrid access femtocells: A stochastic geometric analysis. *arXiv preprint arXiv:1108.1257*, 2011.

[171] Y. Zhu and D. Guo. Isotropic MIMO interference channels without CSIT: The loss of degrees of freedom. In *Allerton Conference on Commun., Control, and Computing*, pages 1338–1344, 2009.

Vita

Ping Xia received his B.E. in Information Electronics and Engineering with high honor from Tsinghua University, China in 2008 and M.S. in Electrical and Computer Engineering from University of Texas at Austin in 2010. Currently, he is a Ph.D. candidate in Wireless Networking and Communications Group (WNCG) at the Department of Electrical and Computer Engineering, UT Austin. His Ph.D. research focuses on interference management in heterogeneous cellular networks comprising macro, pico and femto cells. He held intern positions at Huawei North America R&D Center in summer 2011 working on interference cancellation in heterogeneous WCDMA networks, and Qualcomm in summer 2012 working on interference management in dual-SIM TD-SCDMA handsets.

Permanent email: xpneville@gmail.com

This dissertation was typeset with LaTeX[†] by the author.

[†]LaTeX is a document preparation system developed by Leslie Lamport as a special version of Donald Knuth's TeX Program.